University of East Anglia

Investigating the role of integrins α5β1 and α7β1 in satellite cell function and adult skeletal muscle regeneration

Paul Lonsdale

A thesis submitted for the degree of Doctor of Philosophy on 19th December 2025

This copy of the thesis has been supplied on condition that anyone who consults it is understood to recognise that its copyright rests with the author and that use of any information derived therefrom must be in accordance with current UK Copyright Law. In addition, any quotation or extract must include full attribution.

norwich research park Doctoral Training Partnership

UKRI Biotechnology and Biological Sciences Research Council

Abstract.

Satellite cells (SCs) are exogenous muscle stem cells that respond to injury or degenerative disease in order to maintain functional movement and strength throughout our lifetimes. SCs respond to a variety of signals in order to achieve either repair or hypertrophy of stressed or damaged muscle fibres. They rely upon a myriad of cell surface signalling receptors to translate their environment and respond to cues, including two members of the heterodimeric integrin family, α5β1 and α7β1. Integrin α5β1 is a fibronectin receptor and α7β1 is a laminin receptor.

In this study, the regenerative capacity of adult skeletal muscle in three knock-out (KO) variants, integrin α5 conditional KO (cKO), integrin α7 KO and a double KO (DKO) were tested against each other and wild-type (WT) controls at various time points after an induced acute injury. The use of genetically modified mice, engineered using conditional Cre-Lox recombination technology, allowed for SCs to be labelled with tdTomato (tdT), and the otherwise embryonically lethal *Itga5* to be ablated specifically in the SCs of *Itga7* +/+ or *Itga7* α*7-/-* adult mice. The effects of an induced injury and regenerative capacity were then assessed using the size of muscle fibres, SC numbers and α-smooth muscle actin expression, at either 10 days or 30 days post injury, as indicators of regenerative efficiency relative to WT controls. SC kinetics and dynamics were also analysed using time lapse microscopy and immunofluorescence on isolated myofibres and associated SCs. Histological and computational analysis of images not only revealed that both integrins, α5β1 and α7β1, are required for regeneration to proceed, but also that SC migration, proliferation and self-renewal are particularly dependent upon integrin α7, whilst integrin α5 is required for proper SC differentiation.

Access Condition and Agreement

Each deposit in UEA Digital Repository is protected by copyright and other intellectual property rights, and duplication or sale of all or part of any of the Data Collections is not permitted, except that material may be duplicated by you for your research use or for educational purposes in electronic or print form. You must obtain permission from the copyright holder, usually the author, for any other use. Exceptions only apply where a deposit may be explicitly provided under a stated licence, such as a Creative Commons licence or Open Government licence.

Electronic or print copies may not be offered, whether for sale or otherwise to anyone, unless explicitly stated under a Creative Commons or Open Government license. Unauthorised reproduction, editing or reformatting for resale purposes is explicitly prohibited (except where approved by the copyright holder themselves) and UEA reserves the right to take immediate ‘take down’ action on behalf of the copyright and/or rights holder if this Access condition of the UEA Digital Repository is breached. Any material in this database has been supplied on the understanding that it is copyright material and that no quotation from the material may be published without proper acknowledgement.

Table of contents.

Abstract..... i
Table of contents..... ii
List of figures..... vi
List of tables..... ix
Abbreviations..... x
Acknowledgments..... xii
Chapter 1. Introduction..... 1
1.1 Skeletal muscle..... 2
1.1.1 Skeletal muscle in health and disease..... 2
1.1.2 Skeletal muscle structure and function..... 3
1.1.3. Myofibres..... 5
1.1.4. Myogenesis..... 7
1.1.5. ECM remodelling during myogenesis..... 10
1.1.6. Satellite cells..... 12
1.1.7. The satellite cell niche..... 16
1.1.8. The basal lamina (basement membrane)..... 17
1.2. **Integrins**..... 18
1.2.1. Integrin structure..... 19
1.2.2. Integrin signalling..... 21
1.2.3. Integrins during skeletal muscle development..... 23
1.2.4. Integrin $\alpha 7\beta 1$..... 25
1.2.5. Integrin $\alpha 5\beta 1$..... 28
1.2.6. Functional association between integrin $\alpha 5\beta 1$ and $\alpha 7\beta 1$..... 30
1.3. Aims..... 30

Chapter 2. Materials & Methods..... 31
2.1. Mouse lines..... 32
2.1.1. Constitutive $\alpha 7$ KO mice..... 32
2.1.2. Conditional $\alpha 5$ KO mice..... 33
2.1.3. DKO mice..... 33
2.1.4. Ai14 Rosa26-stop-flox-tdTomato reporter mice..... 34
2.1.5. Animal maintenance..... 35
2.2. Molecular biology techniques..... 35

2.2.1. PCR genotyping..... 35
2.2.2. Agarose gel electrophoresis..... 37
2.3. Cardiotoxin (CTX) induced muscle injury..... 38
2.4. Dissection of mouse hindlimbs..... 38
2.4.1. Tibialis anterior (TA) – regeneration experiments..... 38
2.4.2. Extensor digitorum longus (EDL) – individual myofibre isolation..... 38
2.5. Histology..... 39
2.5.1. Tissue fixation..... 39
2.5.2. TESPA (3-aminopropyl – triethoxysilane) slide coating..... 39
2.5.3. Cryosectioning..... 40
2.5.4. Hematoxylin and eosin (H&E) staining..... 40
2.5.5. Immunofluorescence on muscle sections..... 41
2.5.6. Immunofluorescence on isolated myofibres..... 42
2.6. Tissue culture..... 44
2.6.1. Coating of culture plates..... 44
2.6.2. Culture of differentiating satellite cells..... 44
2.6.3. Culture of proliferating satellite cells..... 44
2.6.4. Culture of isolated myofibres in 3D collagen I gels..... 45
2.6.5. Labelling of satellite cells with 5'-ethynyl-2'-deoxyuridine (EdU)..... 46
2.7. Flow cytometry..... 46
2.7.1. Click-It EdU reaction..... 46
2.7.2. Analysis of cells with flow cytometer..... 47
2.8. Microscopy.....48
2.8.1. Imaging of muscle sections..... 48
2.8.2. Imaging of muscle fibres..... 48
2.8.3. Time-lapse microscopy..... 48
2.9. Image analysis and data acquisition..... 48
2.9.1. Analysis of stained muscle sections..... 48
2.9.2. Analysis of ex vivo muscle regeneration..... 50
2.9.3 Analysis of time-lapse videos..... 50
2.10 Graphs and statistics..... 50

Chapter 3. Integrins α5β1 and α7β1 are essential for efficient muscle regeneration after an acute injury 51
3.1. Introduction 52
3.2. Genotyping of integrin KO mice 53
3.3. Histological analysis of injured muscle at 10 DPI and 30 DPI. 54
3.4. Quantitative analysis of regenerating myofibres and 10 DPI and 30 DPI 57
3.5. Persistent -smooth muscle actin expression is observed in integrin deficient regenerating myofibres at 10 DPI 60
3.6. Mice lacking integrin α7 display reduced numbers of SCs in vivo 62
3.7. Summary 66

Chapter 4. Integrin α7β1 is essential for satellite cell migration and proliferation 68
4.1. Introduction 69
4.2. Expression of integrin α5β1 in quiescent and activated satellite cells 70
4.3. Time lapse analysis of satellite cell migration on isolated myofibres 72
4.4. Time lapse analysis of satellite cell proliferation on isolated myofibres 73
4.5. Satellite cells lacking integrin α7β1 demonstrate increased cell cycle arrest / mitotic catastrophe 75
4.6. Summary 77

Chapter 5. Integrins regulate satellite cell differentiation and self-renewal 79
5.1. Introduction 80
5.2. Ex-vivo satellite cell proliferation is particularly dependent upon integrin α7β1 81
5.3. Expression of Pax7 and Myf5 in quiescent satellite cells 83
5.4. Expression of Pax7, Myf5 and MyoD in activated satellite cells at 24 hours after isolation 85

5.5. Expression of Pax7, MyoD and MyoG in myogenic progenitors at 48 hours after isolation..... 86
5.6. Expression of Pax7, MyoD and MyoG in myogenic progenitors at 72 hours after isolation..... 90
5.7. Expression of Pax7, MyoD and MyoG in myogenic progenitors at 96 hours after isolation..... 92
5.8. Summary..... 95

Chapter 6. Discussion..... 97
6.1. Discussion..... 98
6.1.1. Impaired muscle regeneration after an acute injury in vivo..... 98
6.1.2. Integrin deficient satellite cell migration..... 101
6.1.3. Integrin deficient satellite cell proliferation and cell cycle progression..... 102
6.1.4. Integrin deficient satellite cell differentiation and self-renewal. 105
6.2. Conclusions..... 106
6.3. Future work..... 107

References.
Appendix.

List of figures

Figure 1.1. Integrin α7β1 and the DGC..... 3
Figure 1.2. Hierarchical structure of skeletal muscle..... 4
Figure 1.3. Structure of the sarcomere and molecular components of contraction..... 5
Figure 1.4. Distribution of different MyHCs detected by immunofluorescence in mouse soleus..... 6
Figure 1.5. Stages of skeletal myogenesis from the embryo to the adult.. 9
Figure 1.6. Adult myogenic lineage progression and expression profile of key myogenic regulatory factors..... 10
Figure 1.7. ECM composition in regenerating skeletal muscle.....12
Figure 1.8. The satellite cell niche..... 13
Figure 1.9. Schematic representation of the cycle of satellite cell activation, proliferation and differentiation following muscle injury..... 14
Figure 1.10. Symmetric vs asymmetric satellite cell division..... 15
Figure 1.11. Basic structure of the basal lamina.....18
Figure 1.12. Integrin specificity..... 19
Figure 1.13. Integrin structure and activation..... 20
Figure 1.14. Different modes of integrin signalling..... 22
Figure 1.15. Summary of integrin expression during primary, secondary and adult myogenesis..... 24
Figure 1.16. Schematic representation of integrin location during muscle development in mice..... 25
Figure 1.17. Pathological changes observed in muscle of integrin α7 KO mice..... 26
Figure 1.18. Genomic organisation of *ITGA7* and its splice variants..... 28

Figure 2.1. Targeted disruption of *Itga7*..... 32
Figure 2.2. Inducible targeted inactivation of *Itga5*..... 33
Figure 2.3. Breeding strategy for DKO mice..... 34
Figure 2.4. Cre / Lox mechanism of SC fluorescent labelling..... 35
Figure 2.5. Workflow for image analysis of muscle sections..... 49

Figure 2.6. Sketch of a particle showing minimum (F_{min}) and maximum (F_{max}) Feret diameter..... 49

Figure 3.1. Tamoxifen and CTX protocol..... 53
Figure 3.2. Representative PCR gel images..... 54
Figure 3.3. Representative images of H&E stained transverse sections of the TA. Uninjured, at 10 DPI and 30 DPI..... 56
Figure 3.4. Representative immunofluorescence images of transverse sections of the TA. Stained with nidogen (green) and DAPI (blue). Uninjured, at 10 DPI and 30 DPI..... 58
Figure 3.5. Muscle regeneration is delayed in the α5 cKO and α7 KO but persistently impaired in the DKO..... 59
Figure 3.6. Representative immunofluorescence images of transverse sections of the TA. Stained with nidogen (green), α-SMA (red) and DAPI (blue). Uninjured, at 10 DPI and 30 DPI..... 61
Figure 3.7. Method of SC identification. Sections from the TA of mice expressing tdT in SCs, counter stained with DAPI..... 62
Figure 3.8. Representative images of transverse sections of the TA from mice expressing tdT (red), stained with DAPI (blue). Uninjured, at 10 DPI and 30 DPI..... 63
Figure 3.9. SC numbers are reduced in mice lacking integrin α7..... 64
Figure 3.10. No significant difference in SC number pre and post injury.... 65

Figure 4.1. Integrin α5 is expressed in proliferative myoblasts, not quiescent SCs..... 71
Figure 4.2. Efficient myofibre associated SC migration requires integrin α7β1..... 72
Figure 4.3. The loss of integrin α5β1 and / or α7β1 does not affect the timing of cell divisions after activation..... 73
Figure 4.4. Integrin deficiency in SCs reduces their mitotic potential..... 74
Figure 4.5. Representative flow cytometry outputs..... 75
Figure 4.6. Loss of integrin α7 slows cell cycle entry..... 76
Figure 4.7. The loss of integrin α7 results in reduced cell cycle progression.....77

Figure 5.1. Tamoxifen and myofibre isolation protocol..... 80
Figure 5.2. Expression of MRFs in SCs and progeny during activation, proliferation and differentiation..... 81
Figure 5.3. Integrin α7 is a requirement for efficient SC proliferation..... 83
Figure 5.4. Integrin deficiency increases Myf5 expression in quiescent SCs..... 84
Figure 5.5. Representative images of isolated EDL myofibres and activated SCs immunostained against Pax7, Myf5 and MyoD at T24..... 85
Figure 5.6. Loss of integrins results in fewer MyoD +ve SCs at T24..... 86
Figure 5.7. Representative images of isolated EDL myofibres and proliferating myoblasts immunostained against Pax7, MyoD and MyoG at T48..... 87
Figure 5.8. Loss if integrin α7 results in fewer Pax7 +ve / MyoD -ve myoblasts at T48..... 88
Figure 5.9. Loss of integrin α5 results in fewer MyoG +ve myoblasts at T48..... 89
Figure 5.10. Representative images of isolated EDL myofibres and proliferating myoblasts immunostained against Pax7, MyoD and MyoG at T72..... 90
Figure 5.11. Loss of integrins results in fewer MyoD -ve myoblasts at T72..... 91
Figure 5.12. Loss of integrin α5 results in fewer MyoG +ve myoblast at T72..... 92
Figure 5.13. Representative images of isolated EDL myofibres and proliferating myoblasts immunostained against Pax7, MyoD and MyoG at T96..... 93
Figure 5.14. Loss of integrins slows myoblast differentiation and impairs self-renewal at T96..... 94
Figure 5.15. Loss of integrin α5 results in fewer MyoG +ve myoblast at T96..... 95

Figure 6.1. Graphical summary.....107

List of tables

Table 2.1. Composition of proteinase K lysis buffer..... 36
Table 2.2. Mastermix for PCR genotyping reactions..... 36
Table 2.3. PCR primers used to confirm the predicted genotype.. 36
Table 2.4. PCR programme for integrin α5..... 37
Table 2.5. PCR programme for integrin α7, Cre and tdTomato..... 37
Table 2.6. Composition of gel electrophoresis reagents..... 37
Table 2.7. Composition of fixation reagents..... 39
Table 2.8. Timing of sequential immersions for TESPA coating..... 39
Table 2.9. H&E protocol..... 41
Table 2.10. Composition of immunofluorescence reagents..... 42
Table 2.11. Primary antibodies..... 43
Table 2.12. Secondary antibodies + DAPI..... 44
Table 2.13. Composition of cell culture media..... 45
Table 2.14. Composition of 4X medium for collagen I gel (per 48 well plate)..... 46
Table 2.15. Composition of collagen I gel (per 48 well plate)..... 46
Table 2.16. Click-iT reaction cocktail preparation (per reaction)..... 47
Table 2.17. Cytoflex filter specification..... 47

Abbreviations

α-SMA	Alpha smooth muscle actin.
bp	Base pairs.
BM	Basement membrane.
BMRC	Biomedical research centre.
BSA	Bovine serum albumin.
CTX	Cardiotoxin.
^{o}C	Celsius.
cKO	Conditional knock out.
Cre	Cre-recombinase.
DKO	Double knock out.
DMU	Disease modelling unit.
DPBS	Dulbecco's phosphate buffed saline.
DPI	Days post injury.
DMD	Duchenne muscular dystrophy.
DMEM	Dulbecco's modified eagle medium.
EDL	Extensor digitorum longus.
EDTA	Ethylenediaminetetraacetic acid.
FGF	Fibroblast growth factor.
Fig	Figure.
FACS	Fluorescence activated cell sorting.
g	Grams.
H&E	Hematoxylin & eosin.
hrs	Hours.
IP	Intraperitoneal.
KO	Knockout.
μg	Micrograms.
μl	Microlitres.
mg	milligrams.
ml	millilitres.
MRF	Muscle regulatory factor
MyoG	Myogenin.
MyHC	Myosin heavy chain.
NGS	Normal goat serum.

Pax	Paired box.
PFA	Paraformaldehyde.
Pen/strep	Penicillin and streptomycin.
PBS	Phosphate buffed saline.
PCR	Polymerase chain reaction.
ROS	Reactive oxygen species.
SCs	Satellite cells.
SEM	Standard error of the mean.
TA	Tibialis anterior.
WT	Wildtype.
Wnt	Wingless.

Acknowledgments

First and foremost, a massive thank you goes to my supervisor and mentor, Prof. Uli Mayer. Your unwavering academic and personal support is what has got me through this PhD journey, even though at times I didn't think I would make it. I owe you so much, in so many ways, including my future scientific career and I am eternally grateful. To my secondary supervisor, Prof. Andrea Munsterberg, thank you for always being an optimist at lab meetings and believing in me. I would also like to say a huge thank you to Dr Ernst Pöschl. Your ever enthusiastic technical guidance, questioning and anecdotes taught me so much and made my time in the lab such an enjoyable experience. Special mentions must also go to Dr Tim Pearson and Dr Shannon Conway who were both instrumental in my BMRC survival. Tim, you are a good friend and experimental guide. I have benefitted immeasurably from your vast experience. Shannon, you were my bedrock for years at the BMRC, then you had to graduate (how dare you!) and left me to fend for myself, your permanent smile and positivity were sorely missed. Thank you also to all of the technicians and staff at the BMRC and DMU, your tireless work doesn't go unnoticed, you are the unsung heroes of so many publications and PhD theses.

To my family, Rach, thank you for putting up with me over the last 4 years. It has been tough at times, but your unconditional love and support have got me through. Poppy and Maya, everything I have achieved is because I want a better life for you. Hopefully we will now have more opportunities to experience the world together as you grow up. You can literally do anything if you set your mind to it, this thesis is proof of that. Mum, Rob, Janet and Colin, you have helped more than you know, this would never have been possible without your help, thank you.

To my close friends, 'Auntie' Sharon, I don't think you realise quite how much you have made this possible, taking on childcare duties and school runs gave me time when crucially needed. Completing a PhD is not easy at the best of times, but you have made mine much easier than it could have been. Justin and Ross, my brothers from other mothers, you are both constant positive influences on me and my girls. You remind me to enjoy life and never take myself, or anyone else, too seriously.

Last but not least. Dad, my scientific inspiration, this is for you.

Chapter 1.
Introduction.

1.1. Skeletal muscle.

1.1.1. Skeletal muscle in health and disease.

With the exception of the morbidly obese, skeletal muscle is the most abundant tissue in the human body, accounting for approximately 30 % - 40 % of total adult body mass (Janssen et al., 2000). It allows for movement, respiration, strength and stability whilst also facilitating numerous metabolic and homeostatic processes which can become perturbed if the muscle becomes dysfunctional or vice versa. Metabolic disruption within skeletal muscle can contribute to several conditions including, but not limited to, obesity, Pompe's disease and numerous mitochondrial disorders (Koopman et al., 2014; Pezzo., 2013). Whereas muscle wasting conditions such as sarcopenia, cachexia and the muscular dystrophies all result in altered muscle metabolism (Heydemann., 2018; Ryall et al., 2008). Healthy skeletal muscle is the largest secretory organ in the body, capable of autocrine, paracrine and endocrine signalling (Pedersen., 2013). The numerous cytokines and other signalling peptides expressed within muscle fibres have collectively been termed 'myokines'. Recent evidence indicates that myokine expression and secretion is critical for many homeostatic processes (Severinsen & Pedersen., 2020). These crucial signalling molecules can be significantly altered when muscle becomes dysfunctional and that this can have far reaching effects throughout the body (Jo et al., 2022).

Duchenne muscular dystrophy (DMD) is the most common form of muscular dystrophy, affecting approximately 1:5000 live male births (Crisafulli et al., 2020). It is characterised by progressive degeneration of skeletal muscle in conjunction with cardiomyopathy first manifesting at around 3 years of age, ultimately leading to fatal cardiac and respiratory complications by the age of 30. It is a recessive X-linked condition caused by one or more mutations in the dystrophin gene, resulting in a lack of functional dystrophin protein. Dystrophin, when bound to other key proteins, forms the dystrophin glycoprotein complex (DGC) (Figure 1.1). It provides an essential link between the cytoskeleton of muscle fibres and the surrounding ECM via interaction with a muscle specific laminin containing α2, β1 or β2 and γ1 chains (laminin-211 or -221). The link between the DGC and laminin is key to the protection and stabilisation of the muscle fibre and when lost results in contraction induced injury to the sarcolemma resulting in sequential rounds of degeneration/regeneration (Rahimov & Kunkel., 2013), ultimately leading to muscle wasting and a reduced capacity for force

transmission. Dystrophic muscle also displays an altered insulin response and contains fewer, sometimes aberrant mitochondria (Schneider et al., 2018). This leads to decreased levels of intracellular ATP and an increase in reactive oxygen species (ROS), resulting in a reduced capacity to fulfil the metabolic demands associated with muscle contraction. Integrin $\alpha 7\beta 1$ acts as a complementary laminin receptor in adult skeletal muscle, contributing to the functional interaction between the cytoskeleton, sarcolemma and basal lamina via extracellular binding of laminin-211 or -221 and intracellular interaction with the actin cytoskeleton via binding proteins vinculin and talin, as shown in figure 1.1.

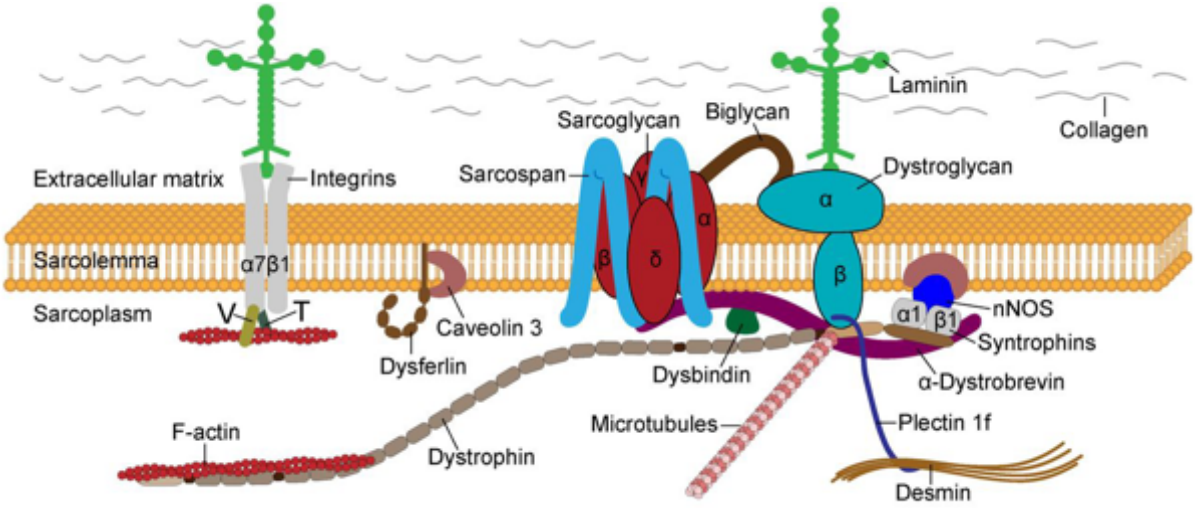


Figure 1.1. Integrin α7β1 and the DGC. Heterodimeric integrin $\alpha 7\beta 1$ on the left and multimeric DGC on the right both bind laminin-211 or -221 in the basement membrane. Figure taken from Rahimov, F. & Kunkel, L. M. 2013

1.1.2. Skeletal muscle structure and function.

Skeletal muscle is a composite tissue with broad functionality and large regenerative capacity in response to acute injury. Whilst its primary function is to facilitate locomotion and respiration, it also plays a vital role in metabolism and thermogenesis (Periasamy et al., 2017), acting as storage for both glycogen and essential amino acids (Jensen et al., 2011; White., 2021). Although highly complex in terms of composition and architecture, it is generally characterised by its contractile multinucleated fibres which can adapt to various stimuli including mechanical stress, oxidative stress or environmentally induced conditions, such as hypoxia, through either atrophy, hypertrophy or via changes in fibre metabolic capacity. Each muscle is hierarchically compartmentalised into gradually larger

units by distinct layers of collagen rich connective tissue, resulting in the recognisable cross-sectional appearance shown in figure 1.2.

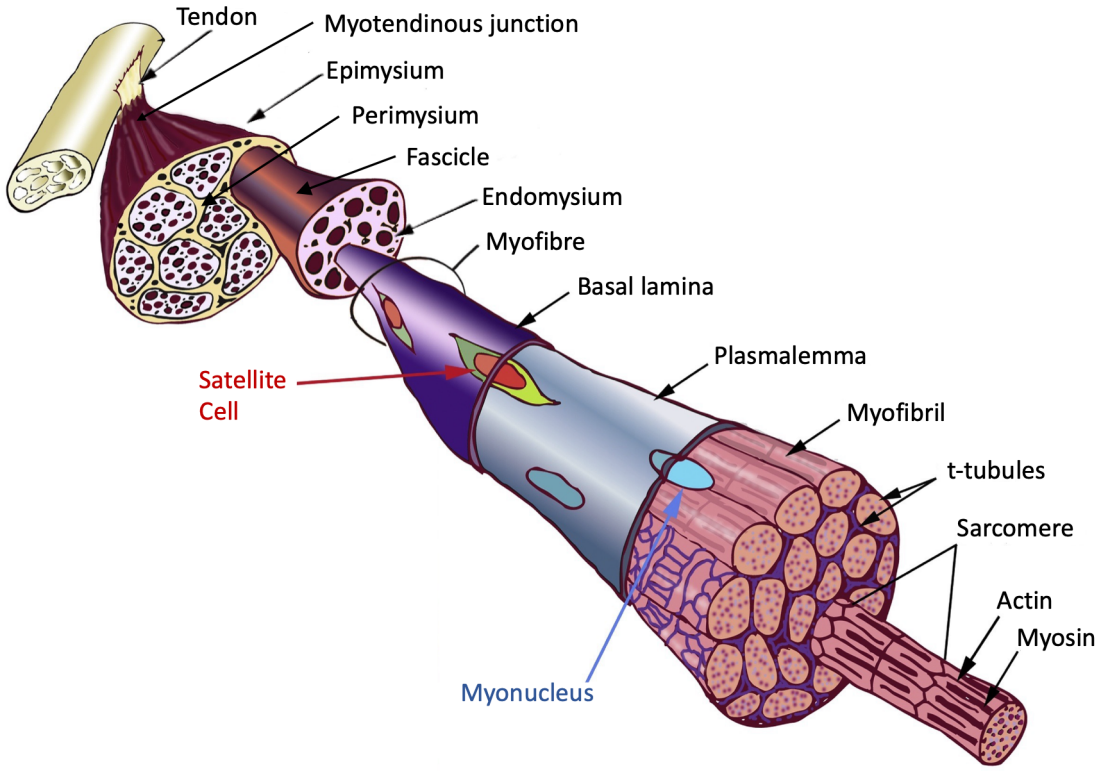


Figure 1.2. Hierarchical structure of skeletal muscle. Bundles of myofibrils, which contain the contractile sarcomeres, are compartmentalised into myofibres by the plasmalemma and encapsulated by the basal lamina. Myofibres are supported by the endomysium and bundled into fascicles which are themselves surrounded by the perimysium. The epimysium encapsulates the entire muscle to ensure isolated contraction. Each muscle is anchored by a tendon via the myotendinous junction. Figure modified from Zammit., 2017.

The epimysium is the outer most layer, it acts as a sheath around the entire muscle that allows for separation and isolated operation. Beneath that, the perimysium surrounds and supports bundles of myofibres known as fascicles. Within each fascicle, individual myofibres are surrounded by the endomysium but separated from it by the plasmalemma and basal lamina, highlighted in figure 1.2. Skeletal muscle contracts and elicits movement in response to electrical stimulation, delivered by motor neurons via neuromuscular junctions (NMJs) to individual myofibres. Upon contraction, the force generated is transmitted through the tendon to the bone via specialised, interdigitated, load bearing regions known as the myotendinous junction (MTJ). The contractile apparatus is integrated within a complex network of extra cellular matrix (ECM) primarily composed of collagens

I, III and VI along with elastin and various glycoproteins and proteoglycans (Csapo et al., 2020; Loreti & Sacco., 2022).

1.1.3. Myofibres.

Although numerous cell types contribute to the overarching composition of skeletal muscle, the individual cellular unit, around which everything else is built, is the myofibre. Each myofibre contains the necessary organelles required for normal cellular function and ATP production, whilst the cytoskeleton is arranged into myofibrils of thin actin and thick myosin filaments. The thin and thick filaments overlap at regular intervals along the myofibril to form the functional units of contraction, the sarcomere (fig. 1.3).Sarcomeric contraction relies upon a Ca^{2+} driven conformational change in troponin and tropomyosin to reveal binding sites on the thin filament (fig. 1.3), increasing the binding affinity of myosin to actin, thereby initiating the interaction and movement of myosin thick filaments across actin thin filaments in an ATP dependant manner.

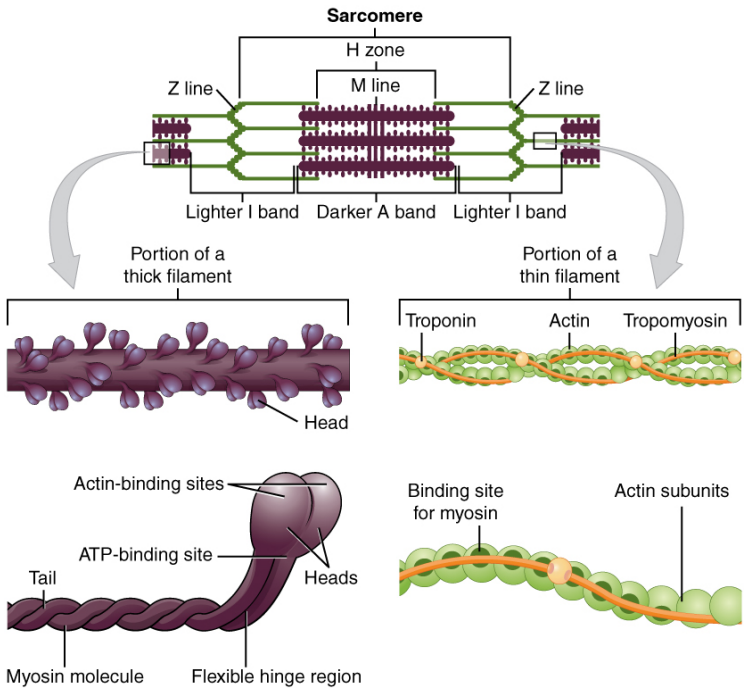


Figure 1.3. Structure of the sarcomere and molecular components of contraction. (Top) Sarcomeric organisation showing the overlap between thin actin and thick myosin filaments. **(Left)** Portion of thick filament and myosin molecule. Each myosin molecule has a flexible hinge region, two globular heads and bindings sites for ATP and actin. **(Right)** Portion of thin filament composed from actin arranged in a helical formation. Myosin binding sites are partially covered by tropomyosin and troponin until Ca^{2+} causes conformational change and exposes the binding site. Figure taken from Openstax.

Skeletal muscle is a heterogeneous tissue composed from a variety of fibre types and subtypes. In rodents myofibres can be broadly categorised into four groups based upon their contractile and metabolic properties. Type 1 fibres or so called 'slow twitch' fibres have a relatively slow contraction velocity, high oxidative capacity and high resistance to fatigue due to large numbers of mitochondria. Type 2, or 'Fast twitch' fibres can be further subdivided into three groups based upon the expression of specific myosin heavy chain (MyHC) isoforms, mitochondrial density, and metabolism: type 2A (oxidative), type 2B (glycolytic) and type 2D (oxidative/glycolytic). Humans however only express type 1, type 2A and type 2B myofibres (Pette & Staron., 2000; Talbot & Maves., 2016). The make-up of each muscle with respect to fibre type varies depending on the functional demands placed upon it. Skeletal stability or endurance exercise generally employs muscles with a higher degree of oxidative fibres, whereas bursts of speed or strength generally relies upon muscles with a mixed fibre profile or a predominantly glycolytic fibre composition. Numerous studies have demonstrated the presence of hybrid fibre types which display mixed MyHC expression and intermediate phenotypes with respect to contraction and metabolism (Biral et al., 1988; Larsson et al., 1978; Schiaffino., 2010), as shown in figure 1.4. These hybrid fibres, although potentially a permanent feature, could be fibres that are transitioning between phenotypes in response to environmental or physiological challenges. Myofibre plasticity has been demonstrated in numerous studies and offers a mechanism by which skeletal muscle can adapt to the ever-changing demands placed upon it. Traditionally myosin ATPase staining has been used to identify fibre types based upon distinctions between different isoforms of the myofibrillar enzyme ATPase

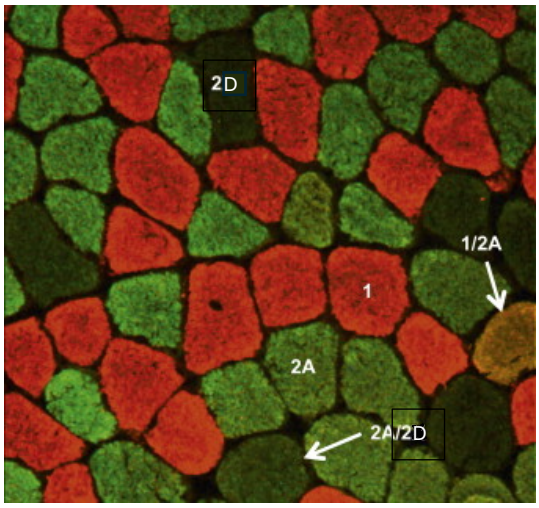


Figure 1.4. Distribution of different MyHCs detected by immunofluorescence in mouse soleus. Predominantly oxidative type 1 and 2A fibres. Fewer type 2D fibres are also present, whereas type 2B fibres are absent. Hybrid type 1/2A and type 2A/2D fibres are indicated by the arrows. Figure taken from Schiaffino., 2010.

(Behan et al., 2002). Using this method, it is possible to identify as many as seven distinct fibre types (Scott et al., 2001), however, it also suffers from numerous limitations and so has been superseded by immunofluorescence staining using specific antibodies directed against various MyHC isoforms (Fig. 1.4).

1.1.4 Myogenesis.

Developmental, neonatal and regenerative myogenesis is orchestrated by the same sequential expression of muscle specific transcription factors. The paired box transcription factors Pax3 and Pax7 mark myogenic specification in the developing vertebrate embryo, whilst the basic helix-loop-helix (bHLH) muscle regulatory factors (MRFs) Myf5, MyoD, Myf6 (also called MRF4) and Myogenin (MyoG) are required to induce proliferation, commitment and eventual terminal differentiation of embryonic stem cells into functional, contractile muscle tissue (Robson., 2017). Developmental myogenesis is defined as either primary or secondary (Fig. 1.5) depending on timing, transcriptional profile of the precursors and the target of subsequent fusion. In mouse, primary myogenesis takes place between embryonic day (E) 8 – E14.5 (Hernandez-Torres et al., 2017; Zammit., 2017). Pax3+ myogenic progenitor cells (MPCs) are first found in the mesoderm of the developing embryo and subsequently in the dermomyotome of maturing somites, Pax3+ MPCs begin to express Myf5 and Myf6 at ~E8 (Asfour et al., 2018; Ott et al., 1999), thereby becoming committed MPCs. The MPCs subsequently delaminate from the dermomyotome and contribute towards the formation of the underlying myotome prior to differentiating into mono-nucleated myocytes (Asfour et al., 2018; Chal & Pourquie., 2017; Ott et al., 1999). A subset of the Pax3+ MPCs delay expression of the MRFs until they have undergone an epithelial to mesenchymal transition (EMT) and migrated to further afield areas of the developing embryo. This Pax3+ / Pax7+ migratory population eventually contribute to the musculature in the limbs, diaphragm, neck, jaw and an area of the tongue (Chal & Pourquie., 2017; Zammit., 2017). Once the initial wave of myoblasts is depleted from the myotome, it receives a further contribution of Pax3 / Pax7 expressing stem cells from the dermomyotome at ~E10.5 – E11.5 (Zammit., 2017). Myf6 downregulation coincides with MyoD upregulation around E11.5 and this, along with MyoG expression, directs myocyte fusion into multi-nucleated primary myofibres (Chal & Pourquie., 2017; Zammit., 2017). Secondary myogenesis begins around E12.5 in mouse, Pax3 is downregulated in MPCs of

hypaxial (trunk) muscles, leaving a population of Pax7+ MPCs. Secondary myofibres are generated when Pax7+/Myf5+/Myod+ cells proliferate, before Myf5 downregulation is accompanied by Myf6 and MyoG upregulation, initiating differentiation and eventual fusion with either themselves or primary fibres (Bentzinger et al., 2012; Chal & Pourquie., 2017; Zammit., 2017). During this time only embryonic and neonatal MyHCs are expressed. It is also during secondary myogenesis that fibre type is initially determined via innervation. True muscle stem cells are born at around E16 – E18, when satellite cell (SC) precursors localise under the basal lamina where they reside, ready for activation in later life (Chal & Pourquie., 2017).

Postnatal growth, maintenance and regeneration of skeletal muscle is attributed to SCs, a dedicated population of muscle stem cells able to commit to a myogenic fate upon activation, whereby the sequential cascade of MRFs observed during embryonic development is recapitulated. The pathway for postnatal myogenic differentiation, shown in figure 1.6, begins with SC activation and expression of Myf5. MyoD expression marks proliferation and commitment to a myogenic fate followed by MyoG and Myf6 which mark terminal differentiation of myocytes and subsequent fusion into myotubes (Hernandez-Torres et al., 2017 ; Schmidt et al., 2019).

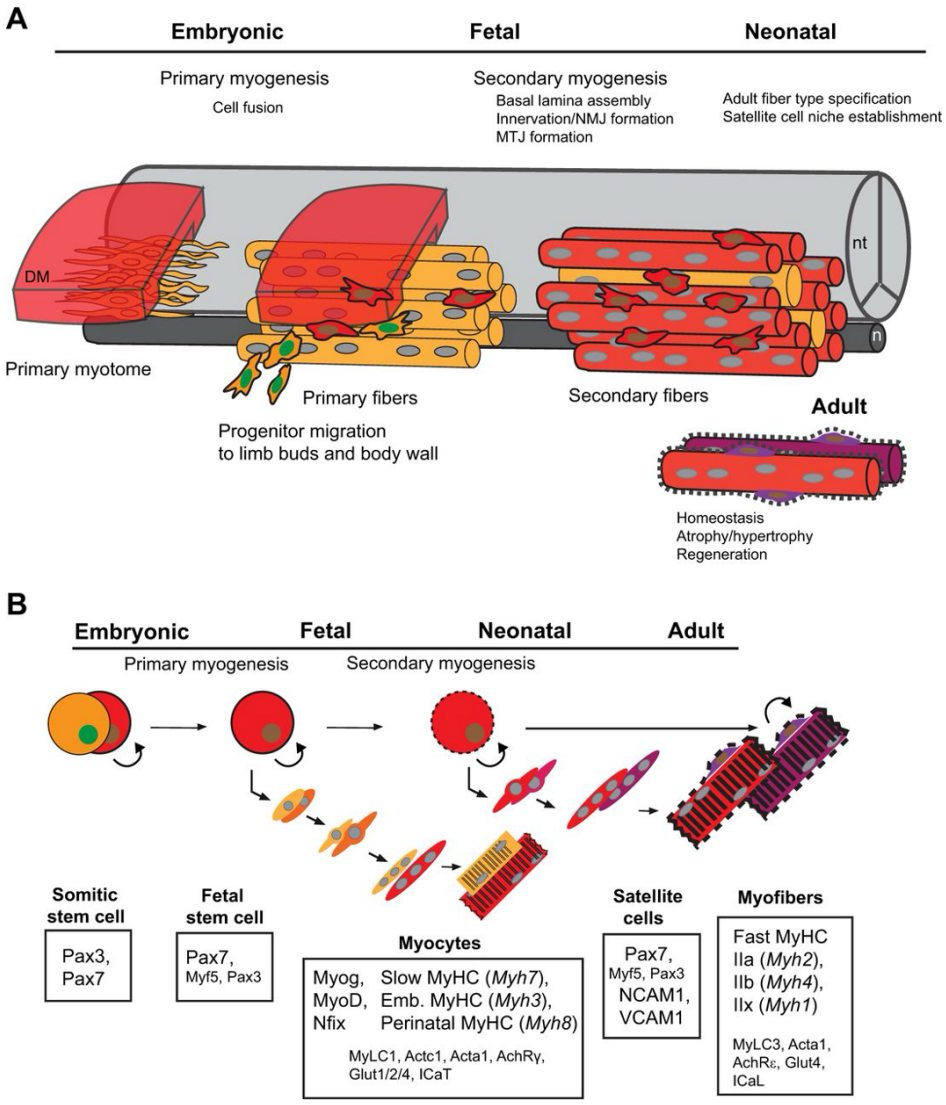


Figure 1.5. Stages of skeletal myogenesis from the embryo to the adult. (A) Developmental sequence of muscle formation. Early myotome (left, yellow) is composed of primary myocytes. During primary myogenesis (middle), Pax3+ progenitors (yellow cytoplasm, green nuclei) delaminate from the dermomyotome and contribute to the formation of primary myofibers (yellow). Some Pax3+ progenitors also migrate to populate the limb buds and body wall (hypaxial domain). During secondary myogenesis (right), Pax7+ myogenic progenitors (red cytoplasm, brown nuclei) contribute to secondary (red) fiber formation. During this phase, satellite cell precursors (purple cytoplasm, brown nuclei) localize under the basal lamina (dotted line) of the fibers where they can be found in adult muscles. nt, neural tube; n, notochord; DM, dermomyotome; MTJ, myotendinous junction; NMJ, neuromuscular junction. **(B)** Differentiation of somitic progenitors toward skeletal muscles and adult satellite cells. Myogenic stem cells contribute to fetal myogenesis while maintaining a pool of progenitors, which eventually become located on mature myofibers in the satellite cell niche. For each step, markers for the intermediates and differentiated skeletal myofibers are shown. Figure taken from Chal & Pourquie., 2017.

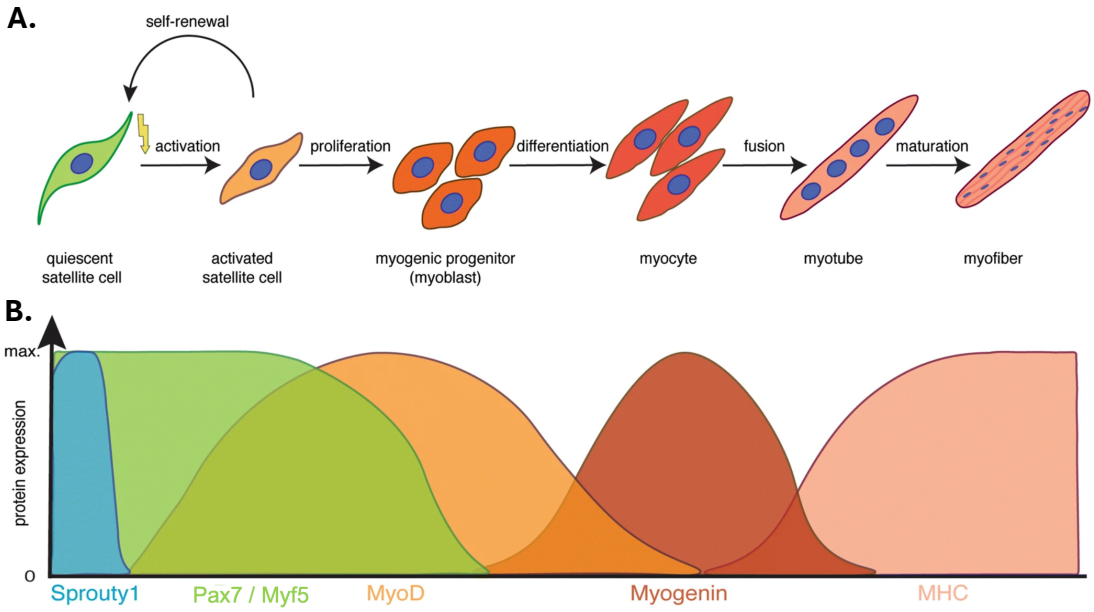


Figure 1.6. Adult myogenic lineage progression and expression profile of key myogenic regulatory factors. (A) Schematic illustration of the myogenic lineage progression. Satellite cells are activated, start to proliferate, thereby generating myogenic progenitor cells. Upon differentiation, myoblasts differentiate into myocytes, which fuse to form myotubes and mature to become myofibres. **(B)** Expression profile of key modulators of myogenic lineage progression. Figure modified from Schmidt et al., 2019.

1.1.5. ECM remodelling during myogenesis.

There is actually very little objective evidence regarding the composition of skeletal muscle ECM throughout primary, secondary and adult regenerative myogenesis. What is clear however, is that the ECM is in an almost perpetual state of remodelling depending upon developmental timepoint, exercise load, or injury. This remodelling process is governed by secretions from numerous resident cell types, including SCs, fibroblasts and fibro-adipogenic progenitors (FAPs), in conjunction with delicately balanced levels of specific matrix metalloproteinases (MMPs) and their respective inhibitors, tissue inhibitors of matrix metalloproteinases (TIMPs). In uninjured adult muscle, levels of MMPs are relatively low, but MMP-2 and MMP-9 which degrade laminin, fibronectin, collagen type IV and proteoglycans, as well MMP-1 and MMP-13 which degrade collagens type I and III respectively are present (Chen & Liu., 2009).

The ECM composition of skeletal muscle during embryonic, primary myogenesis is generally characterised by high levels of fibronectin with tenascin

C, laminin 111, numerous collagen isoforms including types I, III, IV, V, VI, XI, XII, XIV, XV, XVIII and various other proteoglycans (Gillies & Lieber., 2012). This environment supports the migration of Pax 3 / 7+ progenitors into the limb buds and promotes their proliferation and differentiation via Wnt7a signalling (Bentzinger et al., 2013). Post-natally, during secondary myogenesis, and as the skeletal muscle ECM matures into the epi-, endo- and perimysium there is a shift in composition. Fibronectin is downregulated, laminin 111 is replaced by laminin 211 / 221, whilst the array of collagens is significantly reduced to types I and III and VI, depending on the specific region in question (Gillies & Lieber., 2012). This shift likely promotes the structural integrity required by the significant load bearing demands placed upon skeletal muscle throughout its lifetime.

After an acute injury, regeneration occurs in 3 distinct phases (Ahmad et al., 2023). There is the initial degeneration of muscle fibres and associated inflammation. During this time MMPs begin to break down the existing ECM, resident cells including SCs, fibroblast and FAPs become ‘activated’ and begin to secrete high levels of fibronectin and collagen IV, as shown in figure 1.8. Phase two involves the proliferation and expansion of the SC pool and the start of regeneration. During this time the ECM is still rich in fibronectin to allow for rapid cell migration, and new muscle fibres begin to be formed, transiently expressing α-SMA at 4 – 9 dpi. Phase 3 involves hypertrophy and maturation of newly formed muscle fibres and their surrounding ECM, which eventually reestablishes the hierarchical structure shown in Fig. 1.2.

When the process of regeneration fails to resolve fully, possibly due to repeated injury, fibrosis occurs. Skeletal muscle fibrosis is generally characterised by the aberrant accumulation of ECM, primarily fibrillar collagens, in conjunction with fatty deposits, which replace the functional contractile tissue, thereby limiting the muscles capability to contract fully (Loomis. & Smith. 2023). The main drivers of fibrosis in skeletal muscle are thought to be myofibroblasts and FAPs (Hinz. & Lagares., 2020). They are both resident non-myogenic cells which reside in the interstitial space, become activated after injury and begin to secrete ECM proteins in order to facilitate and support regeneration. However, if the SC cell pool is depleted due to repeated injuries, or regeneration does not proceed normally for some reason, FAPs in particular, become resistant to apoptosis and assume a fibrotic phenotype, continuously depositing ECM, resulting in fibrosis (Loomis. & Smith. 2023).

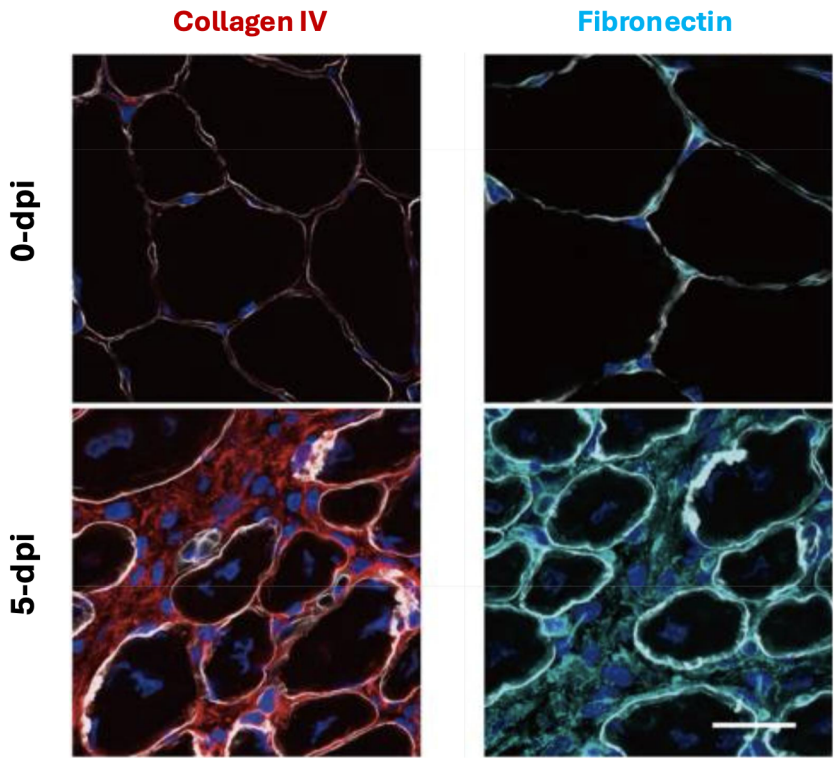


Figure 1.7. ECM composition in regenerating skeletal muscle. Immunostaining of mouse skeletal muscle cross sections at 0 or 5 dpi showing collagen IV (red), fibronectin (turquoise), laminin a2 (white) and DAPI (blue). Scale bar = 20 um. Figure modified from Schuler et al. 2022.

1.1.6. Satellite Cells.

SCs were first described in 1961 by Alexander Mauro (Mauro., 1961). His research confirmed the presence and location of quiescent satellite cells using electron micrographs of frog tibialis anticus muscles. Mauro described SCs as almost indistinguishable from myonuclei, apart from their unique position on the periphery of the myofibre. He also speculated their importance to adult skeletal muscle regeneration. A year prior to the publication of Mauro's work, Bintliff and Walker had shown the presence of multiple mononucleated cells accumulating at the site of an induced injury in the hind limbs of mice, prior to the formation of new myofibres (Bintliff & Walker., 1960). These two seminal papers initiated a wave of research into the topic which persists today. Subsequent studies have given us a wealth of knowledge detailing the origins of SCs along with the processes and molecular mechanisms governing regenerative myogenesis. Armand et al. used chick-quail chimeras to demonstrate that avian limb musculature and SCs both originated from somites, potentially indicating a common origin for all myogenic cells (Armand et al., 1983). More recently, progressive improvements in mouse

genetics have allowed for lineage tracing experiments using inducible fluorescent reporters and Cre-stop-flox techniques, controlled by muscle specific promoters, to give us further insights into the embryonic origins of muscle progenitors and SCs.

In adults, quiescent SCs maintain the expression of Pax7 and reside within a specialised niche between the sarcolemma and basal lamina surrounding each myofibre (Fig. 1.7). They are activated in response to various stimuli, including stretching, exercise, injury, and electrical stimulation (Seale et al., 2000). The activated SCs then re-enter the cell cycle, proliferate and differentiate into committed myoblasts, before undergoing fusion as myocytes to achieve either hyperplasia or hypertrophy to repair or maintain skeletal muscle, as shown in figure 1.9. The absolute requirement for SCs during adult regenerative myogenesis was demonstrated by inducing the expression of diphtheria toxin A in Pax7+ cells, whereby a complete loss of regeneration was observed after an acute injury (Lepper et al., 2011).

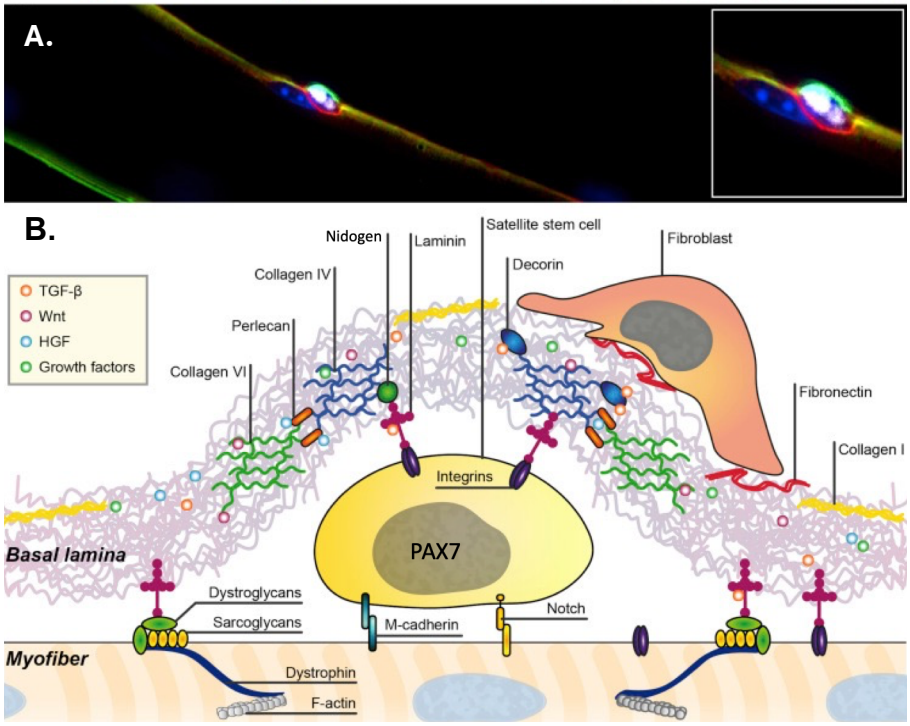


Figure 1.8. The satellite cell niche. (A) Immunofluorescence of single isolated myofibre, stained for Pax7 (white), laminin (green), dystrophin (red) and DAPI (blue). **(B)** Schematic representation of the satellite cell niche. Figure modified from Brun et al., 2017.

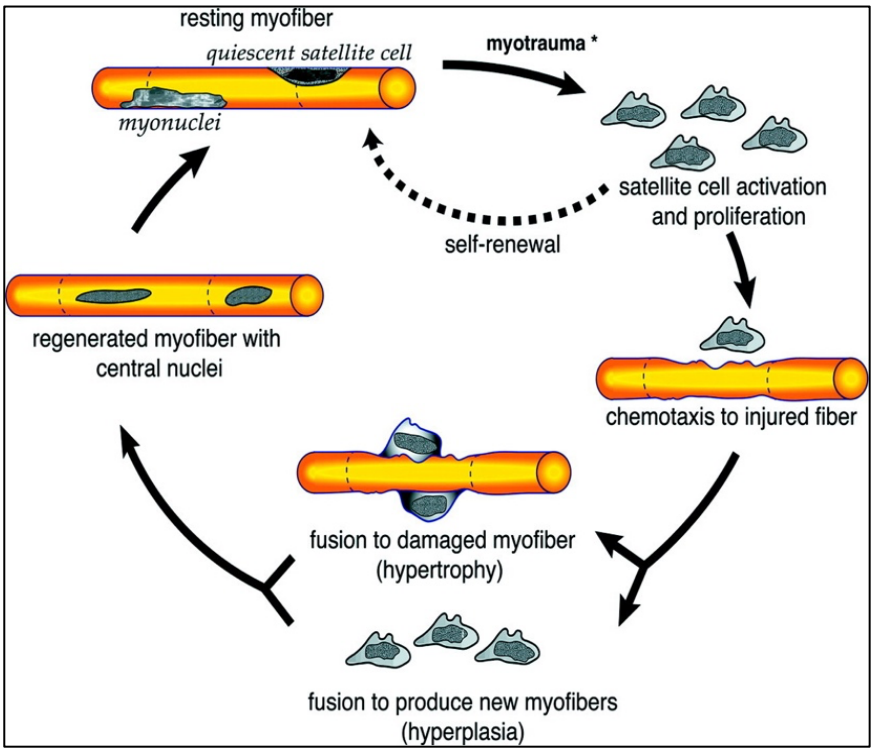


Figure 1.9. Schematic representation of the cycle of satellite cell activation, proliferation and differentiation following muscle injury. Satellite cells are activated in response to myotrauma, they initially undergo asymmetric cell division to maintain stem cell numbers (self-renewal). Committed myoblast continue to proliferate and migrate to the site of injury prior to fusion with either themselves (hyperplasia) or damaged myofibres (hypertrophy). Figure taken from Hawke & Garry., 2001.

Classically, with the exception of a Pax3+ subpopulation in the diaphragm, trunk and forelimbs, SCs have been described as a homogenous population (Bischoff., 1994; Relaix et al., 2006). Recent evidence, however, indicates widespread heterogeneity in terms of gene expression (Cho & Doles., 2017) and subsequent potential for either self-renewal or myogenic commitment (Kuang et al., 2007; Rocheteau et al., 2012). Lineage tracing experiments using the Myf5-Cre/R26R-YFP reporter mouse line identified heterogeneity in terms of Myf5 expression. Around 10% of SCs were shown to be Myf5- and undergo asymmetric cell division to produce both committed progenitor (Pax7+/Myf5+) and stem cell (Pax7+/Myf5-) daughters (Kuang et al., 2007), as shown in figure 1.10. In this way, a stable population of monopotent stem cells is maintained, whilst still producing the large numbers of proliferative myoblasts required for effective maintenance and regeneration.

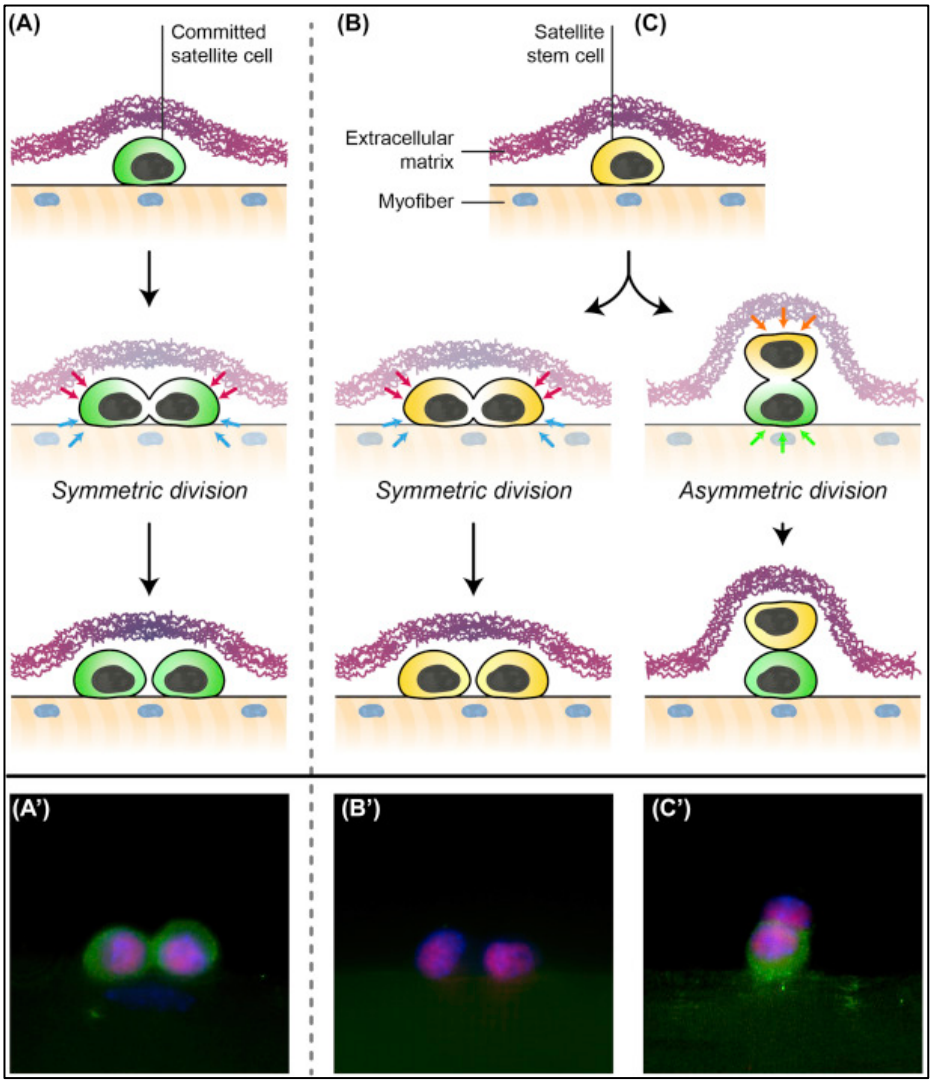


Figure 1.10. Symmetric vs asymmetric satellite cell division. (**A & B)** Committed satellite cells and satellite stem cells undergo symmetric cell division parallel to the myofibre. (**C)** Satellite stem cells can also perform asymmetric cell division in an apical/basal orientation. The daughter cell which maintains contact with the basal lamina is Myf5- whilst the daughter cell in contact with the myofibre becomes Myf5+ and commits to myogenesis. (**A', B' & C')** Immunofluorescence of EDL myofibres stained with Pax7 (red), GFP (for Myf5, green), and DAPI (blue), (**A')** symmetric division in committed satellite cells, (**B')** symmetric division in satellite stem cells and **C')** asymmetric division in satellite stem cells. Figure taken from Brun et al., 2017.

Given the complex multifactorial nature of adult myogenesis, it is not surprising that a large number of signalling pathways have previously been implicated in regulating SC function and adult skeletal muscle regeneration. These include, but are not limited to, Fibroblast growth factor (FGF) (Pawlikowski et al., 2017; Rozo et al., 2016; Zofkie et al., 2021), Notch (Bjornson et al., 2012; Conboy & Rando, 2002; Liu et al., 2018; Mourikis et al., 2012), Wnt (Otto et al.,

2008; Schmidt et al., 2019), Sonic hedgehog (SHH) (Cruz-Migoni et al., 2019; Strace et al., 2009) and c-MET signalling via its ligand hepatocyte growth factor (HGF). SHH signalling for example, is known to be a critical regulator of embryonic myogenesis, however, it also influences adult myogenesis both directly via action upon SCs, and indirectly by inducing interstitial fibroblasts to produce various growth factors (Piccioni et al., 2014). Cilium-mediated SHH signalling has also been shown to play a critical role in the maintenance of SC quiescence, whereby cell cycle entry and subsequent progression rely upon de-repression of SHH (Cruz-Migoni et al., 2019). Cruz-Migoni and colleagues proposed a model in which the disassembly of the primary cilia acts as a switch, inducing a change in SHH signalling from a repressive to an active state, thereby allowing SCs to exit their niche, proliferate and affect regeneration. Notch signalling has also been shown to be fundamental to the maintenance of SC quiescence (Conboy & Rando., 2002; Mourikis et al., 2012). However, upon activation, in order to facilitate appropriate SC differentiation, there is a switch from Notch to Wnt signalling, with multiple Wnt ligands being expressed in a temporally controlled manner. Wnt5a, Wnt5b and Wnt7a are all upregulated during the early stages of regeneration, with Wnt3a and Wnt7b being upregulated later in the process (Liu et al., 2018).

1.1.7. The Satellite Cell Niche.

The SC niche is a specific microenvironment defined as the space between the basal lamina and sarcolemma of the underlying muscle fibre, as shown in figures 1.2 & 1.7. It is essential for proper regulation of SC fate and presents vital ligands, providing the necessary signals to induce either quiescence or activation as required by the ever-changing physiological stimuli unfolding around it. Interaction between SCs and their niche is critical, not only for the maintenance of quiescence (Pisconti et al., 2016; Sampath et al., 2018), but also for the SC to establish polarity, which in turn influences cell fate decisions upon activation (Kuang., 2008; Ono et al., 2015; Seale et al., 2000). Cell surface receptors such as integrin $\alpha 7\beta 1$ and M-cadherin are asymmetrically expressed on the surface of SCs, interacting with the basal lamina and sarcolemma respectively in order to establish an apical/basal orientation, as shown in figure 1.8. Whilst the niche remains unperturbed, Pax7 expression within SCs is maintained. However, upon injury or stress, the signals reaching the SCs change. Damage to muscle fibres causes infiltration by immune cells such as neutrophils and macrophages which

in turn release pro-inflammatory cytokines such as IL-6 and TNF-α (Tidball & Villalta. 2010). There is also significant alteration to the composition of the surrounding ECM after injury, altering the adhesive signals, whilst damage to blood vessels causes vascular endothelial cells to release a number of growth factors, including HGF. This combination of signals promotes SC activation and proliferation (Charge & Rudnicki. 2004).

1.1.8. The basal lamina (basement membrane).

The basal lamina is a thin, highly specialised, mesh-like membrane of ECM which is present in nearly all human tissues (Fig. 1.11). It acts as a semi-permeable barrier between tissues / cells which is able to act as both an adhesive substrate and signalling scaffold (Yamada & Sekiguchi, 2018). In skeletal muscle it surrounds individual muscle fibres and is composed of laminins (primarily laminin-211), collagen IV, nidogen, agrin, biglycan and the heparan sulphate proteoglycan perlecan (Ahmad et al., 2020). Collagen IV is the most abundant component of the basal lamina (Yurchenco & Orear, 1994). It is a helical trimer with three known isoforms composed from a combination of six different α-chains, α1 - α6. The most commonly expressed isoform has two α1 chains and an α2 chain (Sado et al., 1998). Like laminin, a trimeric glycoprotein which is composed of α, β and γ chains (Cheng et al., 1997), collagen IV self-assembles into a sheet like structure which then indirectly associates with laminin via the cross-linking interaction of nidogen and perlecan as shown in fig. 1.11 (Aumailley, 2013; Mouw & Weaver, 2014). Core molecules of the basal lamina are functionally linked to the actin cytoskeleton and directly influence cellular behaviour, affecting intracellular signalling via interaction with various cell-surface receptors, such as integrins (Hynes, 1992). Laminin binding for example, has been shown to influence chromatin remodelling and gene expression (Domogatskaya et al., 2012), thereby inducing changes in myoblast shape, enhancing migration and stimulating proliferation (Ocalan et al., 1988; Timpl & Brown, 1996). The signalling potential of the basal lamina is increased further by its ability to sequester various growth factors (Ishihara et al., 2018; Jayadev & Sherwood, 2017) and modulated further still by the action of ECM-modifying enzymes, such as matrix metalloproteases (MMPs), that are constantly remodelling the ECM composition in response to both intra and extracellular cues (Hirunsai et al., 2015; Kim et al., 2019).

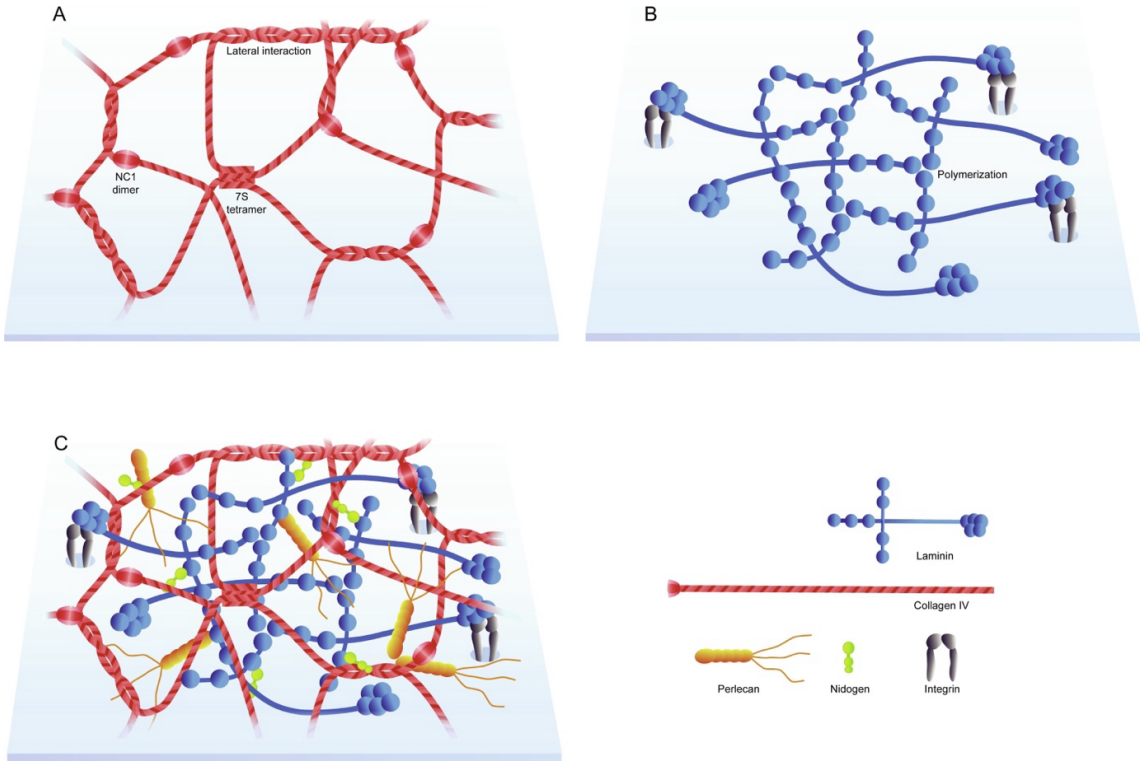


Figure 1.11. Basic structure of the basal lamina. A) Collagen IV network. **B)** Laminin network. **C)** Schematic representation of the basal lamina and its major components. Figure taken from Yamada & Sekiguchi, 2018.

1.2. Integrins.

Integrins are heterodimeric transmembrane glycoproteins consisting of non-covalently associated alpha (α) and beta (β) subunits. They were first described by Richard Hynes in 1976 as “integral membrane proteins” responsible for linking the internal actin cytoskeleton with the ECM component fibronectin (Hynes, 1976). However, it took a further ten years of research to clearly identify the sequence and structure of the first known integrin (Tamkun et al., 1986). Homologues were subsequently quickly identified along with various ligands, revealing a large family of cell surface adhesion proteins responsible for regulating dynamic cell-cell and numerous cell-ECM interactions as shown in figure 1.12 (Barczyk et al., 2010; Hynes, 1987). Ligand binding specificity is governed by their complement of alpha (α) and beta (β) subunits (Fig. 1.12). Although numerous integrins share the same ligand, for instance, eight are known to bind fibronectin and five bind laminins, many have specialised and irreplaceable functions (Sun et al., 2019). The picture is complicated further by the presence of alternative splice variants, each with varying ligands, functions, and downstream consequences upon activation. The β1-subunit is by far the most promiscuous integrin chain,

contributing to 11 known heterodimers, as shown in figure 1.11. In humans there are five main cytoplasmic splice variants, mice however lack all but β1A and β1D (Armulik, 2002). The β1A splice variant is ubiquitously expressed, whereas β1D is specific to cardiac and skeletal muscle (Soto-Ribeiro et al., 2019). The two murine splice variants display non-reciprocal functional compensation, β1A can compensate for the loss of β1D, however, the loss of β1A results in embryonic lethality (Nawrotzki et al., 2003).

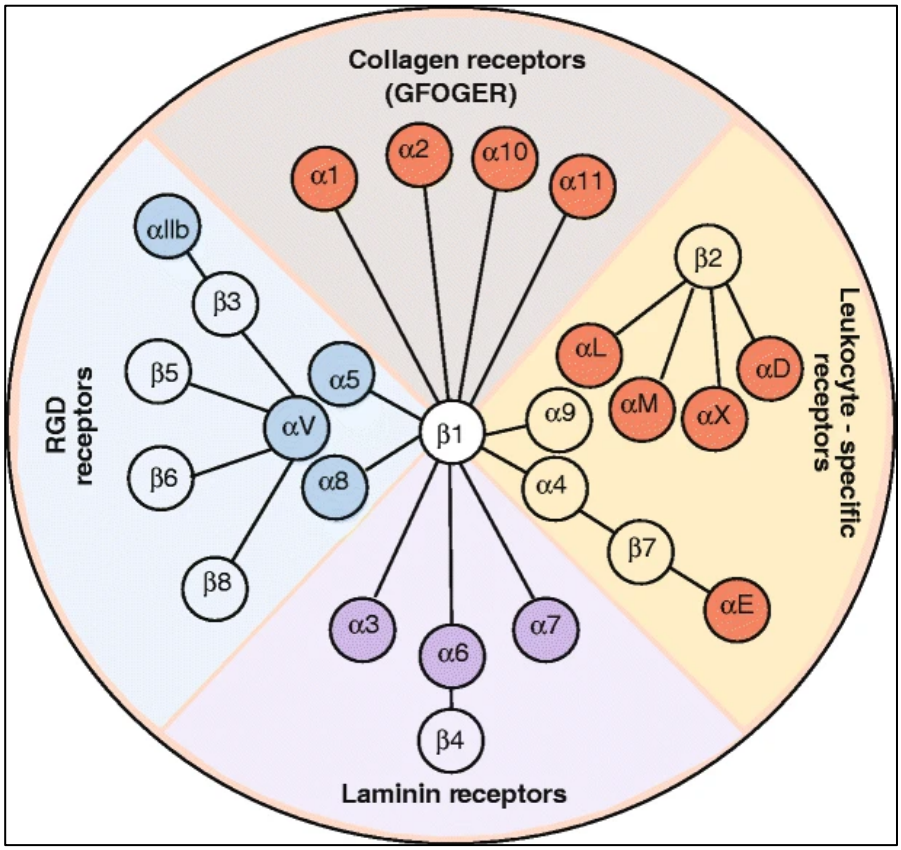


Figure 1.12. Integrin specificity. There are 24 integrin heterodimers found in vertebrates, composed of 18 α and 8 β subunits. They are the primary receptors for ECM components which can be broadly categorised into four groups. Laminin receptors, Collagen receptors, RGD receptors and leukocyte specific receptors. Integrin α5β1 is an RGD receptor for fibronectin, whilst α7β1 is a laminin receptor. Figure taken from Barczyk et al., 2010.

1.2.1 Integrin structure and activation.

The structure of a prototypical integrin consists of a large extracellular domain, responsible for ligand binding, a transmembrane domain and a short cytoplasmic domain which indirectly interacts with the actin cytoskeleton via multi-component protein scaffolds (Giancotti, 2000). The extracellular domain of the α-subunit consists of two calf domains, a thigh domain and a seven bladed β-propellor responsible for ligand binding (Fig. 1.13). Eight of the eighteen α-subunits also possess an additional a-I domain which contains a metal ion dependant adhesion site (MIDAS) (Lee et al., 1995). The extracellular region of the β-subunit also possesses an I-like domain, preceded by four EGF-like folds which terminate with a β sheet prior to the transmembrane domain, as shown in figure 1.13.

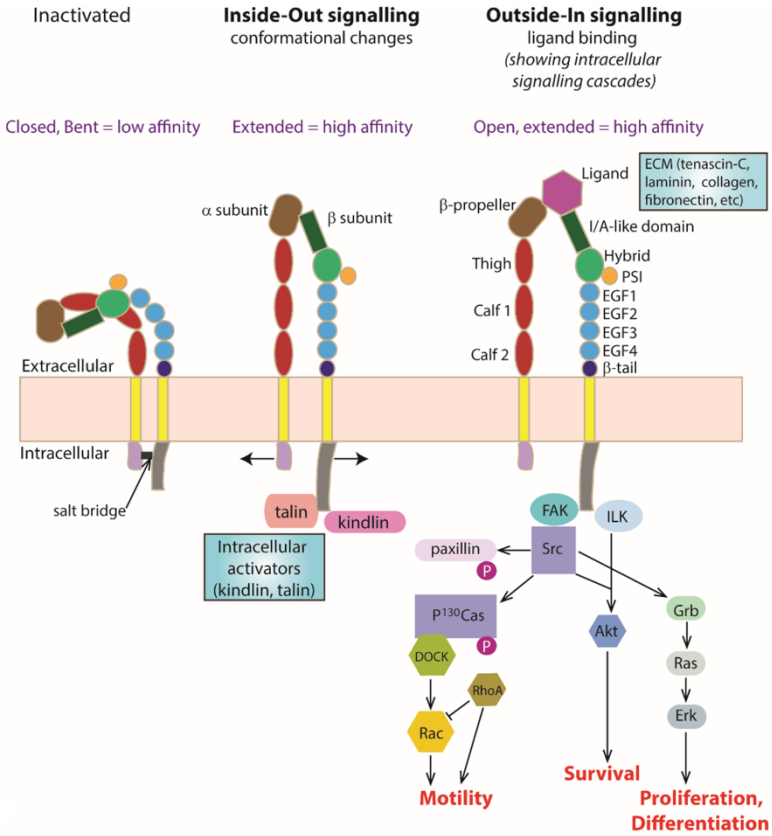


Figure 1.13. Integrin structure and activation. Integrin activation leads to intracellular signalling cascades, resulting in processes such as cell motility, survival and differentiation. Inactivated integrins exists with a closed and bent extracellular conformation with very low ligand binding affinity. With Inside–Out signalling, intracellular activators, such as kindlin and talin, bind the β subunit's cytoplasmic tail leading to an extended (active) conformation with increased ligand binding affinity. With Outside–In signalling, binding of an extracellular ligand, such as fibronectin or laminin, occurs as a result of integrin activation and results an open and extended conformational change with high ligand binding affinity. Figure taken from Cheah & Andrews, 2018.

1.2.2. Integrin signalling.

Although initially described as relatively simple adhesion proteins, today they are seen as complex bi-directional signalling receptors, capable of both 'inside-out' or 'outside-in' signalling, which can modulate different intracellular signalling pathways, thereby contributing to the regulation of many fundamental cellular processes such as migration, proliferation, differentiation and survival (Davies, 2001; Rozo et al., 2016). Recent evidence has also characterised a third mechanism of intracellular integrin signalling, termed 'inside-in' signalling, where integrins transmit signals from endosomes whilst being internalised and recycled away from the cell membrane (Fig. 1.14). Integrins at the cell membrane have been shown to adopt three distinct conformations, with varying affinity for their respective ligands, depending on their activation status; bent closed (inactive low affinity), extended closed (primed – high affinity) and extended open (active – high affinity) (Cheah & Andrews, 2018).

Intracellular stimuli are required to 'activate' integrins and allow the conformational change required for extracellular ligand binding. Prior to activation the α and β subunits are in close proximity, with the receptor assuming a low affinity, bent conformation (Fig.1.13). Inside-out activation and integrin extension is dependent upon the action of talin and kindlin, two adapter proteins which act as scaffolds for interaction with the cytoskeleton and recruitment of downstream signalling affecters (Lu et al., 2022; Moser et al., 2009). Talin and kindlin are recruited to the cytoplasmic tail of the β subunit, which in turn disrupts the salt bridge and close conformation between the α and β subunits, thereby causing partial dissociation and conformational change, resulting in the extension of the extracellular domain, as shown in figure 1.13 (Cheah & Andrews, 2018). Once extended, the ligand binding pocket of the extracellular domain becomes exposed, raising the affinity for its ligand, enabling attachment to the ECM. Post activation, integrins begin to cluster into complexes known as focal adhesions which contribute to the regulation / modulation of numerous intracellular signalling cascades. Ligand binding stimulates further changes in the relationship between the α and β subunits. The subsequent formation of focal adhesions also allows for interaction with a huge number of molecules far beyond that of individual integrin heterodimers, including multiple scaffolding adaptors, G-protein regulators, actin modulators, growth factor receptors, as well as numerous

phosphatases and kinases required for either silencing or activation of downstream signalling cascades (Zamir & Geiger, 2001; Zamir & Geiger, 2001). Integrins possess no intrinsic kinase activity but predominantly rely upon either integrin linked kinase (ILK) or focal adhesion kinase (FAK) to induce the appropriate response to ligand binding. Both ILK and FAK are not only embryonically lethal when absent (Ilic et al., 1995; Sakai et al., 2003), but are also critical to the stability, maintenance, and regeneration of adult skeletal muscle (Graham et al., 2015; Wang et al., 2008), further highlighting the complexity and importance of integrin signalling.

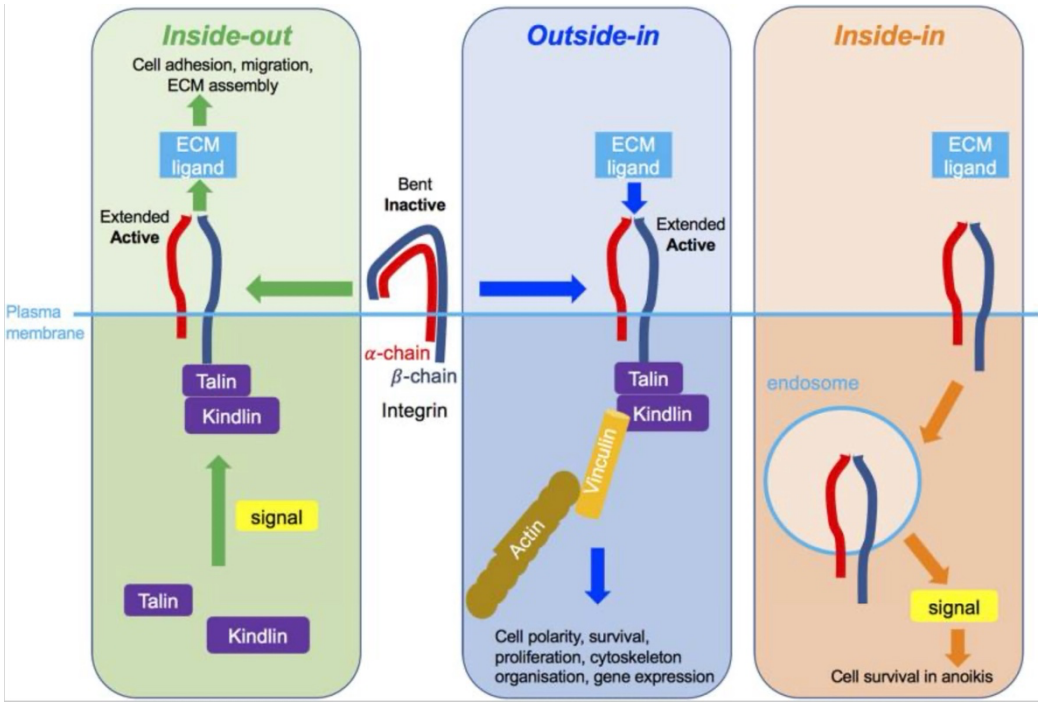


Figure 1.14. Different modes of integrin signalling. Left green box: Inside-out integrin signalling. An intracellular signal triggers the recruitment of key molecules to integrin β1, including talin and kindlin, leading to conformational change, resulting in cell adhesion, migration and/or ECM assembly. Middle blue box: Outside-in integrin signalling. Binding of the ECM leads to the recruitment of several molecules to the cytoplasmic tail of integrin β1, such as talin, kindlin and vinculin, and the connection to the actin cytoskeleton. As a consequence, cell polarity, survival, cytoskeleton organisation or gene expression are promoted. Right organge box: Inside-in signalling, a third mode of integrin signalling, recently described for β1 integrin. The integrin transmits signalling from endosomes. Figure taken from Stanislovas & Kermorgant, 2022.

Beyond their classical role at the plasma membrane, integrins continue to signal following endocytosis through a process termed ‘inside-in’ signalling. After ligand binding and internalisation, integrins are trafficked to early and recycling endosomes, where they remain in an active conformation and act as scaffolds for signalling complexes (De Franceschi et al. 2015). Endosomal integrins have been shown to sustain FAK, Src family kinases, and MAPK/ERK signalling independently of cell adhesion (Alanko et al. 2015; Moreno-Layseca et al. 2019). This compartmentalised signalling regulates cytoskeletal remodelling, cell survival, and migration by allowing integrin-associated adaptors such as talin and kindlin to signal from intracellular membranes (Alanko et al. 2015). In muscle progenitors and satellite cells, integrin trafficking and signalling are particularly important for coordinating responses to mechanical cues, extracellular matrix remodelling, and growth factor signalling during regeneration. Thus, inside-in signalling provides an additional layer of integrin regulation that helps to influence cell fate decisions.

1.2.3. Integrins during skeletal muscle development.

During embryonic and post-natal development, the spatiotemporal expression of numerous integrins and their respective splice variants are tightly orchestrated (Fig.1.15). During primary myogenesis, α4, αv, α5, α6 and α7 are all present and play distinct roles due to the variety of their respective ligands (Fig. 1.12) (Rogers & Mayer, 2006). However, as the musculature develops and matures the profile of integrin expression changes and begins to localise to specific regional structures such as the MTJ or NMJ as shown in figure 1.16. The observable changes in integrin expression that occur throughout development unsurprisingly coincide with distinct changes in the composition of the ECM and basement membranes that occur throughout embryogenesis and postnatal development. During early embryogenesis and primary myogenesis basement membranes contain much higher levels of fibronectin. Postnatally, during secondary myogenesis, the fibronectin found within basement membranes is gradually replaced by laminin (Kuhl et al., 1986). It is unclear if the switch in basement membrane composition is responsible for the altered integrin expression pattern or if the reduction in integrin α5 expression results in the loss of fibronectin.

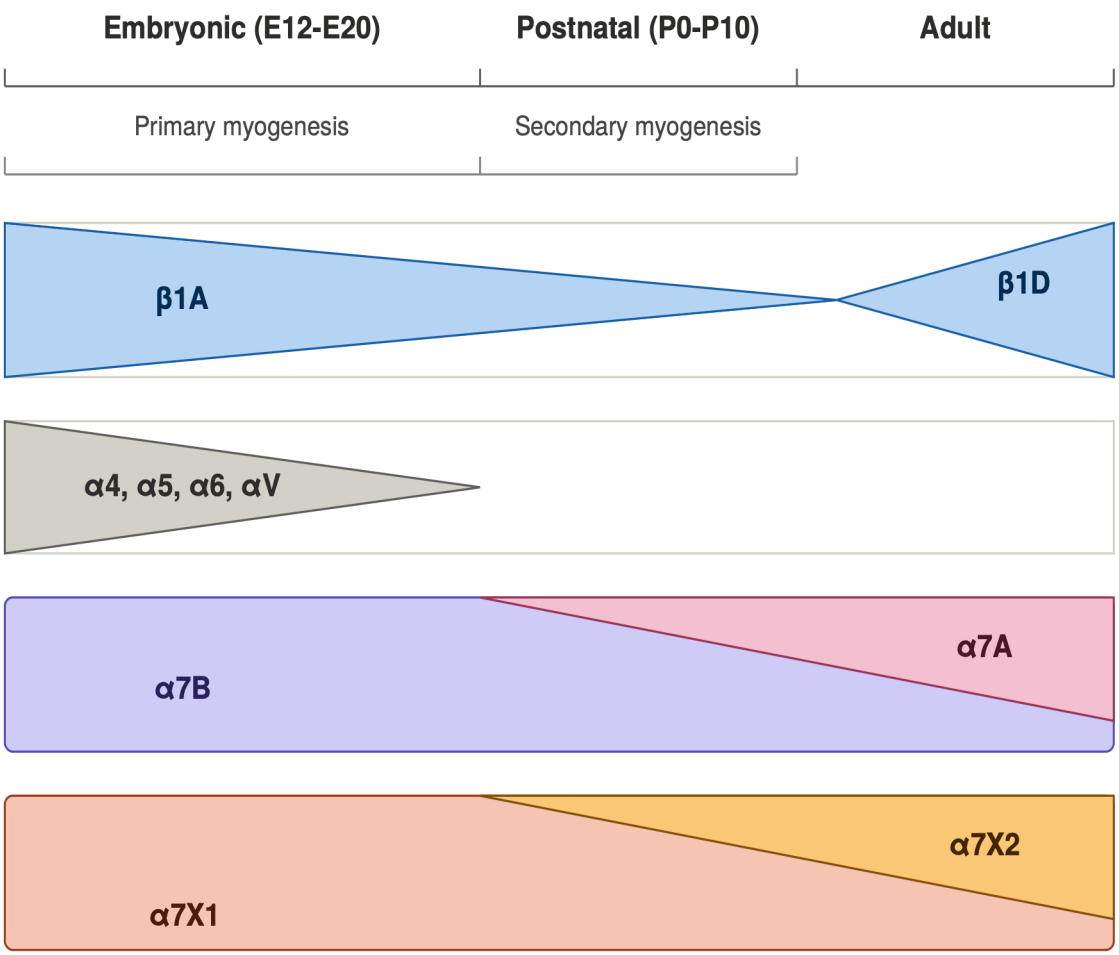


Figure 1.15. Summary of integrin expression during primary, secondary and adult myogenesis. Integrins $\alpha 4$, αv, $\alpha 5$, $\alpha 6$ and $\alpha 7$ are all expressed during primary myogenesis. However, the expression of $\alpha 4$, αv, $\alpha 5$, $\alpha 6$ declines concomitantly with an increase in $\alpha 7$ until it is the predominant integrin in adult tissue. There is also a switch in $\alpha 7$ and β1 splice variants between primary, secondary, and adult myogenesis. Figure modified from Rogers & Mayer, 2006

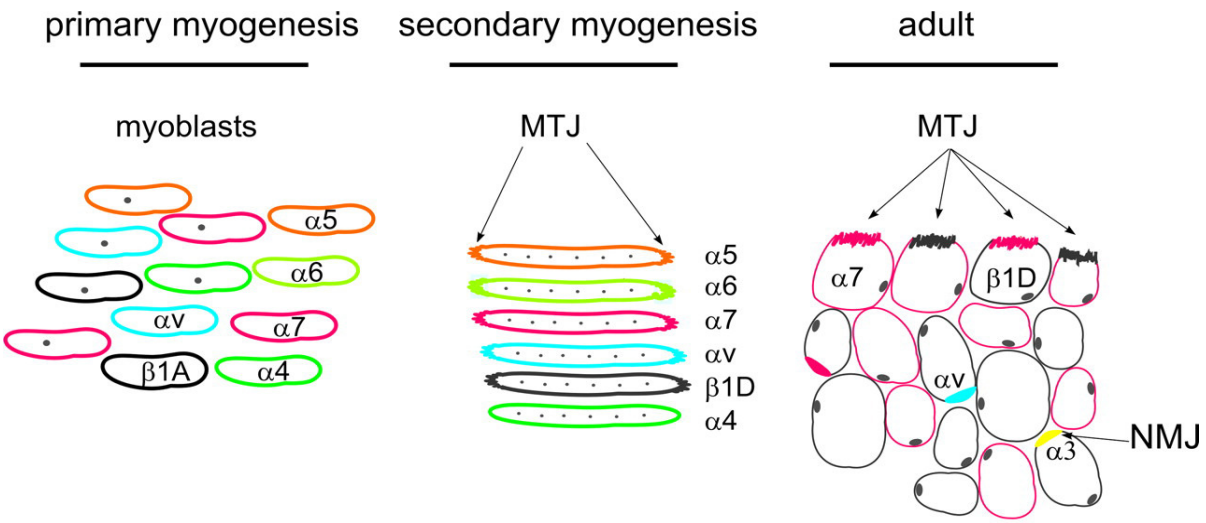


Figure 1.16. Schematic representation of integrin location during muscle development in mice. Migrating myoblasts express integrins α4, αv, α5, α6 and α7 and β1A. During secondary myogenesis β1A is replaced with β1D. In adult musculature only α7β1D is expressed at the MTJ whereas αv and α3 are expressed at the NMJ. Figure taken from Mayer, 2003.

1.2.4. Integrin α7.

Integrin α7β1 is the predominant integrin receptor found in adult skeletal muscle and a canonical marker of both quiescent and activated SCs (Gnocchi et al. 2009). It is also expressed in cardiac muscle, vascular smooth muscle, and a few specialised cell types such as Schwann cells. Although not essential for myogenesis to occur, it has previously been shown to play an important role in the differentiation and migration of myoblasts (Mayer, 2003). In mice, its absence results in altered mendelian ratios due to reduced numbers of live births, distorted muscle fibre morphology and a novel form of progressive muscular dystrophy. Distal regions of muscle fibres are deformed (Fig.1.17 B), MTJ integrity is reduced (Fig. 1.17 D) and the organisation of collagen fibrils at the sarcomere becomes distorted (Fig. 1.17 F) (Mayer et al., 1997; Nawrotzki et al., 2003). The reduced numbers of live births observed in integrin α7 KO mice have been attributed to reduced vasculogenesis and cerebral haemorrhaging in some, but not all, α7 null embryos (Flintoff-Dye et al., 2005). In humans, mutations within the α7 gene (*ITGA7*) presents as a novel form of congenital myopathy (Hayashi et al., 1998).

ITGA7 is located on chromosome 12 in humans but found on chromosome 10 in mice. It is made up from 27 exons which contribute to the four major developmentally regulated splice variants (Fig. 1.18). The extracellular X1 and X2

variants are composed from 1042 and 1038 amino acids respectively, displaying alterations to their ligand-binding regions, resulting in preferential binding to specific laminin isoforms (Von der Mark et al., 2001). The A and B variants contain 57 and 76 amino acids respectively, resulting in significant changes to their cytoplasmic tails (Ziober et al., 1993), possibly indicating differences in downstream intracellular signalling capabilities. Unlike the cytoplasmic variants, only the X2 extracellular variant is expressed in adult skeletal muscle (Von der Mark et al., 2001).

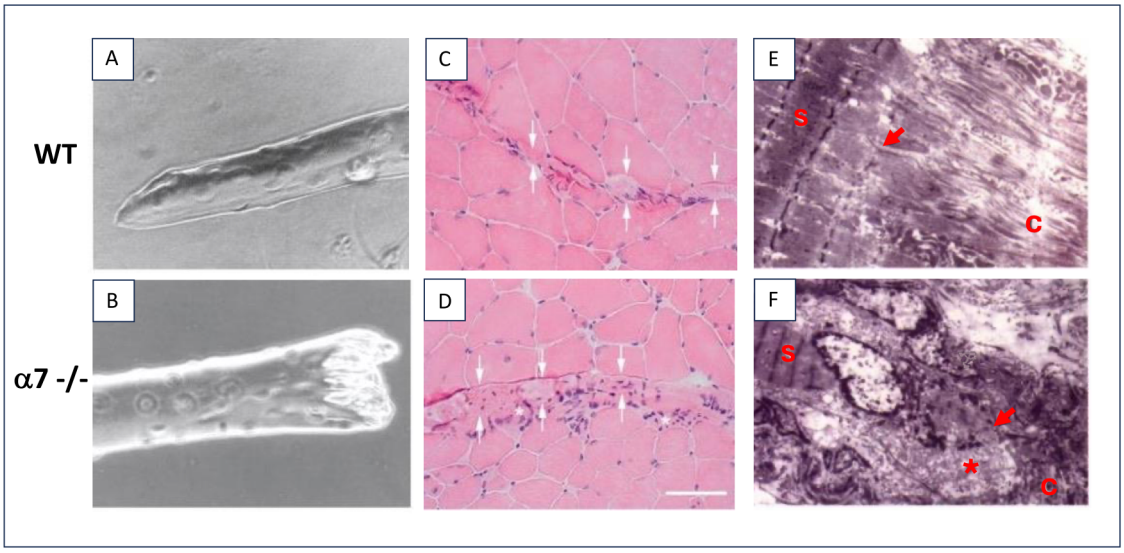


Figure 1.17. Pathological changes observed in muscle of integrin α7 KO mice. (A & B) Phase contrast images of isolated interosseus muscle. Distal regions of *Itga7 -/-* fibres display altered morphology with deformed ends. **(C & D)** Hematoxylin and eosin staining of transverse cryosections taken from the TA muscle. *Itga7 -/-* muscle shows varying fibre diameter, increased presence of centrally nucleated fibres around the MTJ (arrows) and lymphocyte infiltration. Asterisks highlight necrotic fibres. **(E & F)** Electron micrographs of MTJs. Integrin α7 KO mice lack the organised interdigitation of muscle into collagen fibrils (C) from the tendon. The sarcomere (S) is distorted, and basement membrane (arrow) thickened compared to WT, and degenerated cytoplasm is marked (*). Figure modifed from Mayer et al., 1997; Nawrotzki et al. 2003.

Integrin α7β1 is concentrated at the MTJ but can also be detected at neuromuscular junctions (NMJs) and along the length of the sarcolemma (Von der Mark et al., 2001). It acts as a mechanosensor, responding to the transmission of transverse and longitudinal forces between adjoining muscle fibres and from the muscle to tendon at the MTJ, helping to protect the muscle from contraction induced injury. In adult skeletal muscle it acts as a complimentary laminin receptor to the DGC. Mdx mice, which contain a mutation within the *Dmd* gene affecting the DGC, have long been used as a mouse model for Duchenne muscular

dystrophy (DMD). Although mdx mice do not fully recapitulate pathological progression or clinical severity as human DMD patients, double mutant mice lacking both dystrophin and either utrophin (utr), a dystrophin homologue, or integrin α7 do share pathological similarities with human DMD patients. These models demonstrate rapid postnatal muscle fibre degeneration (Burkin et al., 2001; Guo et al., 2006), highlighting the importance of compensatory interactions between the DGC and integrin mediated adhesion in maintaining muscle integrity. Furthermore, Rooney et al., (2009) demonstrated that intramuscular injection of laminin 111, which is normally only expressed during primary and secondary myogenesis, restored muscle regeneration after acute injury in *Itga7 -/-* mice (Rooney et al., 2009). Together, these findings highlight the importance of laminin–integrin α7 interactions in muscle homeostasis and regeneration, leading to extensive previous research due to its potential to compensate for the loss of dystrophin when affected by mutations in the *DMD* gene (Burkin et al., 2001; Divekar. & Mayer., 2014; Heller et al., 2013). However, these previous studies have produced conflicting results as to the efficacy of integrin α7 as a therapeutic target to treat DMD. Although Burkin et al., (2001) rescued the phenotype of mdx/utr -/- mice via transgenic overexpression of integrin α7X2B, a more recent unpublished study from 2014 contradicted these results, observing no difference in the quantity of centrally nucleated fibres, even when each of the *Itga7* splice variants were over expressed in mdx mice. Therefore, concluding that over expression of any integrin α7 splice variant offers no protection against DMD (Divekar. & Mayer., 2014). A possible explanation for the difference observed between the two studies is the differences in their experimental models. Whereas Burkin et al. used the muscle creatine kinase (MCK) promoter to drive the expression integrin α7X2B, Divekar and colleagues used the human skeletal actin (HSA) promoter which becomes active much earlier in development. Integrin Gene therapy approaches using adeno-associated virus (AAV) mediated gene transfer have also shown some promise, Heller et al., (2013) reported overexpression of integrin α7 at the sarcolemma in mdx mice, which in turn resulted in significant stabilisation of muscle fibres and ameliorated further contraction induced injury.

.

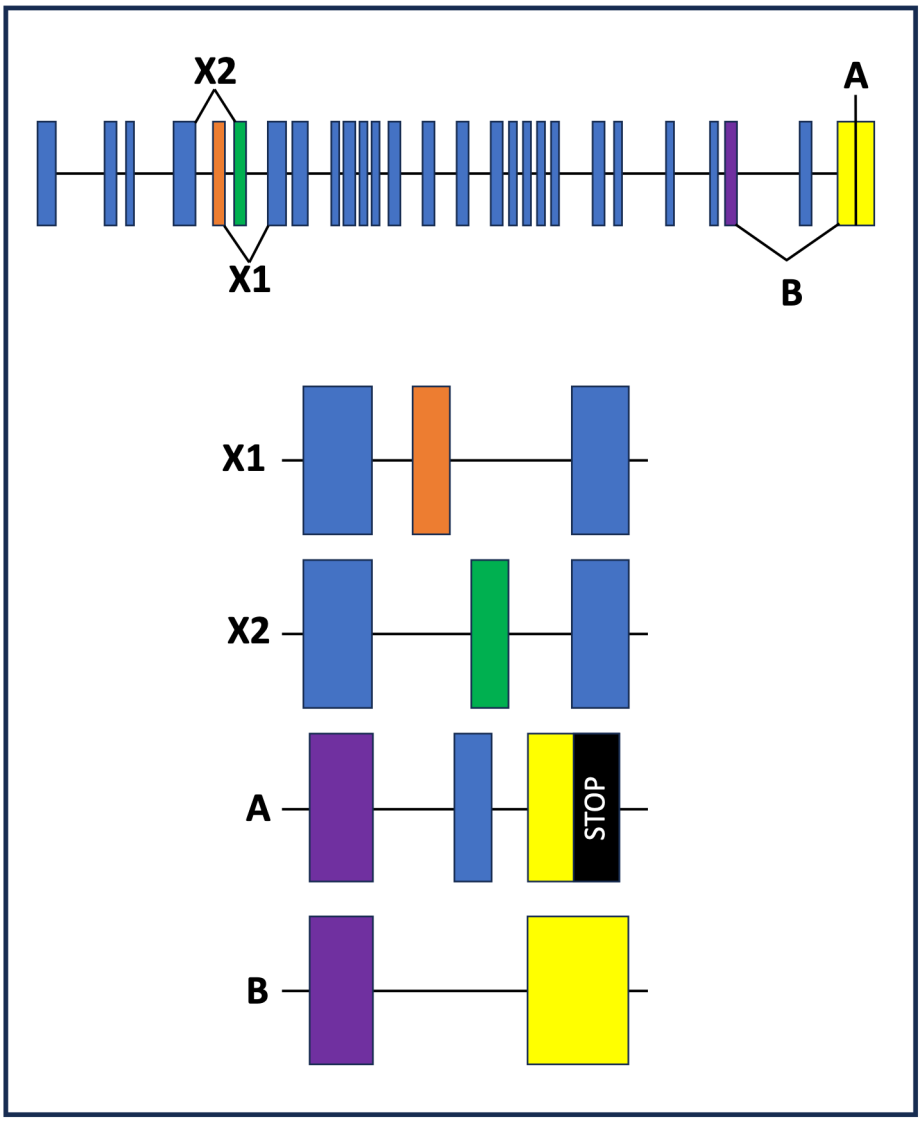


Figure 1.18. Genomic organisation of *ITGA7* and its splice variants. α7X1 contains exons 4, 5 & 7, whereas α7X2 contains 4, 6 & 7. The cytoplasmic A variant has a truncated version of exon 27, whereas the B variant omits exon 26. Figure modified from Vignier et al., 1999.

1.2.5. Integrin α5.

The integrin α5 subunit is 1049 amino acids in length and encoded by the *ITGA5* gene. In humans it is located close to *ITGA7* on chromosome 12, whereas in mice it can be found on chromosome 15. It is not known to undergo any alternative splicing. Integrin α5β1 is an RGD receptor, recognising the RGD (Arg/Gly/Asp) motif within fibronectin. Various other ECM components, including some collagen and laminin isoforms, also contain RGD motifs. However, in most cases they are concealed and do not present as ligands until denaturation or proteolytic cleavage occurs. Proteolytic cleavage of ECM components can generate protein fragments with novel biological functions. Endostatin for

example, a 20 kDa C-terminal fragment of collagen XVIII, can in some contexts act as an alternative ligand for integrin a5β1 (Barczyk et al., 2010). Embryonic cell migration and developmental myogenesis is dependent upon Integrin α5β1, and mutations within *Itga5* have been shown to be embryonically lethal (Yang et al., 1993).

Due to the lethality observed in α5 null embryos, traditional KO approaches could not elucidate the role of integrin α5β1 during the later stages of embryogenesis or in adult tissues. To circumvent this and allow for further studies, mice with chimeric expression of *Itga5* were initially generated (Taverna et al., 1998), then subsequently, tissue specific conditional KOs utilising Cre/Lox techniques. In vitro studies revealed that both α5 null embryonic stem cells (ES) and α5 null myoblasts could differentiate into myotubes, indicating no initial myogenic impairment. However, muscle from adult chimeric α5 -/-;+/+ mice displayed many of the hallmarks associated with muscular dystrophy (Taverna et al., 1998). Taken together, these results suggest that although integrin α5β1 is not required for either primary or secondary myogenesis, it is required for the long-term stability of myotubes and myofibres.

Various studies have reported conflicting results regarding the expression pattern of α5β1 during myogenesis (Enomoto et al., 1993; MacCalman et al., 1992; Steffensen et al., 1992). This could be explained by the different growth requirements of the cell lines used or due to the incomplete isolation of primary cells and the potential presence of integrin α5 expressing fibroblasts in cultures. Blaschuk & Holland (1994) sought to overcome these inconsistencies by using FACS to isolate a homogenous population of human myoblasts which were then analysed to produce a profile of *ITGA5* expression at both mRNA and protein levels. It had been proposed that levels of integrin α5 decrease as myoblasts terminally differentiate (MacCalman et al., 1992), however, Blaschuk & Holland demonstrated that both mRNA and protein levels decreased in response to reduced levels of exogenous growth factors and not necessarily as a direct consequence of terminal differentiation as previously postulated.

1.2.6. Functional association between integrin α5 and α7.

In WT mice, integrin α5 and α7 are both expressed at the MTJ until postnatal day 5 (P5). After this timepoint integrin α5 expression is gradually reduced whilst integrin α7 expression is maintained. By P10 integrin α5 is barely visible at the MTJ having been either displaced or functionally down regulated as direct result of continued expression of integrin α7 (Nawrotzki et al., 2003). In the absence of integrin α7, as demonstrated in integrin α7 KO mice, integrin α5 expression is maintained, and abnormally high levels of fibronectin is recruited to the basement membranes and MTJs of *Itga7 -/-* muscle fibres (Nawrotzki et al., 2003). Immunofluorescence and coimmunoprecipitation experiments revealed the continued presence and interaction of integrin α5 and β1D at the MTJ of integrin α7 KO mice (Nawrotzki et al., 2003 ; Tomatis et al., 1999) demonstrated a functional relationship between integrins α5β1 and α7β1. Integrin α7 was transfected into Chinese hamster ovary (CHO) cells, which in turn reduced integrin α5 expression by 20% - 25% at the cell surface. However, the CHO cells displayed a 70% reduction in fibronectin adhesion and lacked the ability to assemble a fibronectin matrix (Tomatis et al., 1999), thereby demonstrating that integrin α7 negatively regulates both the expression and function of integrin α5.

1.3. Aims.

The aim of this investigation is to uncover the contribution of integrins α5 and α7 to SC function in adult mice, and in turn, how they contribute to maintenance and repair of adult skeletal muscle.

Chapter 3: To investigate the roles of integrins α5 and α7 in adult skeletal muscle regeneration after an acute injury.

Chapter 4: To investigate how the loss of integrins α5 and / or α7 affects SC migration and proliferation.

Chapter 5: To investigate how the loss of integrins α5 and / or α7 affects SC differentiation..

Chapter 2.

Materials & Methods.

2.1. Mouse lines.

The mice used in this study were generated by Prof. U. Mayer and her team prior to the start of this project. Breeding strategies ensured that a constitutive α7 KO (Mayer. 1997), conditional α5 KO (Van der Flier et al. 2010), and double α5 /α7 KO (DKO) were maintained on a 129Sv background in order to study the role of these integrins in adult muscle regeneration, SC activation, differentiation and self-renewal. Male and female mice were used aged between 12 – 16 weeks.

2.1.1 Constitutive integrin α7 KO.

The constitutive integrin $\alpha7^{-/-}$ mouse was originally generated by replacing 1 kb of genomic sequence within *Itga7* with a phosphoglycerate-kinase-neomycin (PGK-neo) cassette by homologous recombination in embryonic stem (ES) cells, as shown in figure 2.1. The targeted region included part of exon 1 that encodes the signal sequence and first 107 bp of mature protein, thereby disrupting all known splice variants. Heterozygous ES cells were then transplanted into pseudopregnant females to produce chimeric founder mice, which were subsequently bred to produce α7-/- mice.

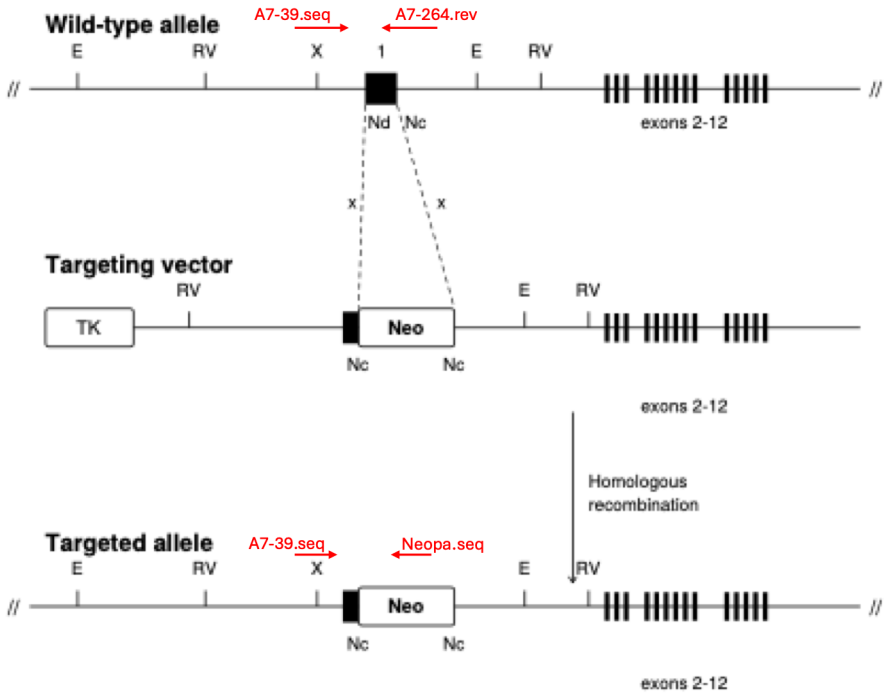


Figure 2.1. Targeted disruption of *Itga7*. Genomic organisation of the 5' terminal region of *Itga7* (top), the targeting vector (middle), the modified allele after homologous recombination (bottom). PCR genotyping primers are shown in red. Primer sequences and expected fragment sizes are shown in table 2.3. Figure modified from Mayer. 1997.

2.1.2. Conditional integrin α5 KO.

The α5 cKO has exon 1 of *Itga5* flanked by lox P sites, as shown in figure 2.2. Homozygous *Itga5* floxed mice (*Itga5*$^{fl/fl}$) were crossed with *Pax7*$^{CreERT2/+}$ mice (Lepper et al., 2011) to generate F1 *Itga5*$^{fl/+}$//*Pax7*$^{CreERT2/+}$ which express a Cre recombinase - ERT2 fusion protein under the control of the endogenous *Pax7* promoter. Subsequent selective breeding strategies were used to generate and maintain *Itga5*$^{fl/fl}$//*Pax7*$^{CreERT2/+}$ mice, ensuring *Itga5* could be inducibly ablated in SCs whilst mice remained heterozygous for *Pax7* expression. Cre-mediated recombination of the lox P sites, excision of exon 1 and disruption of *Itga5* was induced by a series of intraperitoneal (IP) injections of tamoxifen, administered at a dose of 3 mg / 40 g body weight as shown in figure 3.1.

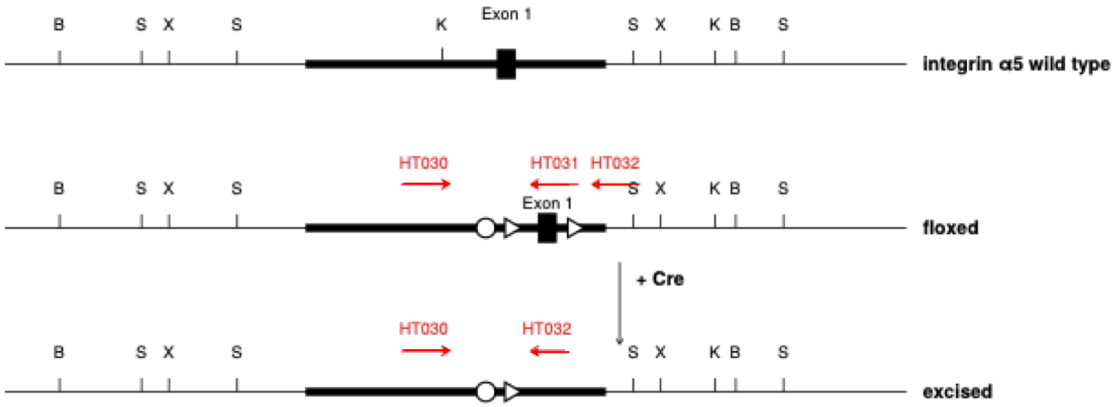


Figure 2.2. Inducible targeted inactivation of *Itga5*. Genomic organisation of 5' terminal region of *Itga5* (top), lox P flanked exon 1 (middle), Cre-mediated excision of exon 1 (bottom). PCR genotyping primers are shown in red. Primer sequences and expected fragment sizes are shown in table 2.3. Figure modified from Van der Flier et al. 2010.

2.1.3. DKO mice.

Selective crossing of the constitutive and conditional integrin KO mice with *Pax7*$^{CreERT2/+}$ mice generated the desired *Itga7*$^{-/-}$//*Itga5*$^{fl/fl}$//*Pax7*$^{CreERT2/+}$ inducible DKO experimental mice, as shown in figure 2.3. Given the reduced number of live *Itga7*$^{-/-}$ births and the complex breeding strategy required, only 1 – 3% of births resulted in the desired *Itga7*$^{-/-}$//*Itga5*$^{fl/fl}$//*Pax7*$^{CreERT2/+}$ genotype.

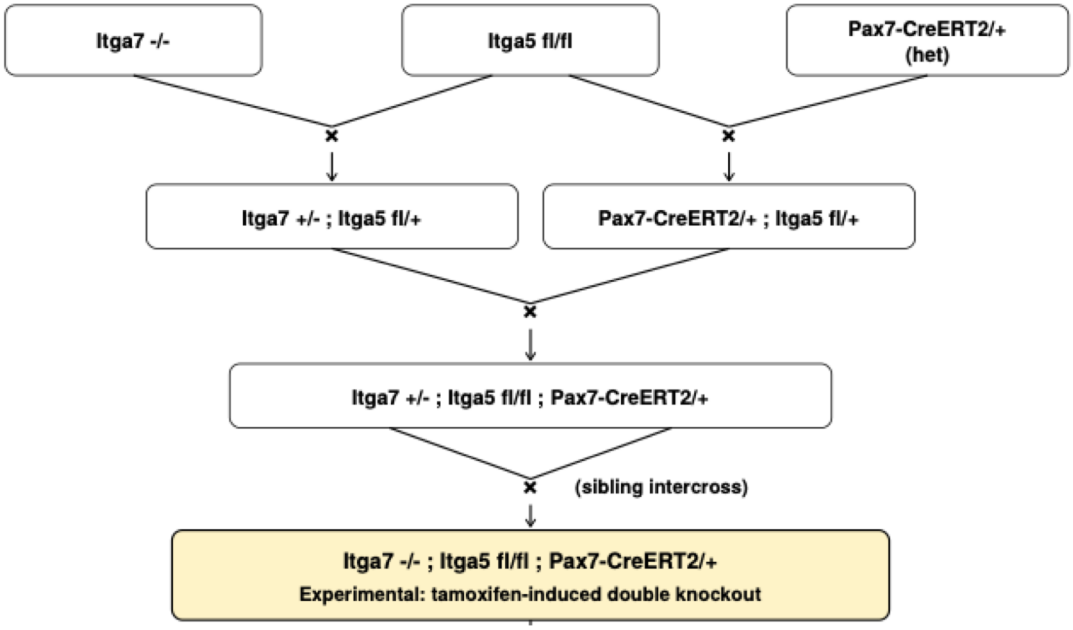


Figure 2.3. Breeding strategy for DKO mice. Schematic diagram of a three-generation breeding scheme used to combine *Itga7*$^{-/-}$ mice and *Itga5*$^{fl/fl}$ mice with the Pax7-CreERT2 driver to generate tamoxifen inducible DKO mice.

2.1.4. Ai14 Rosa26-stop-flox-tdTomato reporter mice.

To visualise and track SCs all previously described strains were crossed with the Ai14 reporter line (Jackson laboratory: B6.Cg(ROSA)26Sor$^{tm14(CAG-tdTomato)Hza}$/J). These mice contain a lox P flanked stop codon, preceding the cDNA of the red fluorescent protein tdTomato (tdT), inserted into the Rosa26 locus, as shown in figure 2.4. Tamoxifen induced Cre-mediated recombination of the lox P sites via IP tamoxifen injections allows for the expression of the tdT exclusively in SCs.

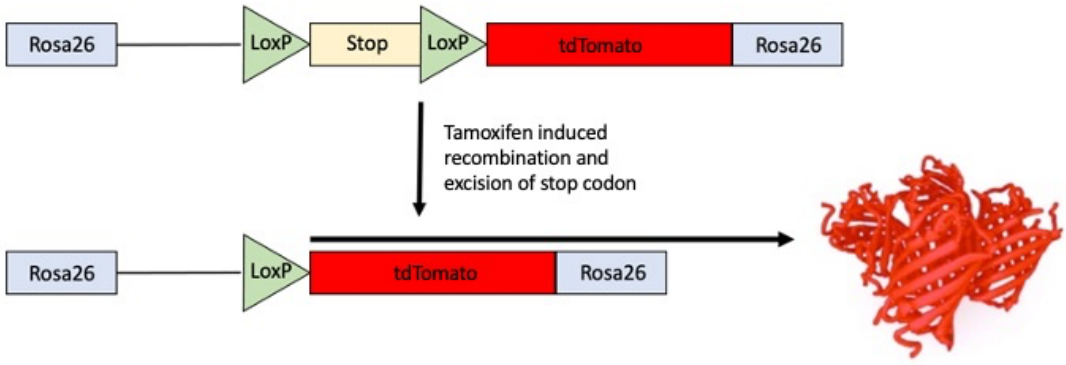


Figure 2.4. Cre / Lox mechanism of SC fluorescent labelling. LoxP sites flank the genomic region to be excised, in this case a stop codon preceding the tdT transgene inserted into the Rosa26 locus. Tamoxifen injections induce the recombination of LoxP sites through the action of Cre recombinase resulting in the excision of the stop codon thereby allowing for transcription and subsequent translation.

2.1.5. Animal maintenance.

All mice were housed in individually ventilated cages in the Disease Modelling Unit (DMU) at the University of East Anglia. Experimental procedures were performed in accordance with the Animal (Scientific Procedures) Act 1986 (ASPA). Mice were ear notched prior to weaning, at post-natal day 20 (P20), for identification and genotyping. Experimental animals were separated by gender, then sacrificed at the desired time point by exposure to gradually increasing CO2 concentrations and cervical dislocation, according to home office schedule 1 protocol.

2.2. Molecular biology techniques.

2.2.1 PCR genotyping.

Ear punches were taken from each of the mice and 50 μl of proteinase K lysis buffer (table 2.1) added to each. The punches were lysed overnight at 55 ^{o}C prior to being diluted 1:10 with distilled H_2O. Each sample was then added to a PCR tube containing the mastermix shown in table 2.2, using the primers described in table 2.3 and thoroughly mixed before loading onto the thermal cycler (Applied Biosystems Veriti) and running on the programmes outlined in tables 2.4 & 2.5.

Table 2.1. Composition of proteinase K lysis buffer.

Reagent	Composition
Proteinase K lysis buffer	0.1 M Tris/HCL, 0.2 M NaCL, 0.2% (w/v) SDS, 5 mM EDTA, 0.1 mg/mL proteinase K.

Table 2.2. Mastermix for PCR genotyping reactions.

Genotype	Primers 20 pmoles/μl (μl)	10X Buffer (μl)	dNTPs 25 mM (μl)	Taq polymerase (μl)	H_2O (μl)	Sample (μl)	Total (μl)
α7	1	5.0	0.5	2.5	38.0	3.0	50
α5	1	5.0	0.5	2.0	38.5	3.0	50
Cre	1	5.0	0.5	2.0	38.5	3.0	50
tdTomato	1	5.0	0.5	2.0	38.5	3.0	50

Table 2.3. PCR primers used to confirm the predicted genotype.

Genotype	Primer	Sequence	Products
α7	A7-39.seq	GAGGGGTGCTGAGGTGAAAG	WT – 230 bp
	A7-264.rev	GCCGGTGGTAAGAACAGTCC	KO – 450 bp
	Neopa.seq	CTGCTCTTTACTGAAGGCTC	
α5	HT030-dwn	GCAGGATTTTACTCTGTGGGC	WT– 692 bp
	HT031-up	TCCTCTGGCGTCCGCCCAA	Floxed – 821 bp
	HT032-up	GAGGTTCTTCCACTGCCTCCTA	Excised – 500 bp
Cre	Cre-UM 15B.rev	GACGGAAATCCATCGCTCGACCAG	Cre +ve – 600 bp
	Cre-UM 19B.seq	GACATGTTCAGGGATCGCCAGGCG	
tdTomato	oIMR9020	AAGGGAGCTGCAGTGGAGTA	WT – 297 bp
	oIMR9021	CCGAAAATCTGTGGGAAGTC	Modified – 197 bp
	oIMR9103	GGCATTAAAGCAGCGTATCC	
	oIMR9105	CTGTTCCTGTACGGCATGG	

Table 2.4. PCR programme for integrin α5.

Stage	Temperature (^{0}C)	Time (S)
1	95	300
2 (x 35 cycles)	95	30
	60	90
	72	60
3	72	600
	4	Hold

Table 2.5. PCR programme for integrin α7, Cre and tdTomato.

Stage	Temperature (^{0}C)	Time (S)
1	95	600
2 (x 10 cycles)	95	45
	65 (minus one degree with each cycle)	60
	72	60
3 (x 25 cycles)	95	45
	55	60
	72	60
4	72	600
	4	Hold

2.2.2. Agarose gel electrophoresis.

Each PCR product had 10 μl of 5X orange G loading dye (table 2.6) added prior to loading into a 2 % (w/v) agarose gel. Gels were run in 1X TAE buffer (table 2.6) at 150V for approximately 40 mins then transferred into 0.5 μg/ml solution of ethidium bromide for 30 mins. Amplicons were then visualised and imaged in a UV trans-illuminator (BIO-RAD).

Table 2.6. Composition of gel electrophoresis reagents.

Reagent	Composition
5X orange G loading dye	50% (v/v) Glycerol, 1X TAE buffer, 0.5% (w/v) Organge G powder.
50X TAE buffer	2 M Tris, 0.05 M EDTA, 1 M Glacial acetic acid.

2.3. Cardiotoxin (CTX) induced muscle injury.

The right tibialis (TA) was injected along its whole length with 50 μl of 10 μM CTX solution (Latoxan) under isoflurane anaesthesia, as demonstrated by Guardiola et al., 2017. The left TA was left as an uninjured control. Muscle regeneration was then allowed to take place for either 10 or 30 days prior to dissection, fixation and further analysis.

Cardiotoxin works by destabilising lipid membranes, creating pores and causing a massive influx of calcium ions which induces metabolic overload and severe hyper contraction of the muscle fibre resulting in acute injury (Fu et al., 2023)

2.4. Dissection of mice hindlimbs

2.4.1. Tibialis anterior (TA) – regeneration experiments.

Post-tamoxifen regime, outlined in chapter 3, mice were sacrificed according to Schedule 1 protocols. The skin on each hindlimb was carefully removed to expose the underlying musculature prior to the removal of the TA along with the associated tendon. Dissection pins were then used to stretch and fix the muscle to parafilm, to avoid contraction, ready for downstream processing.

2.4.2. Extensor digitorum longus (EDL) - individual myofibre isolation.

Dissection proceeded as above, the removal of the TA exposes the underlying EDL which can then be carefully removed. Care was taken to maintain both superior and inferior tendons of the EDL to ensure the muscle is not injured. Each muscle was placed into individual 15 ml falcon tubes and incubated at 37^{o}C in 2 mg/ml CLS-1 collagenase type-1 (Worthington) for 90 minutes with constant agitation. After incubation, each muscle was removed and placed into a 5 cm culture dish, coated with 1% (w/v) bovine serum albumin (BSA), containing 5 ml of DMEM containing GlutaMAX and high glucose (Gibco) + 1% PenStrep .(Gibco). Muscles were then triturated through descending diameter glass Pasteur pipettes to allow dissociation of individual muscle fibres. Individual fibres were collected using a capillary tube and mouth pipette and transferred to appropriate culture media depending on downstream application (detailed in section 2.6). Once cultured for the desired time, fibres were collected into 1.5 ml Eppendorf tubes and fixed in 4% PFA for 10 mins at 37^{o}C, followed by 3X PBS washes and then stored at 4^{o}C.

2.5. Histology.

2.5.1 Tissue fixation.

The TAs excised from mice which expressed tdT were fixed in 2% paraformaldehyde (PFA), prior to freezing in liquid nitrogen cooled isopentane. Whereas muscles taken from mice lacking tdT were frozen directly after dissection and stored at -80^{o} C. PFA fixed muscles were submerged in 2% PFA for a minimum of 5 hours with constant agitation prior to overnight washing in phosphate buffered saline (PBS), then treated with 5% sucrose in PBS for 2 hours followed by 20% sucrose in PBS for a further 2 hours before freezing in liquid nitrogen cooled isopentane.

Table 2.7. Composition of fixation reagents.

Reagent	Composition
10X PBS (pH 7.4)	1.37 M NaCl, 27 mM KCl, 100 mM Na_2HPO_4, 18 mM KH_2PO_4, 5 mM $MgCl_2$.6H2O
2% PFA	2 % PFA (w/v), 1X PBS
Glyoxal (pH 5)	685 mM Glyoxal, 125 mM acetic acid, 3.4 M ethanol

2.5.2. TESPA (3-aminopropyl-triethoxysilane) slide coating.

TESPA coating applies a positive charge to microscope slides, thereby ensuring firm adhesion of biological samples. Slides were immersed in a sequence of reagents and coated with TESPA (Sigma) as described in table 2.8, then left to dry overnight at 37 ^{o}C before being re-boxed and stored at RT.

Table 2.8. Timing of sequential immersions for TESPA coating.

Reagent	Immersion time
Acetone	30 seconds
2.5 % TESPA in acetone	1 minute
Acetone	3 seconds
Acetone	3 seconds
ddH_2O	3 seconds

2.5.3. Cryosectioning.

After dissection and, where applicable, fixation frozen TAs were cut across the belly (widest region) and mounted onto the specimen chuck with OCT. The sample temperature and cryostat chamber were maintained at -24 ºC whilst the blade was kept at -26 ºC. Transverse 10 μm sections were cut and transferred onto TESPA-coated slides, air dried for at least 60 mins and stored at -80 ºC.

2.5.4. Hematoxylin and Eosin (H&E) staining.

Mayer's hematoxylin (Merck) was diluted 1:1 in dH_2O and passed through filter paper, whilst a premixed 0.5% eosin Y solution (Leica) had 0.01% of acetic acid added to increase staining contrast. Slides were defrosted and placed into PBS for ~10 mins. Once the sections were fully rehydrated, slides were placed into the Mayer's haematoxylin solution, before undergoing 'blueing' in running tap water, followed staining in 0.5% eosin Y. Slides were washed quickly in tap water before being dehydrated with washes of gradually increasing concentrations of ethanol (timings are shown in table 2.9). Once fully dehydrated in absolute ethanol slides were cleared with two washes in Histoclear 2 (National Diagnostics), prior to mounting with DPX (ThermoFisher).

Table 2.9. H&E protocol.

Reagent	Time
PBS	10 minutes
Mayer's hematoxylin	5 minutes
Running tap water	10 – 15 minutes
0.5% eosin Y	75 Seconds
Tap water	30 seconds
50% ethanol	15 seconds
70% ethanol	15 seconds
80% ethanol	15 seconds
95% ethanol	15 seconds
95% ethanol	15 seconds
100% ethanol	30 seconds
100% ethanol	1 minute
Histoclear	7 minutes
Histoclear	7 minutes

2.5.5 Immunofluorescence on muscle sections.

Slides were allowed to defrost for 5 min before each section was drawn round with a PAP pen, creating a hydrophobic barrier. Sections were then rehydrated in PBS. Where previously unfixed, sections were fixed for 10 mins in 1% paraformaldehyde (PFA), rinsed in PBS then postfixed for 8 mins in methanol at -20 ^{o}C before a final rinse in tris-buffered saline + 0.1% tween 20 (TBST). After blocking with a 5% normal goat serum (NGS) in TBST solution in a humidified chamber at 37 ^{o}C for 60 mins, 50 μl of primary antibodies (table 2.11) in 2% NGS in TBST were added to the first three sections and incubated for either 60 mins at 37 ^{o}C or overnight at 4 ^{o}C. As a negative control, the fourth section on each slide was treated with 2% NGS in TBST lacking the primary antibodies. Slides were then washed three times for 5 mins in TBST, with rocking, prior to adding 50 μl of secondary antibodies (table 2.12) in 2% NGS in TBST + DAPI (0.5 μg/ml) to each section and incubating at room temperature for 60 mins. After washing twice in TBST and once in TBS for 5 mins, sections were mounted in Gelvatol (Sigma), heated to 37 ^{o}C, and stored at 4 ^{o}C prior to imaging.

2.5.6. Immunofluorescence on muscle fibres.

Fibres were permeabilised with 0.5% Triton in TBS at RT for 10 minutes, washed with TBS, then blocked with 10% NGS in TBST at 37 ^{o}C for 2 hrs. Blocking solution was removed and replaced with primary antibodies (table 2.11) in 5% NGS in TBST and incubated overnight at 4 ^{o}C. Following 3 X 15-minute washes in TBST, fibres were incubated in secondary antibodies (table 2.12) in 5% NGS in TBST + DAPI (0.5 μg/ml) for 1 hr at RT. Fibres were then washed twice in TBST for 15 minutes, once in TBS for 15 minutes, then mounted onto slides with Gelvatol and coverslips and left to dry overnight prior to imaging.

Table 2.10. Composition of immunofluorescence reagents.

Reagent	**Composition**
10X TBS (pH 7.4)	1.5 M NaCl, 0.5 M Tris.
TBST	100 ml 10X TBS, 899 ml dH_2O, 1 ml tween-20.
Gelvatol	80 ml 0.01 M KH_2PO_4 (pH 7.2), 0.65 g NaCl, 40 ml glycerin (Sigma), 20 g polyvinylalcohol (Gelvatol, type II, Sigma)

Table 2.11. Primary antibodies.

Target	Primary antibody	Source	Dilution	Manufacturer
Integrin α7B	U31+	Rabbit	1:400	In-house
Integrin α5	CD49e	Rat	1:100	Pharmingen (5S3319)
Integrin β1	U49+	Rabbit	1:400	In-house
Nidogen	U13+	Rabbit	1:800	In-house
Laminin α2	LNα2	Rat	1:20	In-house
Fibronectin	FN2	Rabbit	1:200	In-house
Myf5	Myf5	Rabbit	1:50	Santa Cruz (SC-302)
MyoD	MyoD	Mouse	1:50	Santa Cruz (SC-377460)
MyoD	MyoD	Rabbit	1:50	Santa Cruz (SC-377463)
Myogenin	MyoG	Mouse	1:100	DSHB (AB2146602)
Pax7	Pax7	Mouse	1:10	DSHB (AB528428)
α-smooth muscle actin	α-SMA -Cy3	Mouse	1:400	Sigma (C-6198)
Basement membrane	WGA-488	Wheat	1:200	Invitrogen (W11261)

Table 2.12. Secondary antibodies + DAPI.

Antibody / Nuclear stain	Dilution	Manufacturer
Goat anti-rabbit Cy2	1:200	Jacksons
Goat anti-rabbit Cy3	1:400	Jacksons
Goat anti-mouse Cy2 F(ab')$_2$	1:200	Jacksons
Goat anti-mouse Cy3 F(ab')$_2$	1:400	Jacksons
Goat anti-rabbit Alexa 647	1:250	Invitrogen
Goat anti-rat Alexa 647	1:250	Jacksons
4',6-diamidino-2-phenylindoe (DAPI)	1:500	Sigma

2.6. Tissue Culture.

2.6.1. Coating of culture plates.

Plates were coated with either 1% BSA in PBS or 1 mg/ml Geltrex in DMEM depending on the application.

When fibres were be kept in suspension, 1 ml of 1% BSA spread over the base of a 5 cm culture dish. Excess was removed and the residual BSA was left to air dry for at least 30 minutes prior to adding the appropriate media.

When fibres were required to attach, plates were coated with the basement membrane substitute Geltrex. A 1mg/ml working stock was made in DMEM and kept at 4 ^{o}C. As required, it was spread onto the base of plates and polymerised at 37 ^{o}C before excess was removed and appropriate media added.

2.6.2. Ex vivo regeneration model of isolated myofibres.

Isolated muscle fibres were placed into 5 cm culture dishes, coated with 1% BSA, containing 5 ml of differentiation medium (table 2.13) and incubated for 96hrs. Fibres were collected at 0, 24, 48, 72 and 96 hrs after isolation and fixed as previously described in section 2.4.2, prior to staining for markers of SC differentiation.

2.6.3. Outgrowth of SCs from isolated myofibres.

Isolated muscle fibres were placed into 6-well plates, coated with Geltrex (Gibco), containing 5 ml of proliferation medium + FGF2 (Thermofisher) (table

2.13). Fibres were left undisturbed for 5 days to allow fibres to attach to the plates and for SCs to proliferate away from the fibres (outgrowth). After this initial proliferation stage, the plates were washed with DPBS (Gibco), treated with 0.05% trypsin / EDTA (Gibco) at 37 ^{o}C for 3 – 4 mins, then quenched with D10 media (table 2.13) prior to being transferred into 15 ml falcon tubes. The cell suspension was centrifuged at 400 X g for 8 minutes and the pellet resuspended in proliferation medium without FGF2. The resuspended cells were then replated onto Geltrex coated 10 cm dishes containing 10 ml of proliferation medium without FGF2, and cultured for a further 24 hrs (D5+1), 48 hrs (D5+2) and 72 hrs (D5+3) depending on downstream application.

Table 2.13. Composition of cell culture media.

Media	**Composition**
D10	DMEM + 10% (v/v) fetal bovine serum (FBS)
Differentiation medium (Pasut et al., 2013)	DMEM + 10% (v/v) horse serum (HS) + 0.5% chicken embryo extract (CEE)
Proliferation medium (Pasut et al., 2013)	DMEM + 20% FBS + 10% HS + 1% CEE

2.6.4. Culture of isolated fibres in 3D collagen I gels.

A collagen gel was prepared, as described in tables 2.14 and 2.15, 200 μl was then added to the inner 24 wells of a 48 well plate and kept on ice. Isolated muscle fibres were carefully transferred into each well using a capillary tube and mouth pipette, with 2-3 fibres in each well. The plate was then incubated at 37 ^{o}C for 60 minutes to allow the gel to polymerise. Once set, 200 μl of proliferation media (without CEE) was carefully added on top of the gel. The plate was placed back into the incubator, at 37 ^{o}C for another 60 minutes, prior to timelapse imaging.

Table 2.14. Composition of 4X medium for collagen I gel (per 48 well plate).

Reagent	Volume
10X DMEM	600 μl
100X pyruvate	60 μl
0.5 M $NaHCO_3$	300 μl
H_2O	540 μl

Table 2.15. Composition of collagen I gel (per 48 well plate).

Reagent	Final concentration	Volume
4X medium	1X	1.5 ml
FCS	20%	1.2 ml
HS	5%	300 μl
H_2O	-	50 μl
0.1 M NaOH	9.2 mM	550 μl
Collagen I (5 mg/ml)	2 mg/ml	2.4 ml
Total volume		6 ml

2.6.5. Labelling of satellite cells with 5-ethynyl-2'-deoxyuridine (EdU).

TdT+ve cells at D5+1, D5+2 and D5+3 were prepared as described in section 2.6.3. A 10 mM stock solution of EdU was added to the culture medium to give a final EdU concentration of 10 μM, an additional D5+3 culture was left unlabelled as a negative control. The cells were then incubated for 8 hrs at 37°C prior to washing with 10 ml of DPBS (Gibco) and treatment with 1 ml of 0.05% trypsin / EDTA (Gibco). Following the addition 1 ml of D10 medium, cells were transferred into 15 ml falcon tubes and centrifuged at 400 X g for 8 minutes. The cells were washed in 1 ml of DPBS and centrifuged again at 400 X g for a further 8 minutes. After removal of the DPBS, 2 ml of ice cold 70% ethanol was added in a dropwise fashion and the cells resuspended before storing at -20 °C.

2.7. Flow cytometry.

2.7.1. Click-iT EdU reaction.

The Click-iT EdU Alexa Fluor 488 flow cytometry assay kit (Invitrogen) was used to attach a fluorescent dye to incorporated EdU. Cells previously labelled

with EdU and fixed in 70% ethanol were centrifuged at 400 X g for 10 minutes and the resulting pellet washed in PBS. The Click-iT reaction cocktail was prepared, as shown in table 2.16 and after another 10-minute spin at 400 X g 500 μl of the reaction cocktail was added to each tube. The pellet was resuspended and incubated at room temperature for 30 minutes. The cells were centrifuged again at 400 X g for 10 mins and the resulting pellet resuspended in 500 μl of FACS buffer (5% FBS in PBS) containing Draq5 (Invitrogen) diluted 1:500. Following another 30-minute room temperature incubation, the cells were centrifuged at 400 X g for 10 minutes and washed in 1 ml of FACS buffer. The resuspended cells were transferred to FACS tubes before a final spin at 400 X g and resuspended in 300 μl of FACS buffer prior to analysis.

Table 2.16. Click-iT reaction cocktail preparation (per reaction).

Reaction component	**Volume**
PBS	438 μl
$CuSO_4$	10 μl
Alexa Fluor 488 azide	2 μl
Reaction buffer additive	50 μl
Total volume	500 μl

2.7.2. Analysis of cells with flow cytometer.

The cells were analysed using a Beckman Coulter Cytoflex cytometer using the filter sets outlined in table 2.17 to detect cells positive for tdT, Alexa Fluor 488 and Draq5.

Table 2.17. Cytoflex filter specification.

Fluorophore	**Excitation peak**	**Emission peak**	**Filter**
tdTomato	554 nm	581 nm	**585/42 nm**
Alexa Fluor 488	493 nm	519 nm	**488/8 nm**
Draq5	647 nm	681 nm	**712/25 nm**

2.8. Microscopy.

2.8.1. Imaging of muscle sections.

Fluorescence and brightfield imaging were done at 20x magnification using a Zeiss Axioplan 2 microscope and Axiovision 4.8.2 software in conjunction with Zeiss AxioCan HRm (fluorescence) and HRc (brightfield) cameras.

2.8.2. Imaging of muscle fibres.

Isolated muscle fibres, stained for various markers were imaged and analysed using a Zeiss ApoTome 2 microscope, Axiovision 4.9 software and AxioCam HRm camera.

2.8.3. Time lapse microscopy.

Isolated fibres suspended in a 3D collagen I matrix, as described in section 2.6.4. were placed into the incubation chamber and imaged using a Zeiss Axiovert 200M inverted microscope with an AxioCam HRm camera. Positional data for each fibre was input into Axiovision 4.8.2 and images at each position taken every 15 minutes for 96 hrs.

2.9. Image analysis and data acquisition.

2.9.1. Analysis of stained muscle sections.

Fluorescence images of transverse sections were converted into .tiff format and loaded into Ilastik V. 1.3.2post2 (www.ilastik.org), a computer learning tool capable of identifying muscle fibres by dividing an image based upon similarities between individual pixels (colour and intensity). The binary image produced by Ilastik was compared against the original immunofluorescent images and corrected where needed. Binary images of injured muscle had the original DAPI channel overlayed in ImageJ to identify regenerating, centrally nucleated fibres, as shown in Figure 2.5. Non-injured fibres were discounted from the analysis prior to the particles (muscle fibres) being selected and measured in terms of minimal Feret's diameter (F_{min}) (Fig 2.6), according to the procedures outlined in Ruegg & Meinen. 2011. SCs marked by tdT expression were easily identifiable using a fluorescence microscope. Once identified they were counted and the number calculated per mm^2.

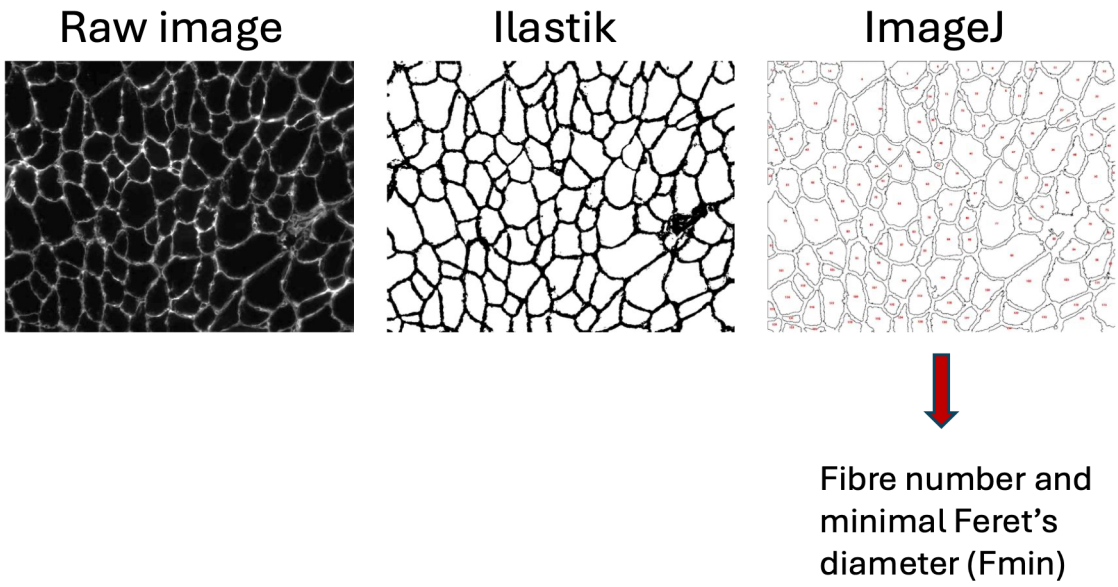


Figure 2.5. Workflow for image analysis of muscle sections. Raw image is converted to .tiff format (left), Ilastik converts immunofluorescence into a binary output (centre), DAPI staining is overlayed to identify regenerating fibres in ImageJ and measures fibres in terms of F_{min} (right).

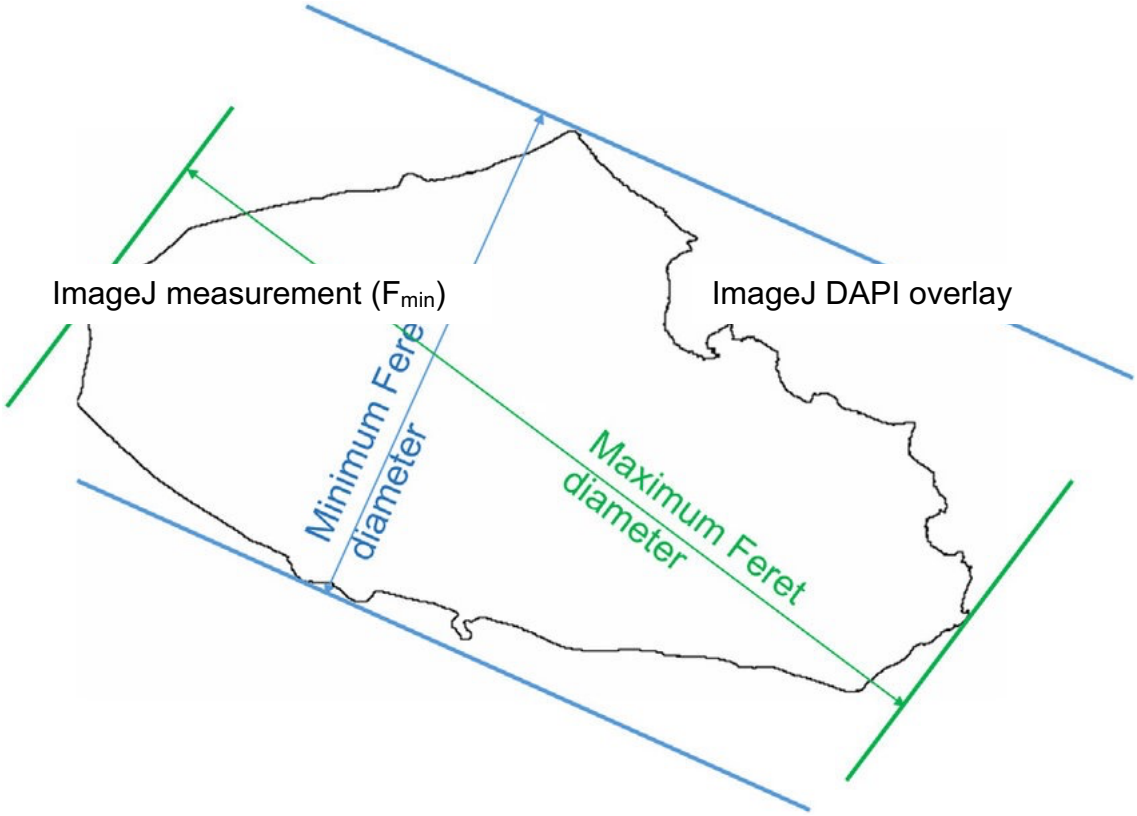


Figure 2.6. Sketch of a particle showing minimum (F_{min}) and maximum (F_{max}) Feret diameter. F_{min} is described as the shortest possible distance between two parallel tangents to a particles outline.

2.9.2. Analysis of ex vivo muscle regeneration.

Isolated fibres, stained for a combination MRFs, were viewed at 20x magnification. SCs were identified by either Pax7 staining or by the presence of tdT. As muscle fibres are too long to image in their entirety, cells were counted manually whilst scrolling along each fibre in real time. Total number of cells, positive or negative for each MRF, at each time point were recorded.

2.9.3. Analysis of time-lapse videos.

SC migration speed was calculated using the MTrackJ plugin in ImageJ. SCs were tracked manually frame by frame and their overall course and distance plotted. Once all frames had been completed the total distance covered could by divided by the time, giving their average migration speed. SC proliferation was calculated by counting the number of times each cell divided over the course of the video.

2.10. Graphs and statistics.

Graphs were produced in either R-studio or GraphPad Prism V.10.6. All statistical analysis was carried out on raw data in GraphPad Prism V.10.6. on Mac OSX. All assumptions for parametric testing were checked, and data transformation was attempted when data did not conform to normal, prior to using non-parametric alternatives.

Chapter 3.

Integrins α5β1 and α7β1 are essential for efficient muscle regeneration after an acute injury.

3.1. Introduction.

To investigate how the loss of integrins α5β1 and α7β1 would impact adult skeletal muscle regeneration after acute injury we used three integrin KO mouse lines (α7 KO, α5 cKO and DKO) and compared these to controls. Integrin α7 KO mice, although viable and fertile, have been shown to develop a post-natal form of progressive muscular dystrophy (Mayer et al. 1997). Integrin α5 KO mice die in-utero prior to E11, whereas mice with chimeric expression of integrin α5 are viable but display signs of muscle degeneration – regeneration in muscles of the head, thorax and limbs (Yang et al. 1993). For these reasons we wanted to investigate how the muscle would respond to an acute injury if either one or both integrins were absent. Given that some functional association / compensation mechanism has been demonstrated between these two integrins (Nawrotzki et al. 2003), the DKO was also used in order to assess the degree of compensation conferred by each when the other is absent.

An acute injury model was employed, whereby the right tibialis anterior (TA) was injected with cardiotoxin (CTX), whilst the contralateral limb remained an uninjured control. Complete muscle regeneration should take around 21 - 28 days. With this in mind, mice were sacrificed at either 10 days post injury (DPI) to assess initial regenerative progress, or at 30 DPI by which point healthy muscle would be fully regenerated. All mice underwent a series of tamoxifen injections, outlined in figure 3.1, thereby inducing the expression of tdT in the SCs of all mice, whilst concurrently excising exon 1 of *Itga5* in the SCs of α5 cKO and DKO strains. The injury was induced via an intra-muscular injection of CTX into the right TA. Tamoxifen injections then continued, as shown in figure 3.1, to ensure maintained ablation of *Itga5* in the rapidly dividing muscle stem cell population. Repeated tamoxifen injections were required to ensure all SCs were targeted, as untargeted cells would have a potential proliferative advantage. The tamoxifen regime also differed between the two models due to the observed negative regenerative effect tamoxifen had on controls if administered every two days for extended periods of time (Lonsdale & Mayer, 2022).

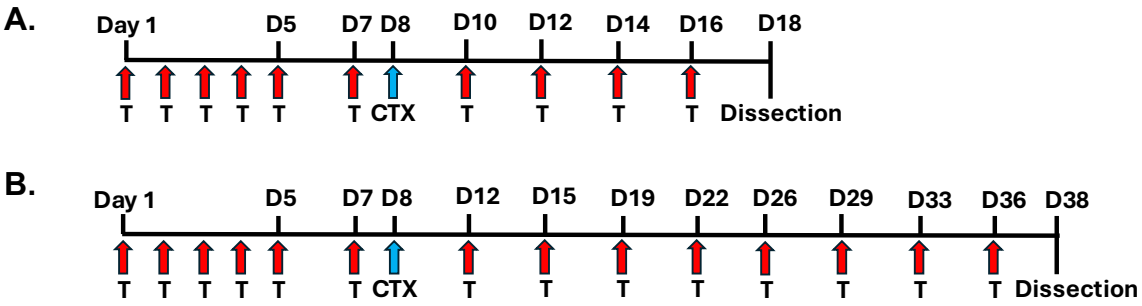


Figure 3.1. Tamoxifen and CTX protocol. The timings of injections and recovery periods observed for (A). 10 DPI and (B). 30 DPI, prior to dissection.
T = Tamoxifen. CTX = Cardiotoxin. Figure taken from Lonsdale & Mayer, 2022.

3.2. Genotyping of integrin KO mice

To guarantee the correct genotype of experimental animals, all mice were genotyped twice. Ear notches were taken at P20 prior to weaning, then tail tips were collected after mice were sacrificed and dissected. Tissue was lysed as described in section 2.2.1 and used as the template in a PCR using the primers shown in table 2.3. The α5 reactions can yield three products, floxed - 821 bp, WT - 692 bp and excised - 500 bp. The α7 reactions can give two products, WT - 230 bp and KO - 450 bp. If a sample is Cre+ve it will yield a single band at 600 bp, whilst tdT will yield a fragment of 297 bp for the WT allele compared to 197 bp for the tomato-modified locus. PCR results clearly showed the desired size amplicons in all mice used for further analysis, as shown in figure 3.2.

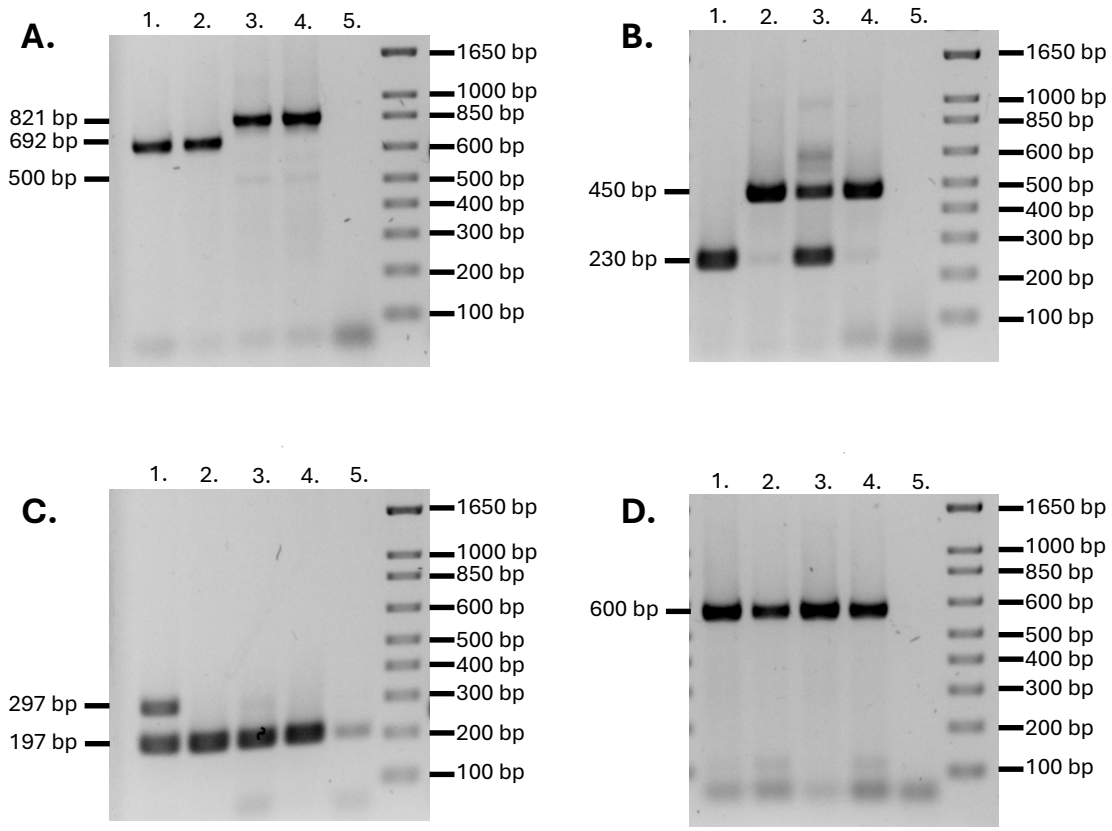


Figure 3.2. Representative PCR gel images. (A) α5. Ln.1. α5+/+. 2. α5+/+. 3. α5fl/fl. 4. α5fl/fl. 5. Blank. 6. 1 kb+ ladder. **(B) α7.** Ln.1. α7+/+. 2. α7-/-. 3. α7+/-. 4. α7-/-. 5. Blank. 6. 1 kb+ ladder. **(C) tdT.** Ln. 1. tdT+/-. 2. tdT-/-. 3. tdT-/-. 4. tdT-/-. 5. Blank. 6. 1 kb+ ladder. **(D) Cre.** Ln. 1. Cre +ve. 2. Cre +ve. 3. Cre +ve. 4. Cre +ve. 5. Blank. 6. 1 kb+ ladder.

3.3. Histological analysis of injured muscle at 10 DPI and 30 DPI.

The left and right TAs were isolated at 10 DPI and 30 DPI, prior to fixation and freezing in liquid nitrogen cooled isopentane. Each frozen muscle was cut transversely at its widest point and sections taken from each portion to allow analysis of the muscle over the majority of its length. H&E staining allowed for easy identification of centrally located nuclei, indicating the muscle had undergone an injury.

Uninjured muscles from all four groups showed no signs of central nucleation and were relatively indistinguishable in terms of gross morphology (Fig. 3.3A, B, C & D). At 10 DPI obvious differences were apparent. All four groups displayed extensive central nucleation, however the degree of regeneration achieved by each was visibly different in terms of both number and size of regenerating myofibres. Control mice showed rapid regeneration, with muscle

morphology looking similar to the uninjured controls (Fig. 3.3A'). The α5 cKO mice showed good numbers of regenerating fibres, however there was significant variability in their size and small regions of fibrosis (Fig. 3.3B'). The α7 KO showed partial regeneration with increased fibrosis, fewer fibres and an increase in fibre size variability (Fig. 3.3C'). The DKO was the most severely impaired with visibly fewer, significantly smaller myofibres and extensive fibrosis (Fig 3.3D'). As expected, by 30 DPI, control mice had undergone complete regeneration (Fig 3.3A''). The α5 cKO and α7 KO also showed improved morphology (Fig 3.3B'' & C''), although fibre size variability and small amounts of fibrosis persisted in the α7 KO. The DKO displayed a persistent regenerative defect with large areas of fibrosis and significantly fewer fibres even at 30 DPI (Fig. 3.3D'').

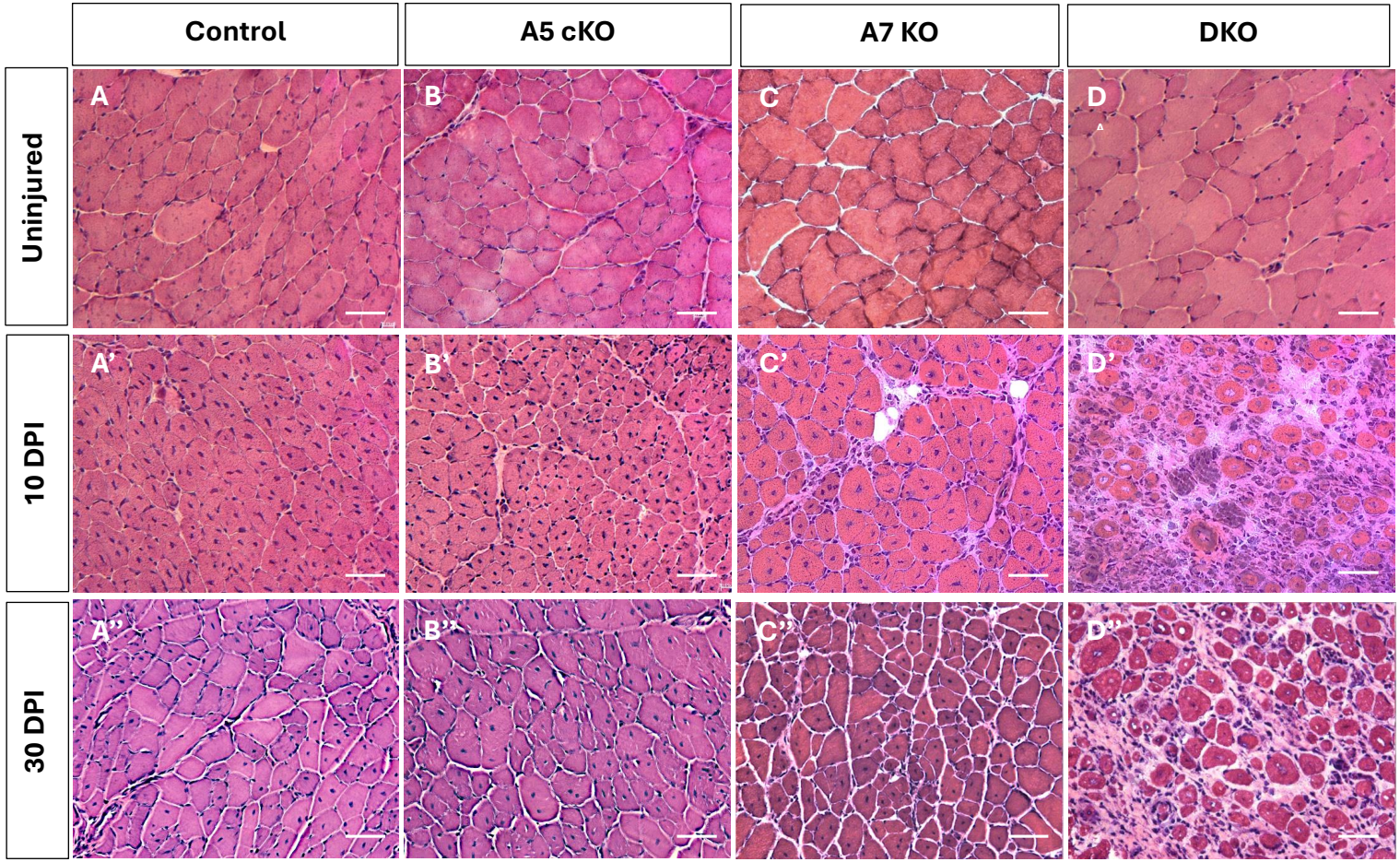


Figure 3.3. Representative images of H&E stained transverse sections of the TA. Uninjured, at 10 DPI and 30 DPI. **(A, A' & A")** Uninjured control, at 10 DPI and 30 DPI respectively. **(B, B' & B")** Uninjured α5 cKO, at 10 DPI and 30 DPI. **(C, C' & C")** Uninjured α7 KO, at 10 DPI and 30 DPI. **(D, D' & D")** Uninjured DKO, at 10 DPI and 30 DPI. Scale bars = 50 μm, n = 7 mice.

3.4. Quantitative analysis of regenerating muscle fibres at 10 DPI and 30 DPI.

Due to the morphological differences observed after H&E staining, quantification of myofibre size was required to statistically confirm the phenotype of each KO model. Sections were taken from two separate regions of each muscle prior to immunostaining of the BM protein nidogen to define the boundary of individual myofibres. Counterstaining with DAPI allowed for visualisation of nuclei and identification of regenerating myofibres. The resulting immunofluorescence images (Fig 3.4.) were processed in Ilastik before the minimum feret diameter (Fmin) for each myofibre could be calculated using ImageJ, as shown in figures 2.5. & 2.6.

As expected, a Kruskal-Wallis test revealed no significant difference between the mean Fmin of uninjured myofibres in each of the four groups (n = 7, K = 0.087, p = 0.993) (Fig 3.5A). The frequency distribution of myofibre size in each group was also well matched at this time point (Fig 3.5A'). At 10 DPI a Kruskal-Wallis test showed no significant difference between the controls and α5 cKO (n = 7, p = >0.999). However, multiple comparisons between each group revealed significant differences between the control, α7 KO (n = 7, p = 0.042) and DKO (n = 7, p = <0.0001) (Fig. 3.5B). The frequency distribution of myofibre size in each KO group had also shifted and diverged compared to controls, confirming a higher proportion of smaller myofibres in the α5 cKO, α7 KO and DKO (Fig. 3.5B'). At 30 DPI most of the differences, in terms of mean Fmin, had been resolved. Although a Kruskal-Wallis test still showed a significant difference between the mean Fmin of the four groups (n = 6, K= 15.13, p = 0.0017), subsequent multiple comparisons between groups revealed this was due to the differences observed in the Fmin of the DKO myofibres compared to both the controls (n = 6, p = 0.001) and α5 cKO (n = 6, p = 0.374), as shown in figures 3.5C & 3.5C'.

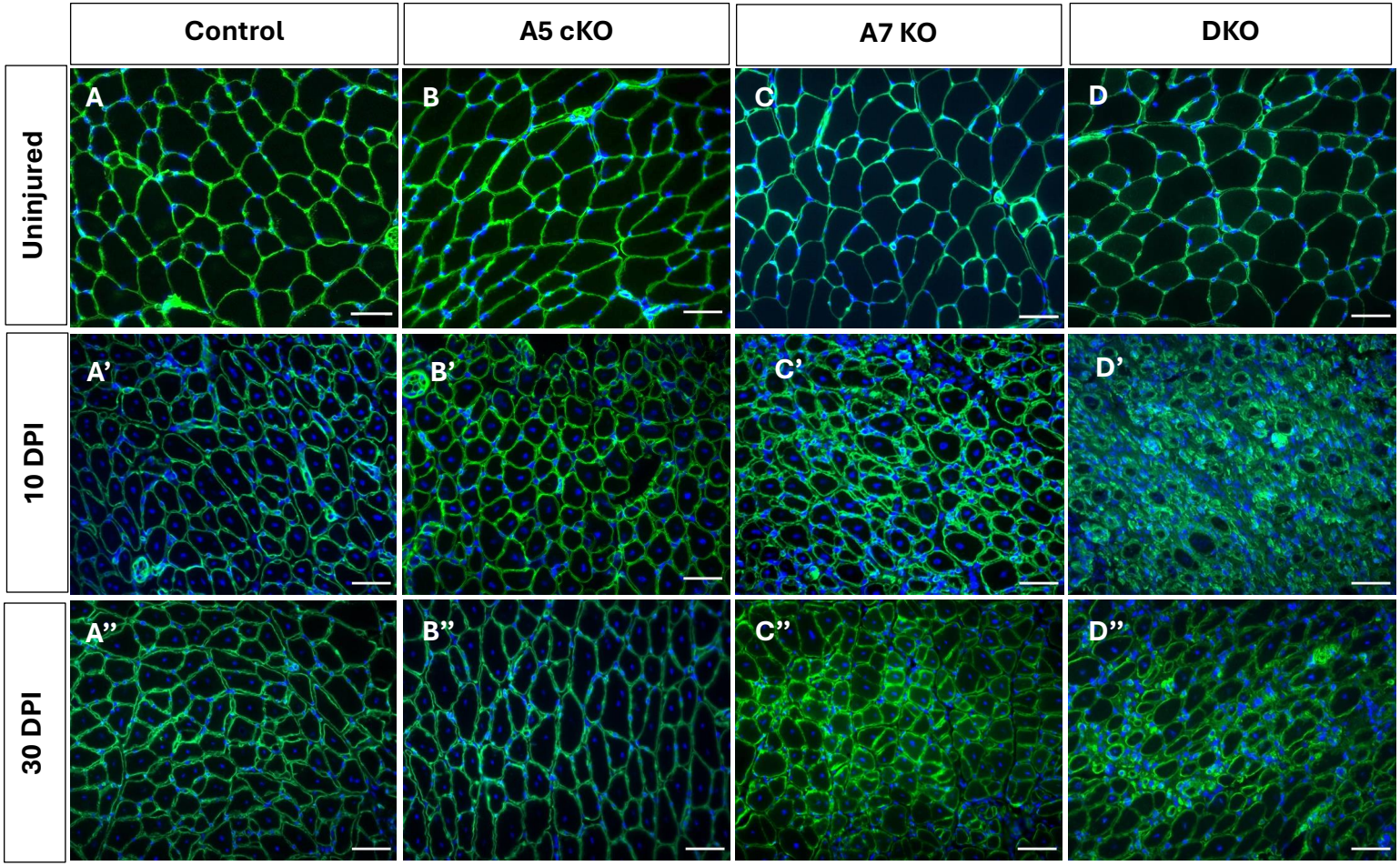


Figure 3.4. Representative immunofluorescence images of transverse sections of the TA. Stained with nidogen (green) and DAPI (blue). Uninjured, at 10 DPI and 30 DPI. (A, A' & A'') Uninjured control, at 10 DPI and 30 DPI respectively. **(B, B' & B'')** Uninjured α5 cKO, at 10 DPI and 30 DPI. **(C, C' & C'')** Uninjured α7 KO, at 10 DPI and 30 DPI. **(D, D' & D'')** Uninjured DKO, at 10 DPI and 30 DPI. Scale bars = 50 μm, n = 7 mice.

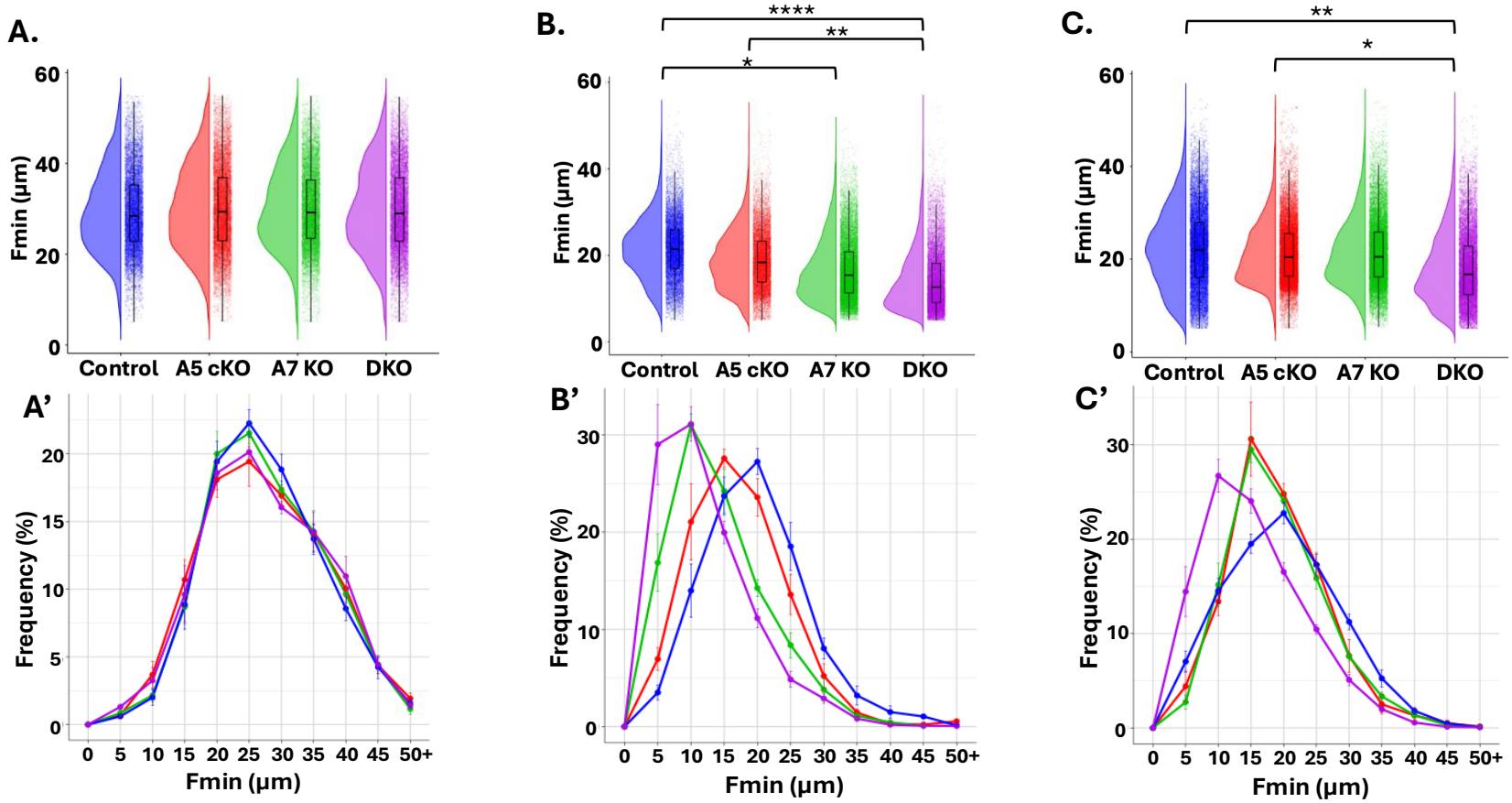


Figure 3.5. Muscle regeneration is delayed in the α5 cKO and α7 KO but persistently impaired in the DKO. (A, B & C) Raincloud plots show size and distribution of myofibre Fmin in control (blue), α5 cKO (red), α7 KO (green) and DKO (purple) in uninjured **(A)**, at 10 DPI **(B),** and 30 DPI **(C)**. Median and interquartile range is shown. **(A', B' & C')** Frequency distribution (+SEM) of myofibre Fmin in control (blue), α5 cKO (red), α7 KO (green) and DKO (purple) in uninjured (A'), at 10 DPI (B') and 30 DPI (C'). n = 7 mice

3.5. Persistent α - smooth muscle actin expression is observed in integrin deficient regenerated myofibres at 10 DPI.

At 10 DPI there are significantly more small myofibres in the integrin KO mice than controls. This was reduced by 30 DPI in both the α5 cKO and α7 KO, however the DKO still had significantly smaller myofibres than controls. To assess the relative stage of myofibre regeneration and the extent of any delay, α - smooth muscle actin (α-SMA) was targeted and visualised. α-SMA is transiently expressed in regenerating myofibres at 4 – 9 DPI, by day 10 it is no longer expressed in maturing myofibres. For this reason, it acts as a good indicator of immature, regenerating myofibres and allows us to establish if regeneration is proceeding at the normal rate. All imaging of α-SMA was taken with consistent exposure times, thereby allowing us to infer that a brighter signal roughly corresponds to an increase in protein expression.

Uninjured myofibres did not express α-SMA (Fig. 3.6A, B, C & D), however it was be clearly seen, highly expressed, in the smooth muscle cells of the blood vessels, as shown in figure 3.5A. By 10 DPI control muscle had regenerated and matured to a point where the transient expression of α-SMA had been downregulated and was no longer visible (Fig. 3.6A'). In the integrin deficient regenerating myofibres α-SMA was still clearly visible (Fig. 3.6B', C' & D'). A significant proportion of myofibres in each of the integrin KOs were still positive for α-SMA, indicating a delay in the regenerative process. The α5 cKO, although obviously delayed compared to controls, had more uniformity in terms of fibre size than the α7 KO and DKO, but still showed low level expression of α-SMA in a large number of fibres (Fig. 3.6B'). The α7 KO presented with a larger number of smaller fibres with higher levels of expression than the α5 cKO (Fig. 3.6C'). The DKO consistently displayed more fibres with higher expression levels than either the α5 cKO or α7 KO at 10 DPI (Fig. 3.6D'), indicating a more retarded regenerative programme when both integrins were absent. At 30 DPI all four groups were negative for α-SMA (Fig. 3.6A'', B'', C'' & D''). Even in the DKO, which still presented with numerous smaller fibres, no α-SMA was visible (Fig 3.6D''). This would indicate that the smaller fibres in the DKO had matured on a molecular level but were possibly unable to undergo fusion or hyperplasia to increase size, as healthy myofibres would.

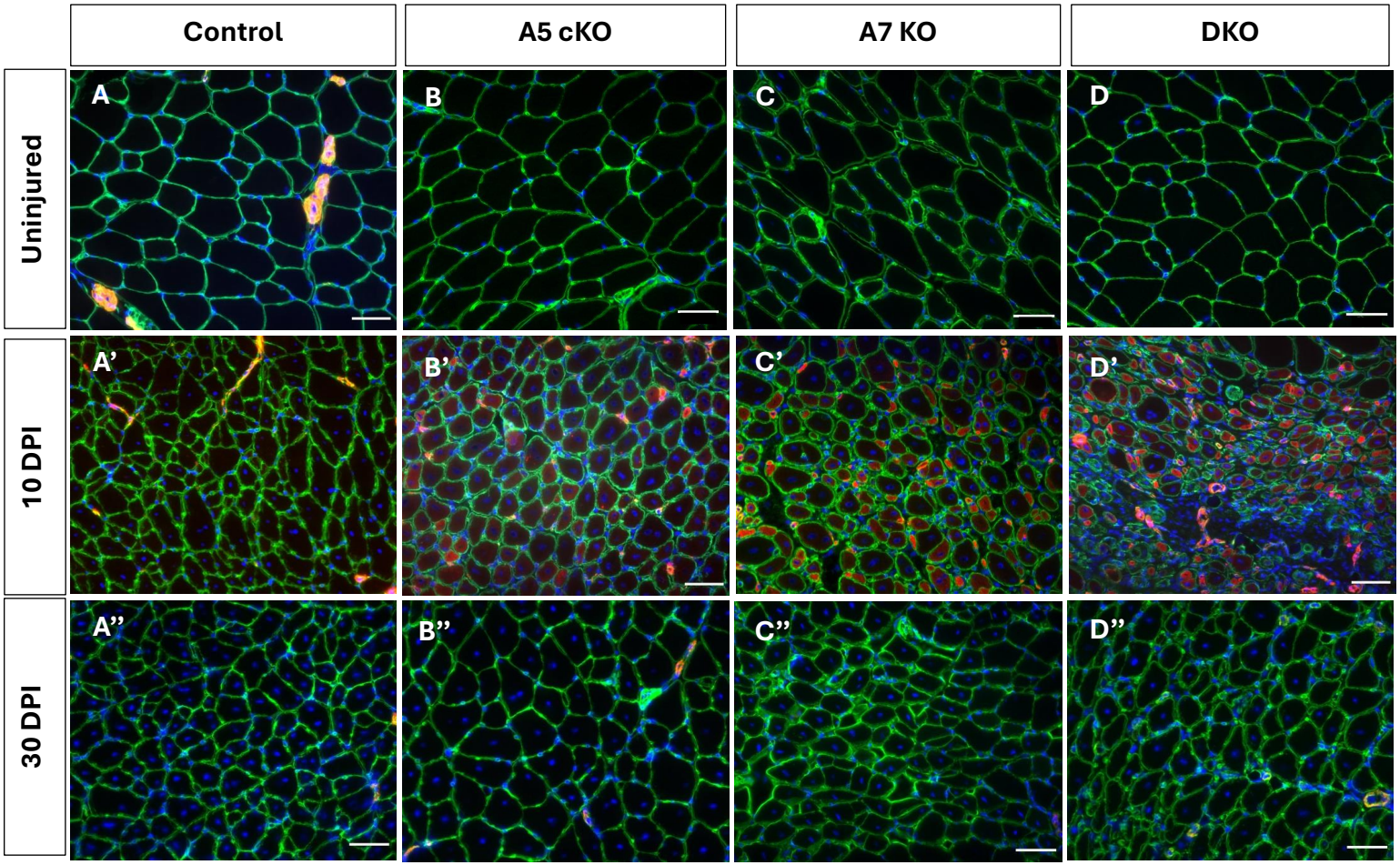


Figure 3.6. Representative immunofluorescence images of transverse sections of the TA. Stained with nidogen (green), α-SMA (red) and DAPI (blue). Uninjured, at 10 DPI and 30 DPI. (A, A' & A'') Uninjured control, at 10 DPI and 30 DPI respectively. **(B, B' & B'')** Uninjured α5 cKO, at 10 DPI and 30 DPI. **(C, C' & C'')** Uninjured α7 KO, at 10 DPI and 30 DPI. **(D, D' & D'')** Uninjured DKO, at 10 DPI and 30 DPI. Scale bars = 50 μm. n = 7 mice.

3.6. Mice lacking integrin α7 display reduced numbers of satellite cells *in-vivo.*

Having demonstrated a delayed regenerative response in the α5 cKO and α7 KO, as well as a persistent defect in the DKO, we wanted to investigate if integrin deficiency altered SC numbers and determine whether this could be a contributing factor. Considering that efficient muscle regeneration is dependent upon a resident quiescent SC population which is activated, then proliferates rapidly after injury, before repopulating the stem cell niche via asymmetric proliferative self-renewal. We hypothesised that fewer SCs, at any stage of the regenerative process (pre, during or after) could potentially lead to a delayed or even impaired outcome.

An acute injury was again induced via CTX injection into the right TA of mice engineered to express the red fluorescent protein tdT. Due to the action of the Cre-recombinase, expressed under the control of the *Pax7* promoter, tdT expression was exclusive to SCs, allowing for easy identification, as shown in figure 3.7. Mature myofibres also become red upon fusion with tdT+ progenitors, but to a lesser extent due to lower cytoplasmic content of the red fluorescent protein. Therefore, to facilitate accurate counting and eliminate false positives, SCs were only counted if they were significantly brighter than the fibre to which they were associated and co-localised with DAPI staining. The number of SCs in uninjured muscle was counted to establish the size of SC pool in each of the four groups. Then repeated at 10 DPI to investigate SC activation and proliferation, prior to counting again at 30 DPI to assess if SC numbers had returned to their per-injury numbers and had undergone self-renewal.

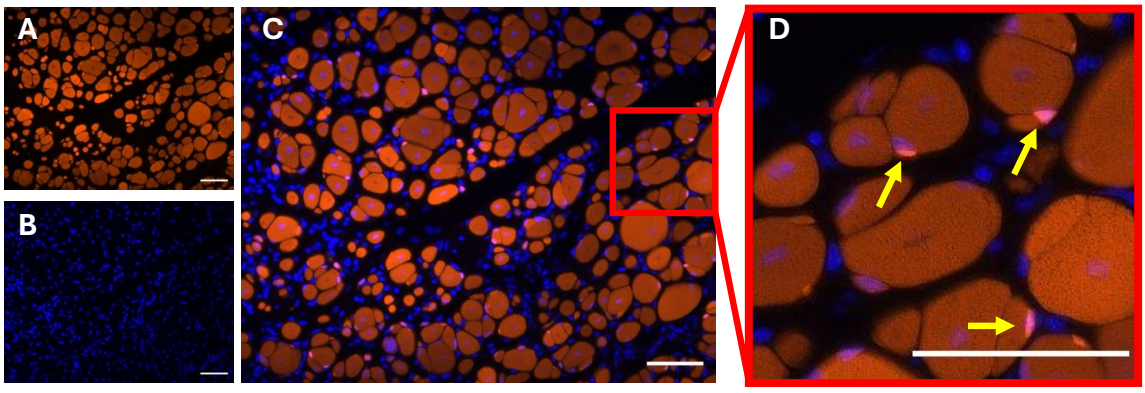


Figure 3.7. Method of SC identification. Sections from the TA of mice expressing tdT in SCs, counter stained with DAPI. (A) tdT. **(B)** DAPI. **(C)** Merge. **(D)** Zoomed view, arrows indicate SCs where high concentration of tdT colocalises with DAPI. Scale bars = 50 μm.

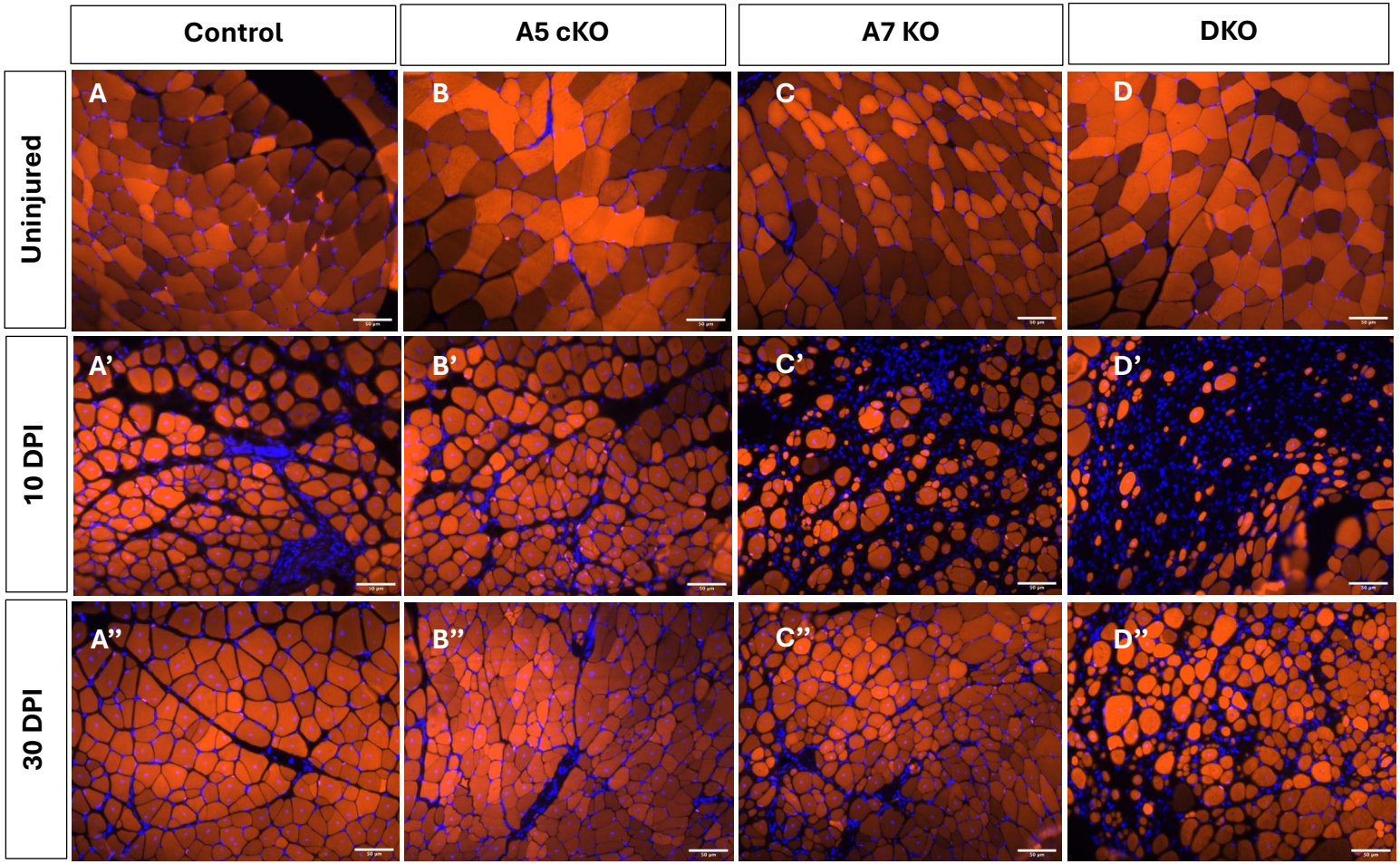


Figure 3.8. Representative images of transverse sections of the TA from mice expressing tdT (red), stained with DAPI (blue). Uninjured, at 10 DPI and 30 DPI. (A, A' & A'') Uninjured control, at 10 DPI and 30 DPI respectively. **(B, B' & B'')** Uninjured α5 cKO, at 10 DPI and 30 DPI. **(C, C' & C'')** Uninjured α7 KO, at 10 DPI and 30 DPI. **(D, D' & D'')** Uninjured DKO, at 10 DPI and 30 DPI. Scale bars = 50 μm. n = 7 mice.

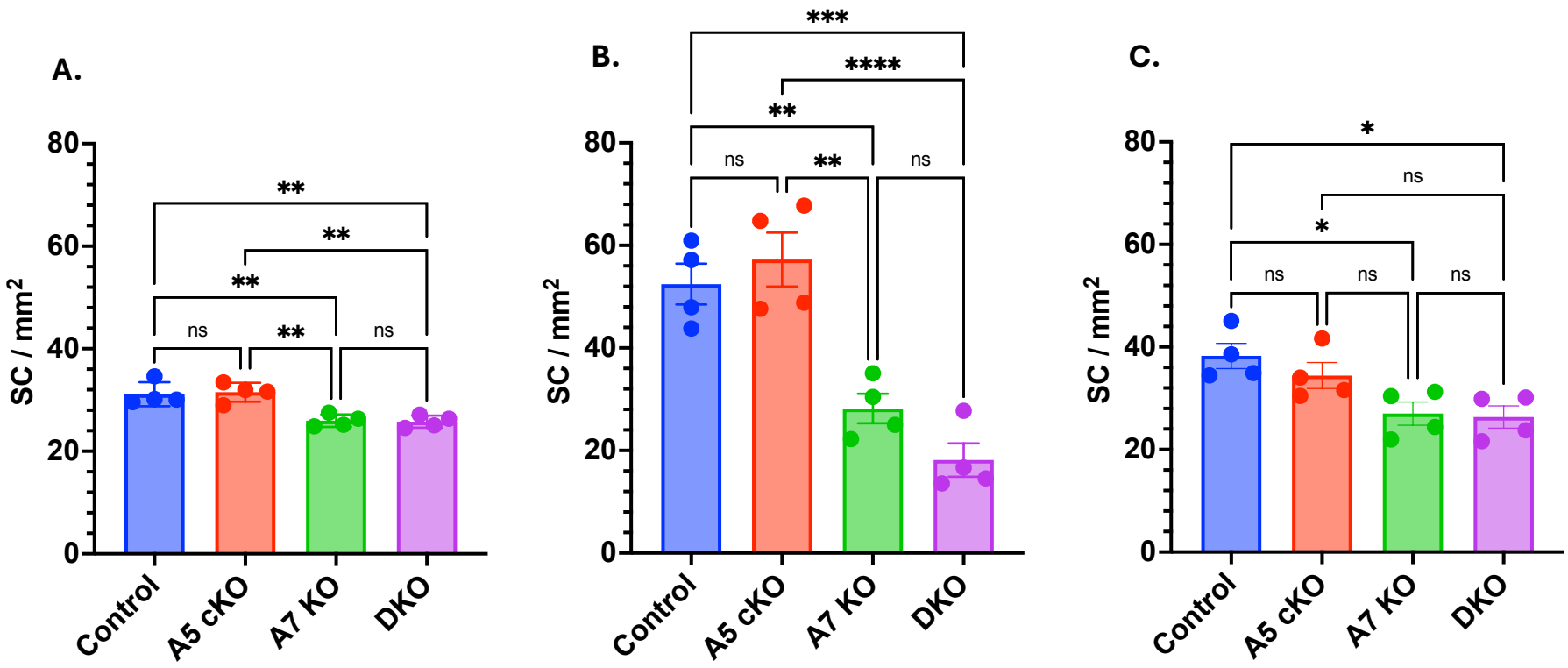


Figure 3.9. SC numbers are reduced in mice lacking integrin α7. Bar charts show mean (+SEM) SC number in control (blue), α5 cKO (red), α7 KO (green) and DKO (purple) in uninjured (A), at 10 DPI (B) and 30 DPI (C). **(A)** Uninjured muscle shows significantly more SCs in control and α5 cKO mice. **(B)** At 10 DPI, numbers of control and α5 cKO SCs increase. **(C)** At 30 DPI, mice lacking integrin α7 have significantly fewer SCs than controls. n = 4 mice.

The results of a one-way ANOVA confirmed that mice lacking integrin α7 had significantly less SCs in uninjured muscle than either control or α5 cKO mice (n = 4, f = 13.44, p = 0.0004), (Fig. 3.9A). These differences became exaggerated at 10 DPI (n = 4, f = 22.83, p = <0.0001), (Fig. 3.9B). Whereas control and α5 cKO mice displayed a strong proliferative response to injury, increasing by 2.01-fold and 2.13-fold respectively, α7 KO mice only managed to marginally increase SC number by 1.09-fold. In contrast, the mean number of SC / mm^2 in the DKO actually decreased 1.30-fold. Demonstrating that SCs lacking integrin α7 have a clear defect in either activation or proliferation. At 10 DPI caspase 3 staining showed no difference between groups, indicating that the difference in cell numbers was not a result of increased apoptosis (data not shown). At 30 DPI, mice lacking integrin α7 still had significantly less SC / mm^2 than controls (n = 4, f = 6.058, p = 0.0094), (Fig. 3.9C). However, within each group, results from paired t-tests showed no significant difference between the number of SCs in uninjured muscle vs 30 DPI (Fig 3.10), indicating a maintained ability to asymmetrically divide, self-renew and repopulate the stem cell niche.

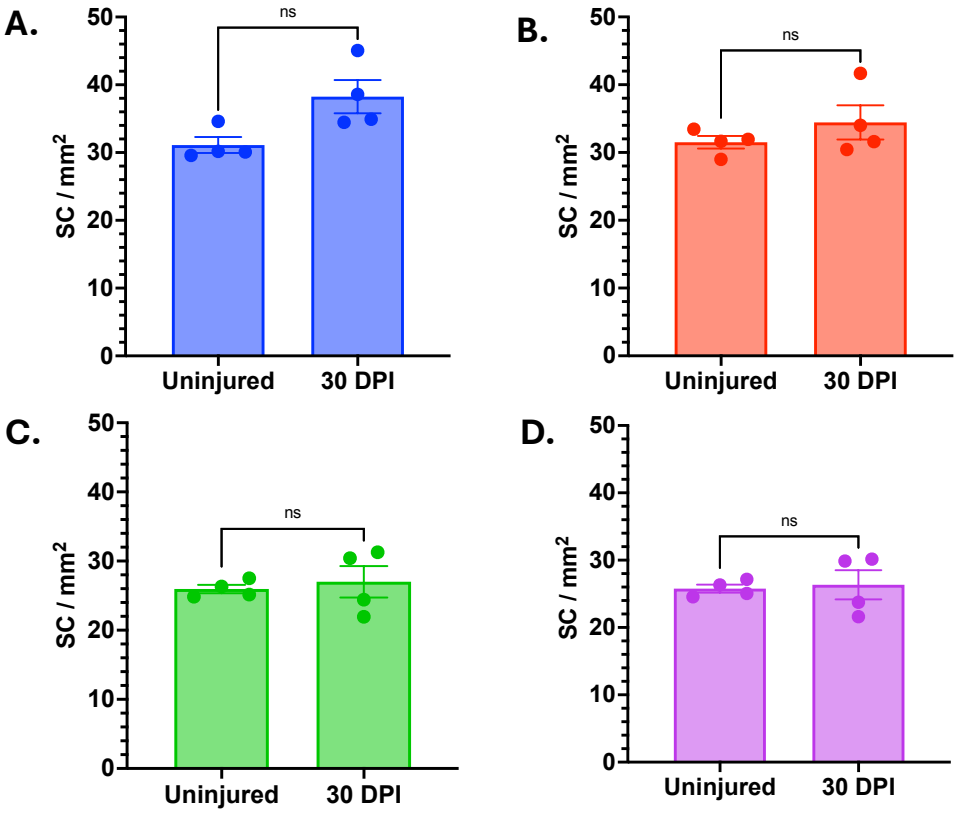


Figure 3.10. No significant difference in SC number pre and post injury. (A) Control (n = 4, p = 0.1072), **(B)** α5 cKO (n = 4, p = 0.2822). **(C)** α7 KO (n = 4, p = 0.5937). **(D)** DKO (n = 4, 0.8440). Paired t-test. Mean +SEM shown. n = 4 mice.

3.7. Summary.

The aim of this chapter was to determine whether adult muscle regeneration was compromised after an acute injury when SCs were lacking either integrin α5β1 and / or α7β1. Both integrins have been previously implicated in defective muscle development / homeostasis, but no studies have yet assessed their impact after an acute injury. We utilised an acute injury model in three KO mouse lines, α5 cKO, α7 KO and DKO and compared these to controls to determine the degree of any defect. A combination of H&E, immunofluorescence and SC labelling with tdT, allowed us to gain insights into how the loss of either α5β1 and / or α7β1 would impact upon not only muscle regeneration at various stages, but also SC proliferation and self-renewal.

Gross morphological differences were clearly apparent at 10 DPI, the α5 cKO showed a delayed regenerative response, followed by the α7 KO which displayed a more acute phenotype. However, the DKO was the most severely affected at this time point showing far fewer, smaller myofibres and increased fibrosis. Thereby demonstrating there is a degree of compensation conferred by each integrin when the other is absent. Even though, as receptors, they do not share the same ECM ligand, both the α5 cKO and α7 KO showed some degree of fibrosis, which was again exacerbated in the DKO. This is indicative of a possible defect in ECM remodelling which is crucial for efficient restructuring of muscle after an acute injury. At 30 DPI, although the α5 cKO and α7 KO mice had managed to recover to an extent, however the α7 KO looked aberrant compared to controls and α5 cKO, primarily due to an increase in myofibre size variability. The DKO was still obviously impaired, again demonstrating an essential need for both integrins if full muscle regeneration is to be achieved.

α-SMA is known to be transiently expressed in ‘young’ myofibres (Makarenkova et al., 2009). The persistent expression of α-SMA confirmed a delayed regenerative response in the integrins KOs. Myofibres remained in an ‘immature’ state for longer when integrin deficient. Interestingly however, the smaller myofibres that persisted in the DKO at 30 DPI had down regulated α-SMA, something that in healthy muscle is observed as myofibres mature and undergo hyperplasia. This could indicate that SCs lacking both integrins struggle to either terminally differentiate or fuse with existing fibres to initiate growth or repair.

Quantification of Fmin statistically confirmed the abnormalities observed using H&E and α-SMA staining. Although all integrin mutants were significantly different to controls, the α7 KO and DKO mice remained statistically similar but were significantly different to the α5 cKO. At 30 DPI the DKO mice remained the only group significantly different in terms of Fmin, further demonstrating that each integrin can partially compensate for the loss of the other.

Uninjured muscle showed fewer SCs in both the α7 KO and DKO, highlighting a crucial role for integrin α7 in maintaining a quiescent population of muscle stem cells prior to injury. Upon injury, only the control and α5 cKO displayed a consistent proliferative response. Demonstrating that integrin α7 is essential for rapid expansion of the stem cell pool, which facilitates the rapid regeneration that skeletal muscle is famous for. However, by 30 DPI, all four groups had replenished their preinjury quota of SCs, thereby demonstrating the crucial ability of asymmetric division of myogenic progenitors in order to replenish any depletion caused by the initial injury, ready for the next round of regeneration, compromised or not.

Chapter 4.

Integrin α7β1 is essential for satellite cell migration and proliferation.

4.1 Introduction.

The results in chapter 3 demonstrate that when SCs are lacking integrin α5β1 and / or α7β1 muscle regeneration becomes compromised. The regenerative shortcomings become more acute and persistent when both integrins are absent. There were also fewer SCs in mice lacking Integrin α7β1 and a clear defect in either activation or proliferation. Integrin α7β1 is the primary laminin binding integrin expressed in skeletal muscle and SCs. It is known to be expressed in quiescent SCs, throughout differentiation, along the sarcolemma of mature muscle fibres and enriched at the MTJ (Liu et al. 2009; Mayer et al. 1997). It allows for direct interaction with the laminin rich BM which encapsulates each myofibre, facilitating myofibre stability under contraction, whilst also supporting SC adhesion and migration. Less is known about the spatiotemporal expression of integrin α5β1, with no evidence in the literature suggesting it is expressed in quiescent SCs. It is expressed during embryonic myogenesis in somites and migratory myogenic precursors in a fibronectin rich environment. It is then gradually replaced with α7β1 postnatally as muscle matures (Nawrotzki et al. 2003), Integrin α5β1 is a fibronectin (FN) receptor, and whilst FN is not a component of the BM in mature skeletal muscle, it is highly expressed after injury, suggesting the expression of α5β1 would be better suited in myoblasts after SC activation, during the early stages of regeneration.

Integrin α7β1 is commonly used as a SC marker as it is known to be expressed throughout quiescence, activation and myoblast differentiation. However, an obvious gap in our knowledge remains regarding the timing of integrin α5β1 expression in SCs or myoblasts during regeneration along with how the loss of either integrin would affect migration, proliferation and cell cycle progression. To address these questions, myofibres were isolated in differentiation media, prior to fixation at various time points (T0, T24, T48 & T72). Immunostaining was carried out to confirm the expression patterns of integrin α5 in control and α7 KO mice. Given that integrins α5β1 and α7β1 are both receptors for ECM components and known to play roles in embryonic and post-natal myogenic precursor cell migration respectively, we used time-lapse microscopy to visualise ex-vivo SC migration on isolated myofibres, to visually confirm and quantify any defect in migration. Proliferation could also be observed and quantified in the time-lapse videos, whilst cell-cycle analysis was carried out via the application of 5-ethynyl-2'-deoxyuridine (Edu) to cultures of isolated SCs, prior

to fixing and labelling with a fluorescent azide via a copper catalysed 'click' reaction. Flow cytometry was then used to determine the percentage of cells which had undergone S-phase and progressed through the G2 check point of the cell-cycle.

4.2. Expression of integrin α5β1 in quiescent and activated SCs.

The profile of integrin expression in SCs is not well characterised, the literature is contradictory regarding all but integrin α7β1, which is widely accepted as the primary integrin expressed in both SCs and mature muscle. To gain further insight into integrin α5β1 expression in SCs, we isolated single myofibres from EDL muscles and placed them into differentiation media. Myofibres were then fixed at various time points (T0, T24, T48 and T72) and stained against integrin α5 (Fig. 4.1A) prior to counting the number of positive cells. Myofibres from control and α7 KO mice were stained to ascertain if the loss of integrin α7 resulted in altered integrin α5 expression.

At T0 and T24 there were no integrin α5 +ve cells in either the control or integrin α7 KO. However, by T48 integrin α5 expression could be seen in 22% of control myoblasts and 26% of α7 KO myoblasts, an independent T-test showed no significant difference between these two populations ($n = 3$, $t = 0.455$ $p = 0.673$). This then increased to 55% and 57% respectively at T72 ($n = 3$, $t = 0.139$, $p = 0.896$) (Fig. 4.1B). This demonstrates that integrin α5 expression begins at least 24 hours after activation, but the number of integrin α5 +ve myoblasts increases rapidly after 48 hours, once cells have begun to proliferate.

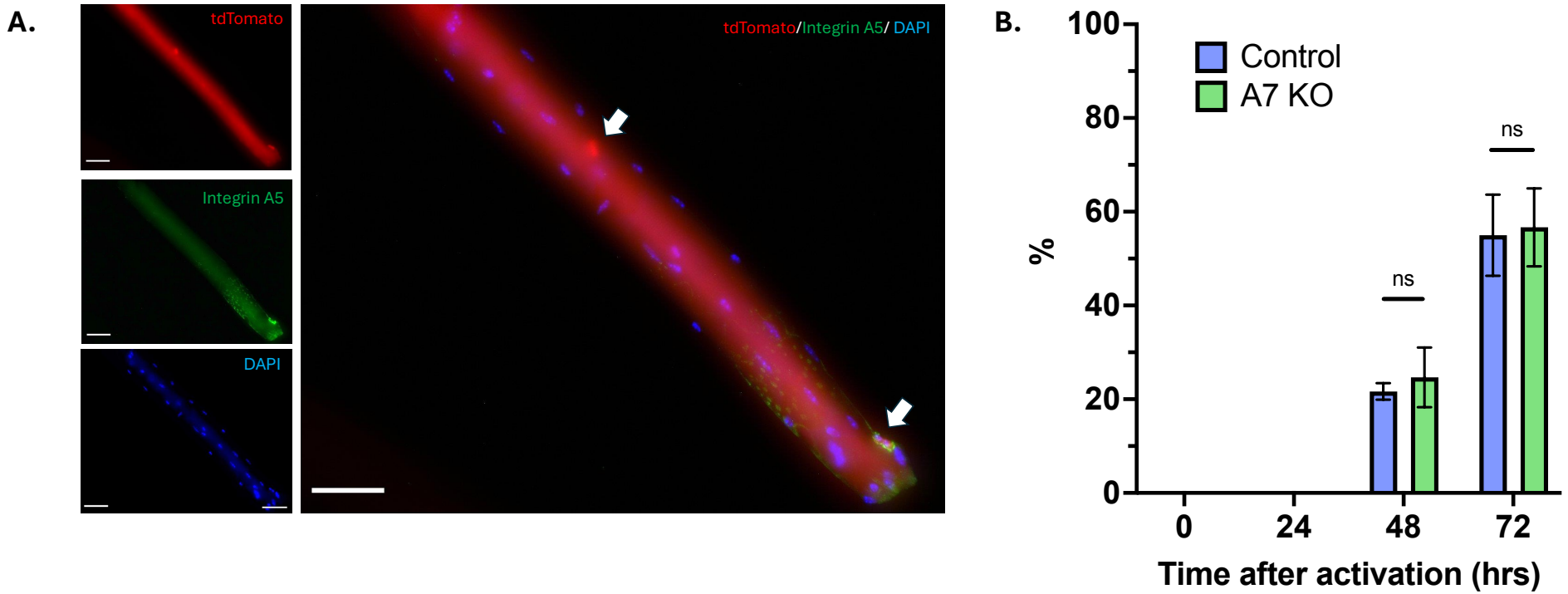


Figure 4.1. Integrin α5 is expressed in proliferative myoblasts, not quiescent SCs. (A) Representative image of isolated EDL myofibre stained against integrin α5 at T48. Arrows show integrin α5 +ve and -ve myoblasts. Scale bar = 50 μm. **(B)** Mean (+SEM) proportion of integrin α5 +ve cells at various time points after isolation / activation (n = 3 mice).

4.3. Time lapse analysis of SC migration on isolated myofibres.

As ECM receptors, integrins allow cells to interact with their environment, whilst integrin clustering enables focal adhesion formation allowing dynamic cell motility and migration. Integrins $\alpha5\beta1$ and $\alpha7\beta1$ are fibronectin and laminin receptors respectively, and whilst laminin is a major component of the BM which surrounds each myofibre, fibronectin is not. To investigate how SC migration speed was affected by the loss of integrins $\alpha5\beta1$ and / or $\alpha7\beta1$, isolated single myofibres from the EDL were mounted in a collagen gel (described in section 2.6.4) and imaged every 15 minutes over 96 hours. The resulting time lapse videos were imported into ImageJ and SC migration distance tracked manually frame by frame. An example of SC tracking is shown in figure 4.2A, the distance each cell travelled was recorded enabling migration speed to be calculated.

Unsurprisingly, given that laminin is a key component of the BM, SCs lacking integrin $\alpha7\beta1$ showed significantly reduced migration speed compared to either controls or $\alpha5$ cKOs (Fig. 4.2B). Control and $\alpha5$ cKO SCs had a mean migration speed of 20.2 μm/hr and 20.3 μm/hr respectively, whereas $\alpha7$ KO and DKO SCs migrated at a reduced 12.5 μm/hr and 13.0 μm/hr respectively.

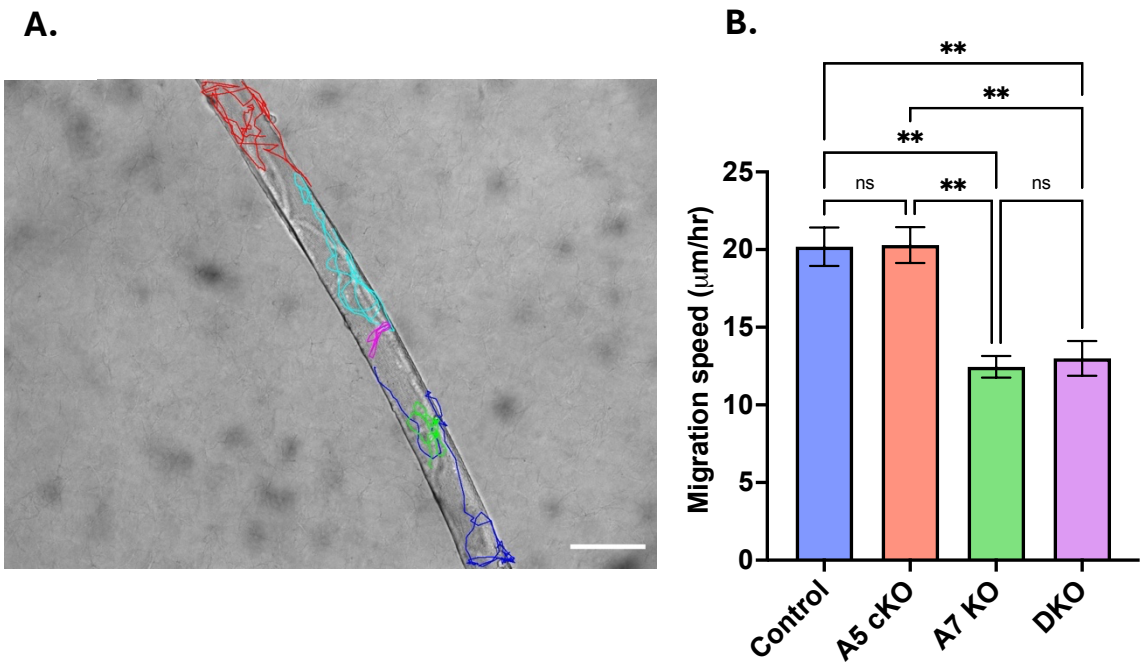


Figure 4.2. Efficient myofibre associated SC migration requires integrin α7β1. (A) Example of time lapse tracking of SCs on isolated EDL myofibres. Each coloured line represents the path taken by an activated SC as it migrates. Scale bar = 50 μm **(B)** Mean (+SEM) migration speed (μm/hr) of SCs on isolated EDL myofibres (n = 4 mice).

4.4. Time lapse analysis of SC proliferation on isolated myofibres.

The in vivo data from chapter 3 indicated a significant proliferative defect when SCs lack integrin α7. To investigate this further we analysed the time lapse videos to establish both the timings and number of each cell division. The timing of the first cell division after activation varied considerably, ranging from 22 – 56 hours. The mean time of the first cell division in the control and α5 cKO groups was 40 hrs and 36 hrs respectively, whilst the first division in the α7 KO and DKO groups occurred at around 33 hrs and 34 hrs after activation respectively. The mean amount of time taken between subsequent divisions was 11 hrs for the control, 10 hrs for the α5 cKO, 12 hrs for the α7 KO and 13 hrs for the DKO. Although integrin deficient cells underwent their first division quicker than controls and integrin α7 deficiency resulted in a marginally elongated doubling time, a one-way ANOVA revealed no significant difference between the mean timing of either the first division (n = 4, f = 0.369, p = 0.777) or second cell divisions (n = 4, f = 0.567, p = 0.646) between any of the four groups (Fig. 4.3). Due to the relatively large variance observed in these data, an increased sample size would be required to assess if this trend is indicative of a difference in phenotype.

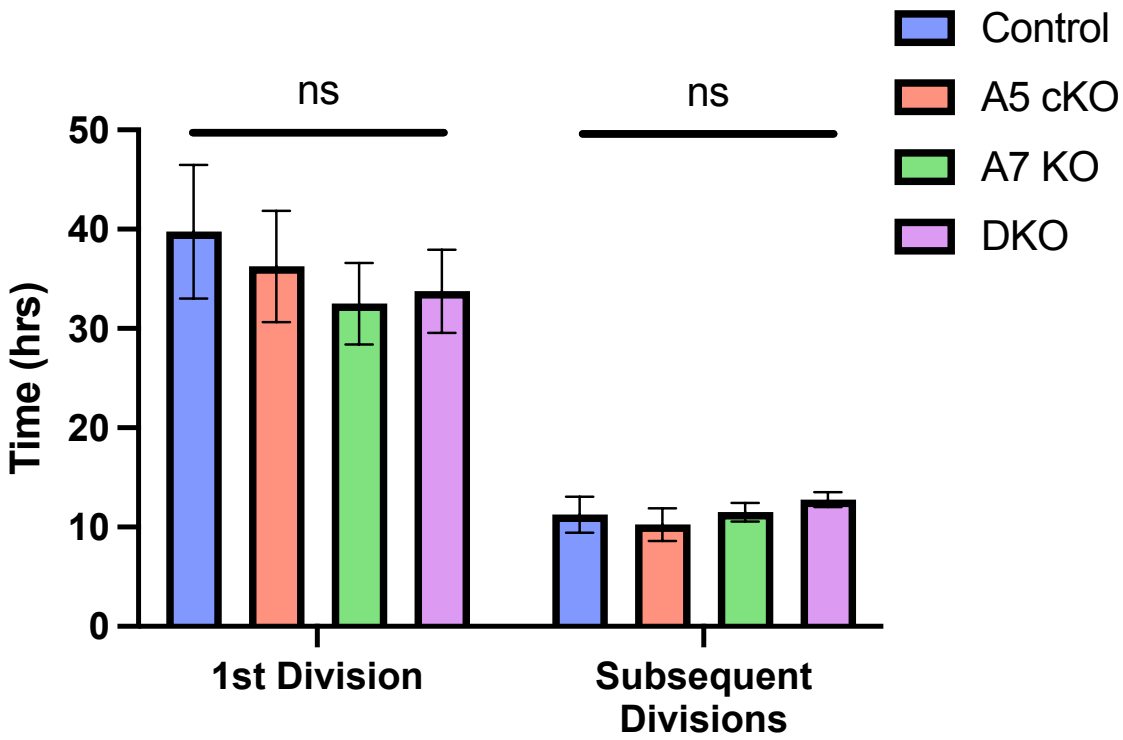


Figure 4.3. The loss of integrin α5β1 and / or α7β1 does not affect the timing of cell divisions after activation. Mean (+SEM) time for SCs to undergo 1st and subsequent divisions (n = 4 mice).

Although no difference in timing was observed, we wanted to assess each genotypes potential for multiple rounds of mitosis, as this could help us understand why there are significantly fewer α7 KO SCs in vivo. Time lapse videos were again analysed and cells tracked to count the total number of divisions they undertook over the 96-hour time course. Although cells lacking integrin α7 are capable of multiple divisions, 45% of α7 KO and 49 % of DKO SCs did not divide. However, significantly fewer control and α5 cKO SCs did not undergo mitosis, 12% and 14% respectively (n = 4, f = 62.68, p = <0.0001) (Fig. 4.4). In contrast, the majority of control and α5 cKO SCs underwent at least 3 rounds of mitosis, 41% and 32% respectively, again demonstrating a significantly increase mitotic potential compared to either the α7 KO or DKO (n = 4, f = 37.15, p = <0.0001) (Fig. 4.4).

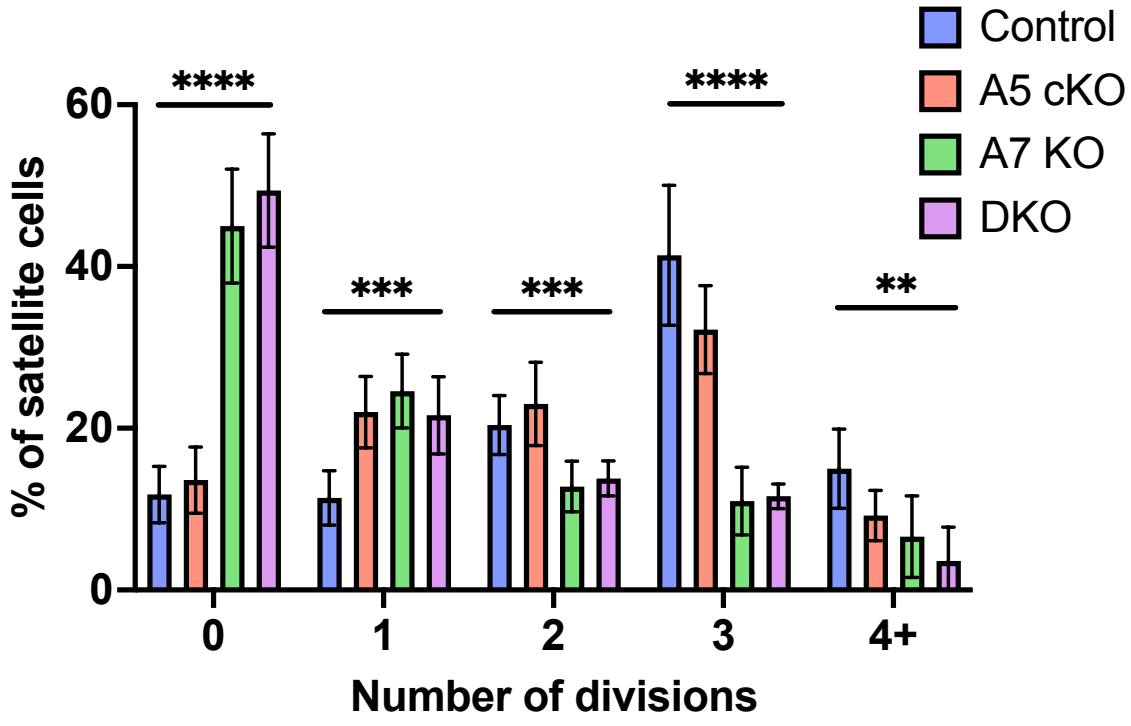


Figure 4.4. Integrin deficiency in SCs reduces their mitotic potential. Mean (+SEM) percentage of SCs which underwent 0, 1, 2, 3 or 4+ divisions. Anova and post-hoc Tukey's test results are shown in Appendix 1.6. (n = 4 mice).

4.5. SCs lacking integrin α7 demonstrate increased cell cycle arrest / mitotic catastrophe.

We have shown that, although not retarded in terms of timing, cells lacking integrin α7 are less capable of multiple rounds of mitosis and more likely to not divide at all. To establish what was driving this behaviour, we again isolated single EDL myofibres and plated them in proliferation media on plates coated with a synthetic BM, Geltrex. This allowed the SCs to proliferate and migrate away from each myofibre, allowing downstream cell culture and administration of EDU to the culture media at day 5+1, +2 and +3 after isolation (D5+1, D5+2 and D5+3). EDU is a thymine analogue which is readily incorporated into DNA during S-phase of the cell cycle. We incubated the cultured primary SCs with EDU for 8 hrs prior to fixation and fluorescence EDU labelling. Fixed cells were counter stained with DRAQ5, a DNA stain which allowed us to assess total DNA content, i.e whether each cell was preparing to divide (4n) or had undergone division and returned to a diploid state (2n). Using flowcytometry, we could then analyse the state of each cell in terms of EDU incorporation and DRAQ5 staining to count the numbers of cells which were either actively preparing for division in S-phase (EDU+ve, 4n) or those which had progressed through the G2 check point and undergone mitosis (EDU+ve, 2n) (Fig 4.5).

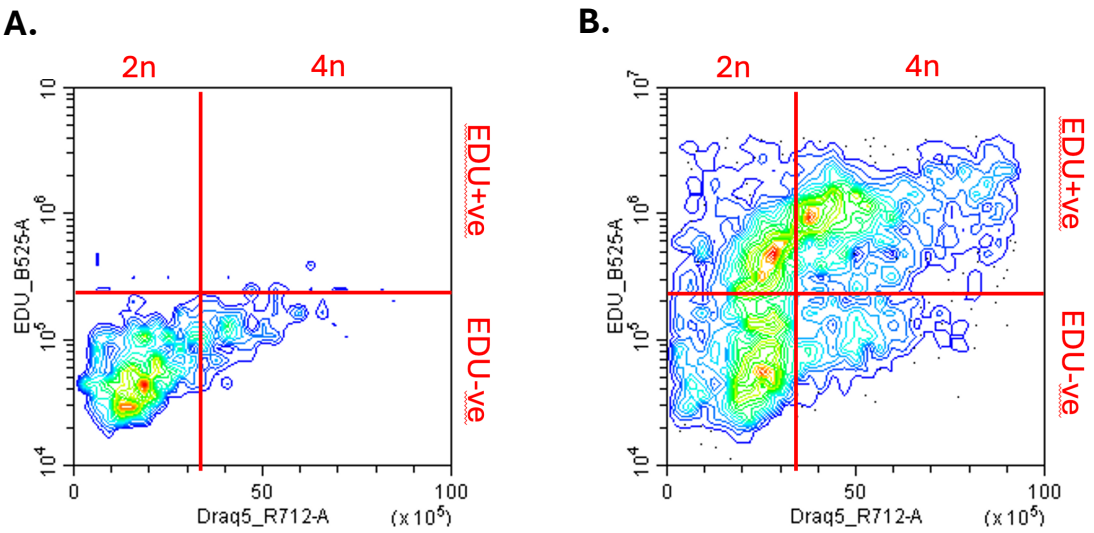


Figure 4.5. Representative flow cytometry outputs. (A) Negative EDU control used to establish gating strategy. **(B)** Example of output from cells stained with EDU and DRAQ5 showing EDU+ve. 2n and 4n populations.

Labelled cells were counted by the flow cytometer, thereby allowing us to initially calculate the total proportion of cells which had incorporated EDU at each measured time point. At D5+1, a one-way ANOVA highlighted that significantly fewer α7 KO and DKO cells had incorporated EDU (n = 4, f = 5.149, p = 0.0162), however there was no significant difference in the proportion of cells which had incorporated EDU at either D5+2 (n = 4, f = 0.617, p = 0.623) or D5+3 (n = 4, f = 1.222, p = 0.363) (Fig. 4.6). We then calculated the mean proportion of EDU+ve cells across all three time points which had returned to a diploid state. Allowing assessment of each genotype in terms of G2 checkpoint progression within the 8-hour EDU incubation period. A one-way ANOVA showed a significantly reduced proportion of EDU+ve α7 KO (9.6%) and DKO (8.4%) cells passed the G2 checkpoint and successfully divided compared to either control (31.5%) or α5 cKO (25.4%) cells (n = 4, f = 25.04, p = <0.0001). A post-hoc Tukey's test however showed no significant difference between the control and α5 cKO or the α7 KO and DKO in terms of cell cycle progression (Fig. 4.7).

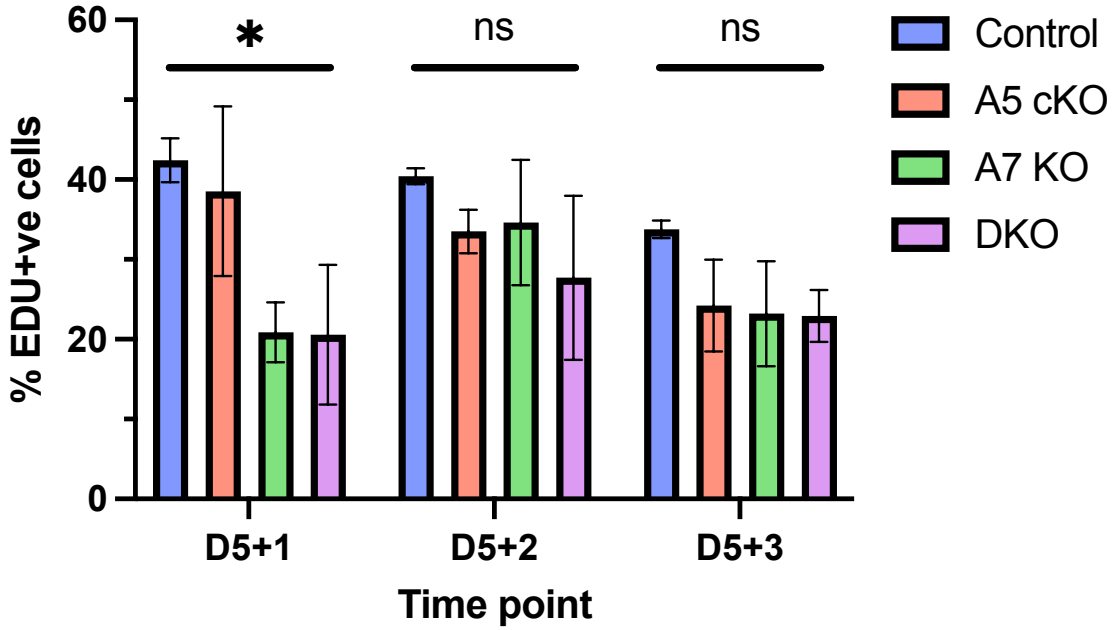


Figure 4.6. Loss of integrin α7 slows cell cycle entry. Mean (+SEM) percentage of cells which have incorporated EDU during S-phase of the cell cycle. At D5+1 significantly fewer α7 KO and DKO cells have initiated S-phase (n = 4 mice). By D5+2 and D5+3 no significant differences were observed.

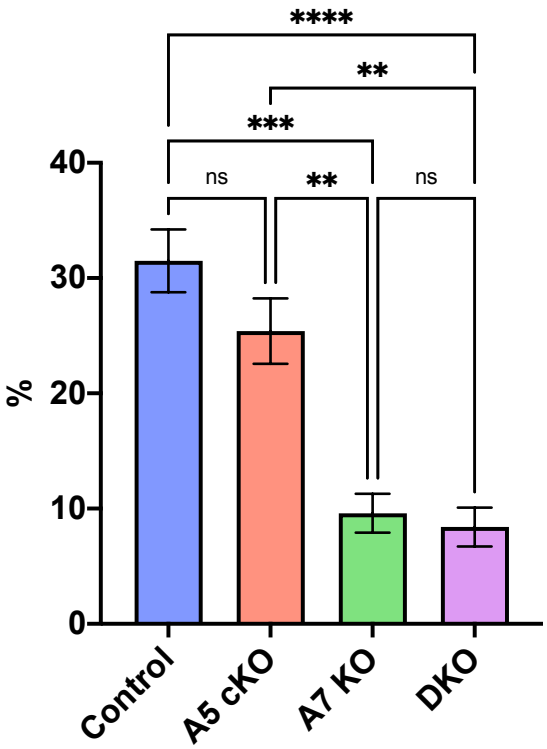


Figure 4.7. The loss of integrin α7 results in reduced cell cycle completion. Mean (+SEM) percentage of cells which returned to a diploid state (2n) after EDU incorporation during S-phase of the cell cycle (n = 4 mice).

4.6. Summary.

The aim of this chapter was to investigate potential mechanistic reasons for the impaired regeneration observed in the previous chapter. We wanted to establish whether SC kinetics and dynamics were negatively affected by the loss of integrins α5β1 and / or α7β1, and if so to what extent. However, before progressing, we initially need to address the obvious gap in our knowledge regarding integrin α5 expression in SCs.

Immunostaining of isolated myofibres and their associated SCs clearly demonstrated that integrin α5 is not expressed in quiescent or recently activated SCs, but that it becomes upregulated between 24 – 48 hrs after activation. This correlates with the rapid proliferative expansion of the myoblast population after injury in vivo, and the approximate timing of the first cell division observed ex vivo.

Time lapse video analysis then demonstrated significant differences in both SC migration speed and mitotic potential. When cells are lacking integrin α7β1, migration speed was negatively affected, whilst α7 KO and DKO cells underwent significantly fewer cell divisions than either control or α5 cKO cells.

Finally, we demonstrated using flowcytometry, that when cells lack integrin $\alpha 7\beta 1$ a smaller proportion were able to proceed from S-phase and fully complete cytokinesis. We demonstrated that there was no difference in the timing of cell divisions between any of the four groups ex vivo, so any delay in cell cycle progression points to a more systemic problem with mitosis after S-phase. The reduced migration speed and proliferative defects observed during this chapter is strong evidence that impaired SC function, as a result of integrin deficiency, contributes to the reduced regenerative capacity observed in chapter 3.

Chapter 5.

Integrin α5β1 and α7β1 regulate proper SC differentiation and self-renewal.

5.1. Introduction.

Previous chapters have shown that integrins α5β1 and α7β1 are essential for muscle regeneration, whilst only α7β1 is a requirement for efficient SC migration and proliferation. Given that the DKO displays such a severe phenotype and integrin α5 expression comes after SC activation, we wanted to investigate how integrin deficiency affects total SC number over time and if it influences the molecular signature of SCs and myoblast as they differentiate. This was achieved by isolating individual myofibres and their associated SCs from dissected EDL muscles. Myofibres were then placed into differentiation media and fixed at specific time points (0, 24, 48, 72 and 96 hrs after isolation) (Fig. 5.1.). Once fixed, SCs and their progeny were stained against a combination of MRFs and counted at each time point, allowing us greater insight into whether integrin deficient SCs proliferate and differentiate appropriately once activated compared to each other and controls.

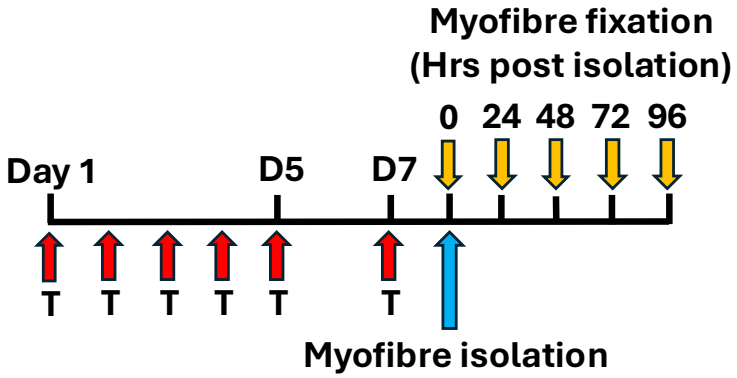


Figure 5.1. Tamoxifen and myofibre isolation protocol. The timings of tamoxifen injections, myofibre isolation and fixation. T = Tamoxifen.

The processes of activation, proliferation, self-renewal and differentiation are mediated by the sequential expressions of specific MRFs, Pax7, Myf5, MyoD and MyoG mark transitions between each stage in the regenerative differentiation pathway. Each has been extensively studied, and their timing and function is well characterised, as shown in figure 5.2. Pax7 is ubiquitously expressed in all quiescent SCs, and whereas Myf5 mRNA transcripts are found in the majority, Myf5 protein levels vary whilst SCs maintain quiescence (Beauchamp et al., 2000). By 24 hrs after activation Myf5 expression becomes consistent and MyoD expression has been upregulated. At around 48 hrs after activation, expression of Pax7 starts to reduce as the majority of cells become committed to a myogenic

fate, however around 10% will adopt a Pax7+ / MyoD- profile, returning to quiescence in order to repopulate the SC niche (Zammit et al., 2004). By 72 hrs after activation, Myf5 expression is downregulated whilst MyoG expression is upregulated (Zammit., 2017), signalling terminal differentiation into myotubes prior to fusion and extension to form myofibres.

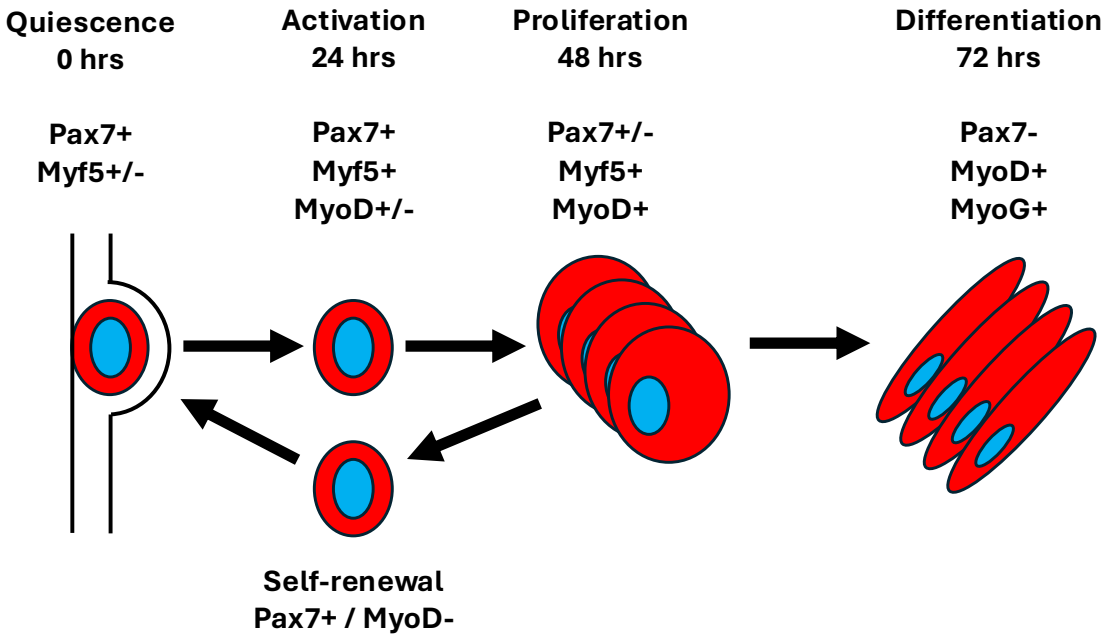


Figure 5.2. Expression of MRFs in SCs and progeny during activation, proliferation and differentiation. Quiescent SCs express Pax7, the majority also express Myf5. Upon activation SCs begin to express MyoD, myogenic commitment is triggered by the downregulation of Pax7, starting at around 48 hrs after activation. A small proportion become destined to replenish the quiescent stem cell population by maintaining Pax7 expression and downregulating MyoD. Those committed to myogenesis start to express MyoG, signalling myogenic progression prior to terminal differentiation and fusion.

5.2. Ex-vivo SC proliferation is particularly dependent upon integrin α7β1.

SCs were previously counted in sections of uninjured muscle and at 10 and 30 DPI, giving us data on how SC numbers change in vivo across the entire regenerative process. Here, total number of myofibre associated muscle progenitors were counted every 24 hrs in each of the four groups, during the first 96 hrs after activation to give us a clearer picture how integrin deficiency affected their dynamics upon activation and during differentiation.

Immediately after isolation, at T0, a one-way ANOVA showed significant differences in the number of SCs on each fibre between the four groups ($n = 5$, $f = 18.7$, $p = <0.0001$). However, a post-hoc Tukey's test showed no significant

difference between either the Control and α5 cKO (n = 5, p = 0.594) or α7 KO and DKO (n = 5, p = 0.956), demonstrating pre-activation numbers of myofibre associated SCs are reduced when integrin α7 is absent. At T24, the same pattern was apparent, there were significantly less α7 KO and DKO SCs compared to either the α5 cKO or control groups (n = 5, f = 19.54, p = <0.0001). By T48, SCs in the control and α5 cKO groups had clearly started to proliferate more rapidly, increasing in number 2.80-fold and 2.72-fold respectively, whilst the α7 KO and DKO had increased by only 2.33-fold and 2.40-fold respectively. A one-way ANOVA again displayed a significant difference between the four groups (n = 5, f = 68.58, p = <0.0001), however there was also a significant difference between the α5 cKO and control at this time point (n = 5, p = 0.0178). By T72 there was still no difference between the number of myogenic progenitors in the α7 KO and DKO (n = 5, p = 0.9472), however, the difference in cell numbers had become more exaggerated between the α5 cKO and control (n = 5, p = 0.0002). By T96, although still significantly different from each other (n = 5, p = 0.0009), both the control and α5 cKO cells had proliferated almost exponentially. showing a 13-fold and 12-fold increase respectively compared to numbers at T0. Although the α7 KO and DKO did proliferate to some extent, it was only a 7-fold increase in the α7 KO and 8-fold increase in the DKO. So not only did they have fewer cells to begin with, the α7 KO and DKO cells proliferated at a slower rate than the α5 cKO or control.

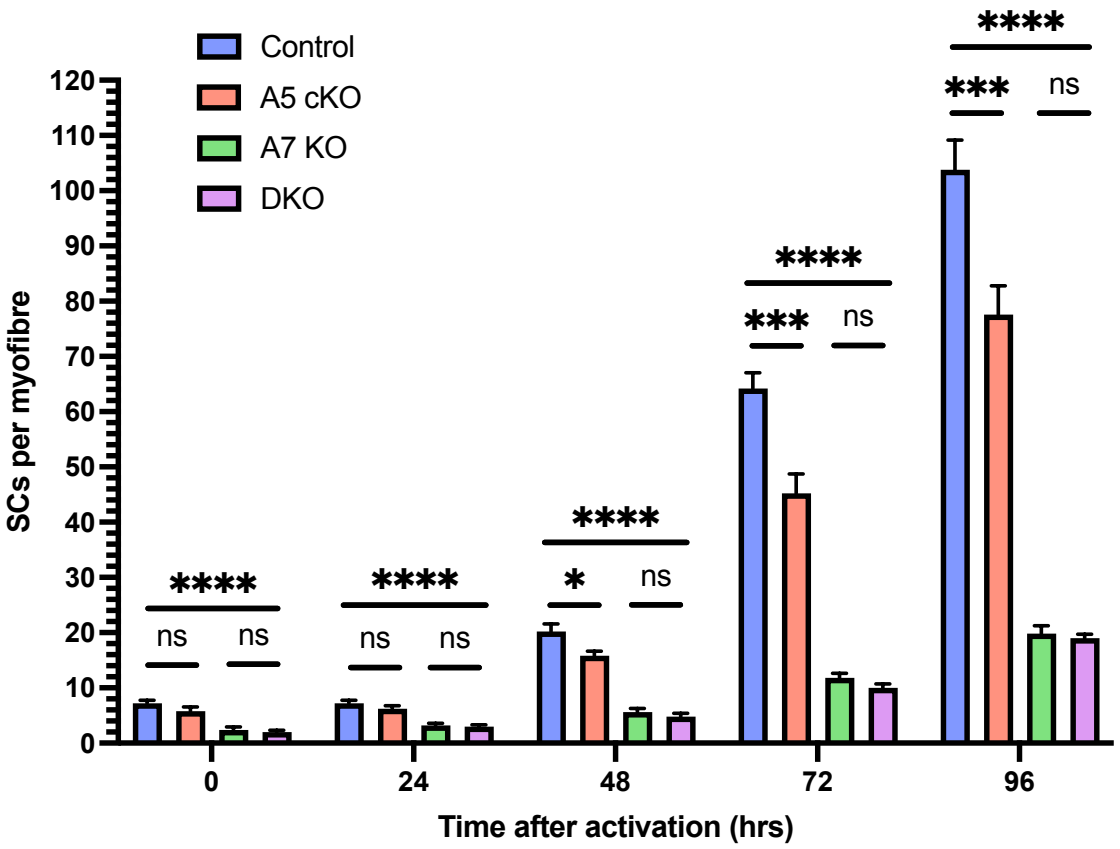


Figure 5.3. Integrin α7 is a requirement for efficient SC proliferation. Mean (+ SEM) number of SCs on isolated EDL myofibres at T0, T24, T48, T72 and T96 after isolation in control (blue), α5 cKO (red), α7 KO (green) and DKO (purple), n = 5 mice.

5.3. Expression of Pax7 and Myf5 in quiescent SCs.

Pax7 is known to be ubiquitously expressed in quiescent SCs, whilst the majority of SCs tend to have some level of Myf5 expression, although it is absent in approximately 10% during quiescence. Immunostaining of isolated EDL myofibres and fluorescence microscopy was used to determine whether Pax7 and Myf5 were properly expressed at T0, as shown if figure 5.4A. Pax7 expression was unsurprisingly seen in 100% of cells at this time point, however, Myf5 expression was observed in significantly higher proportion of cells which lacked integrin α5 and / or integrin α7 (Fig. 5.4B &C), potentially indicating fewer stable stem cells and a higher proportion of 'primed' quiescent cells.

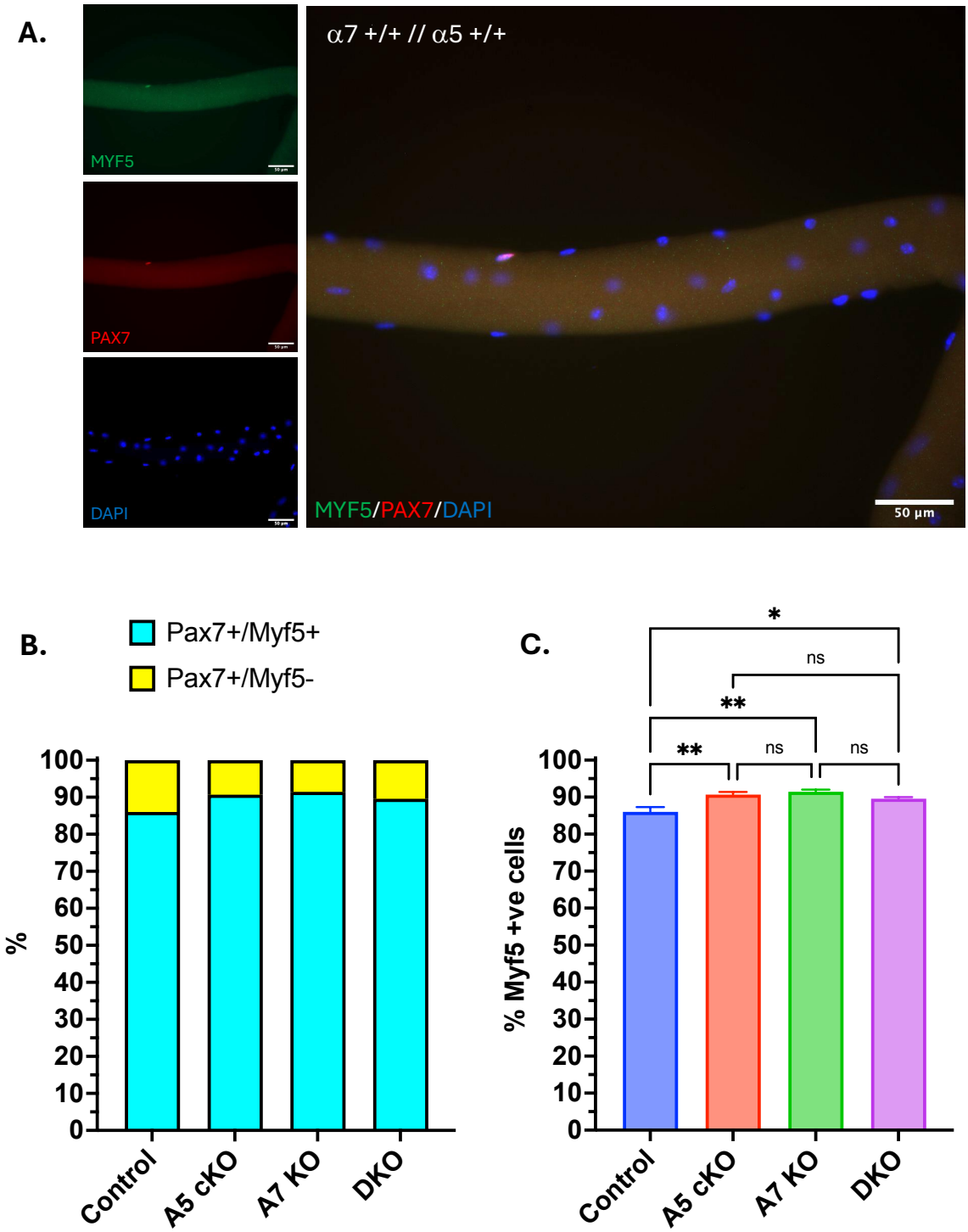


Figure 5.4. Integrin deficiency increases Myf5 expression in quiescent SCs. **(A)** Representative images of isolated EDL myofibres and quiescent SCs immunostained against Pax7 and Myf5 at T0. Scale bar = 50 µm **(B)** Stacked bar chart shows proportional expression of Pax7 and Myf5 at T0 **(C)** Mean (+SEM) percentage of Myf5 +ve SCs per fibre at T0, n = 5 mice.

5.4. Expression of Pax7, Myf5 and MyoD in activated SCs at 24 hrs after isolation.

Upon activation, SCs exit quiescence and enter interphase of the cycle cycle. At this point they migrate out of the BM prior to growth and migration to the site of any injury. Myf5 expression becomes consistent, whilst MyoD expression is upregulated as cells prepare for S-phase and subsequent proliferation. Immunostaining of isolated EDL myofibres and associated activated SCs was used to highlight differences in the temporal expression of Pax7, Myf5 and MyoD at T24 (Fig5.5).

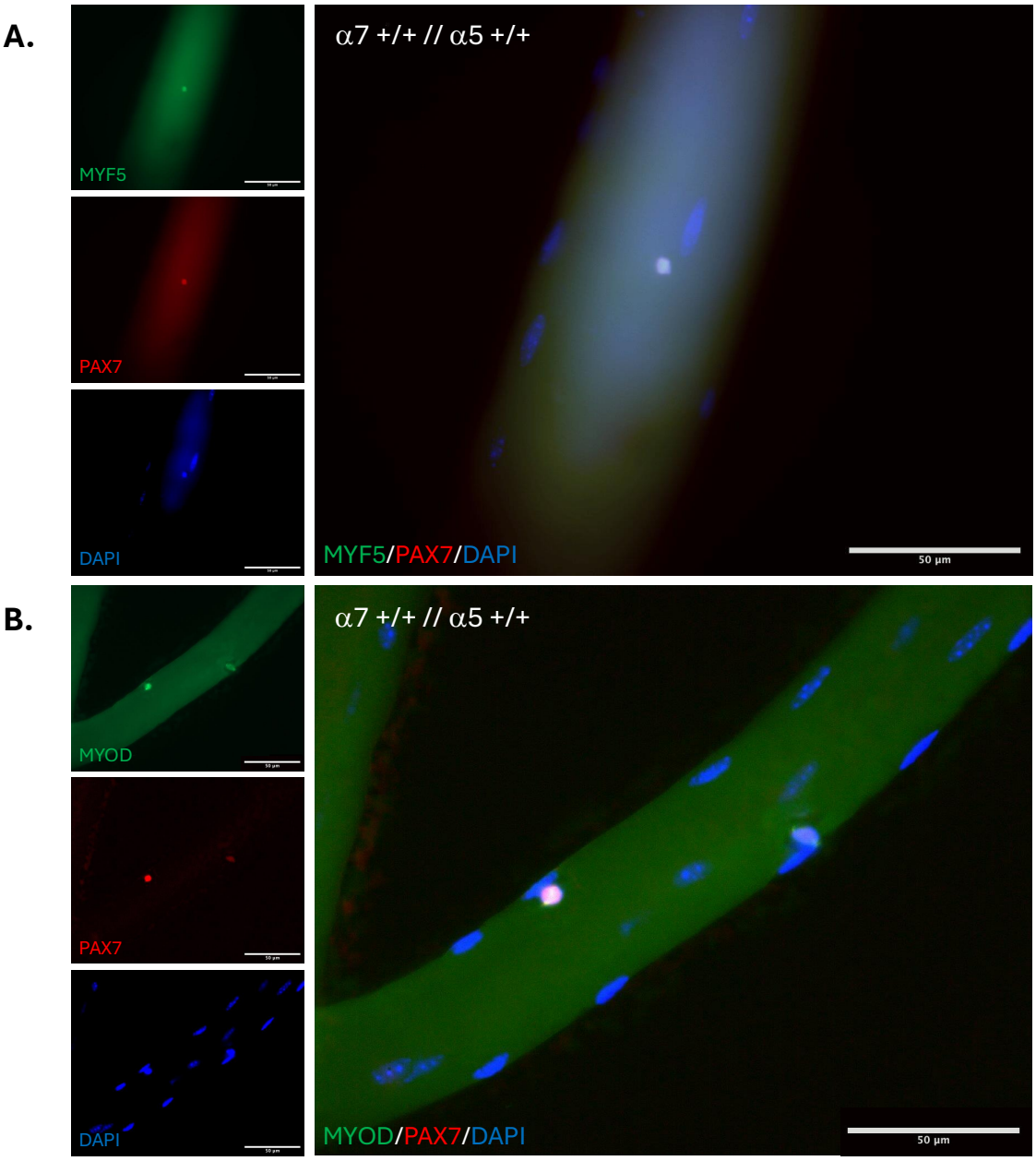


Figure 5.5. Representative images of isolated EDL myofibres and activated SCs immunostained against Pax7, Myf5 and MyoD at T24. (A) Myf5 (Green), Pax7 (Red) and DAPI (Blue). **(B)** MyoD (Green), Pax7 (Red) and DAPI (Blue). Scale bars = 50 µm.

Although significant differences in the mean number of SCs per myofibre were apparent at T24 (n = 5, f = 19.54, p = <0.0001), (Fig. 5.3), a one-way ANOVA highlighted no significant difference in the proportion of activated SCs which express either Pax7 (n = 5, f = 1.977, p = 0.1582) or Myf5 (n = 5, f = 0.902, p = 0.4619), data not shown. In contrast, all integrin KOs showed significantly reduced numbers of MyoD +ve SCs at T24 (n = 5, f = 13.58, p = <0.0001), (Fig. 5.6B), indicating that although activated, there may be delayed growth and proliferation.

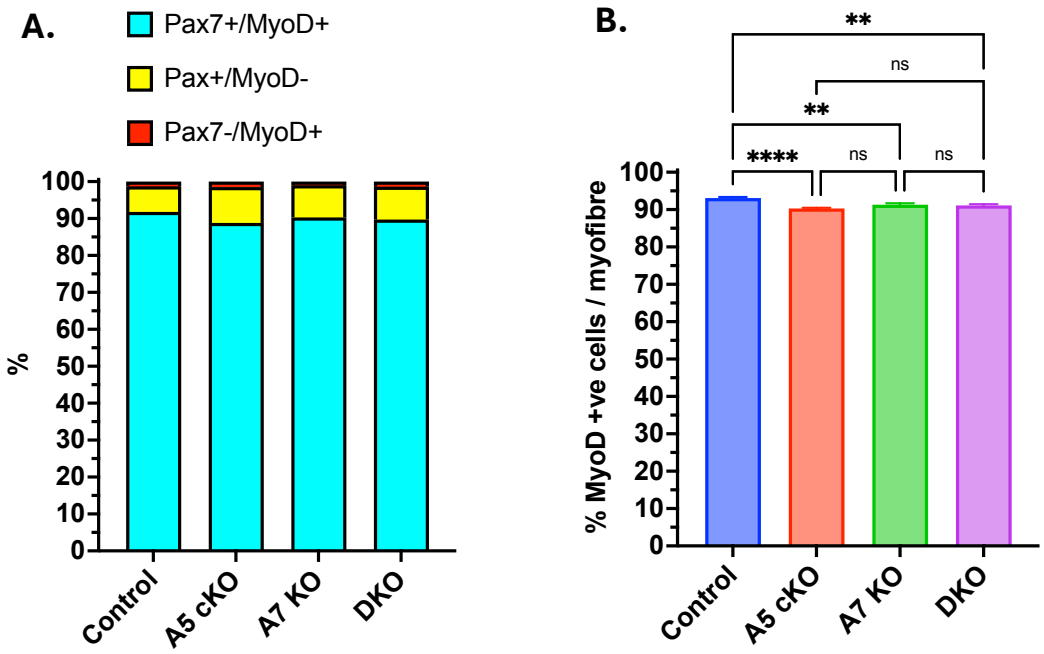


Figure 5.6. Loss of integrins results in fewer MyoD +ve SCs at T24. (A) Stacked bar chart shows proportional expression of Pax7 and MyoD at T24 **(B)** Mean (+SEM) percentage of MyoD +ve SCs per myofibre at T24, n = 5 mice**.**

5.5. Expression of Pax7, MyoD and MyoG in myogenic progenitors at 48 hrs after isolation.

Proliferating myoblast express MyoD (Fig. 5.7) and those that commit to myogenesis start to downregulate Pax7 as they differentiate. Induction of MyoG marks the initiation of terminal differentiation. However, a subset will maintain Pax7 expression becoming Pax7+ / MyoD- to repopulate the stem niche for future rounds of regeneration.

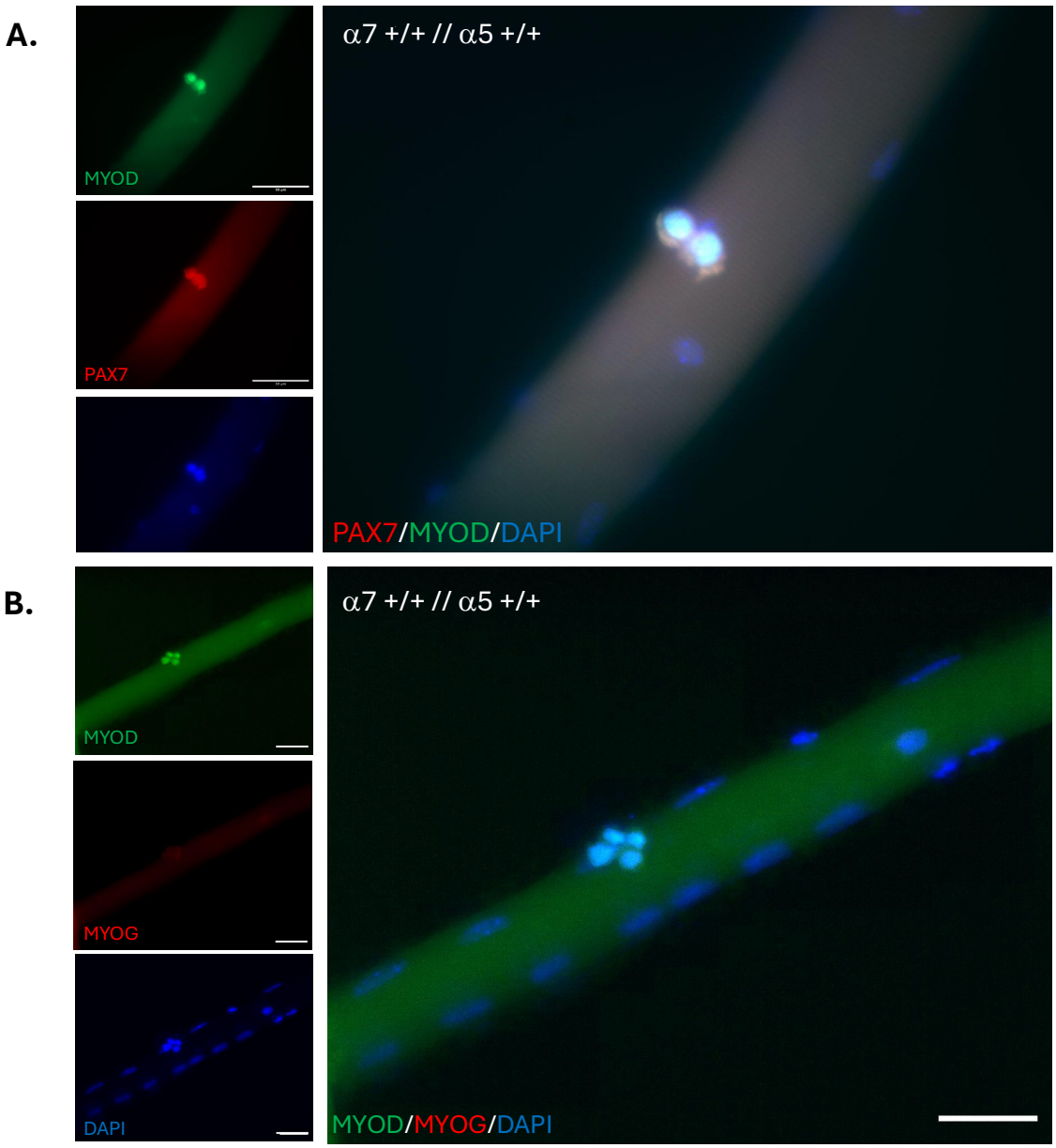


Figure 5.7. Representative images of isolated EDL myofibres and proliferating myoblasts immunostained against Pax7, MyoD and MyoG at T48. (A) MyoD (Green), Pax7 (Red) and DAPI (Blue). **(B)** MyoD (Green), MyoG (Red) and DAPI (Blue). Scale bars = 50 μm.

At T48, as shown in figure 5.7, even though total cell numbers per fibre varied between groups (Fig. 5.3), there was no significant difference in the proportion of Pax7+ / MyoD+ cells ($n = 5$, $f = 0.1782$, $p = 0.9096$) (Fig. 5.8B) or Pax7- / MyoD+ cells ($n = 5$, $f = 1.365$, $p = 0.2892$) (Fig.5.8C). A significant difference was observed in the Pax7+ / MyoD – population though ($n = 5$, $f = 8.336$, $p = 0.0014$). An ad-hoc Tukey test revealed that myofibres from mice lacking integrin α7 (α7 KO and DKO) had proportionally less MyoD- cells at this time point (Fig. 5.8D).

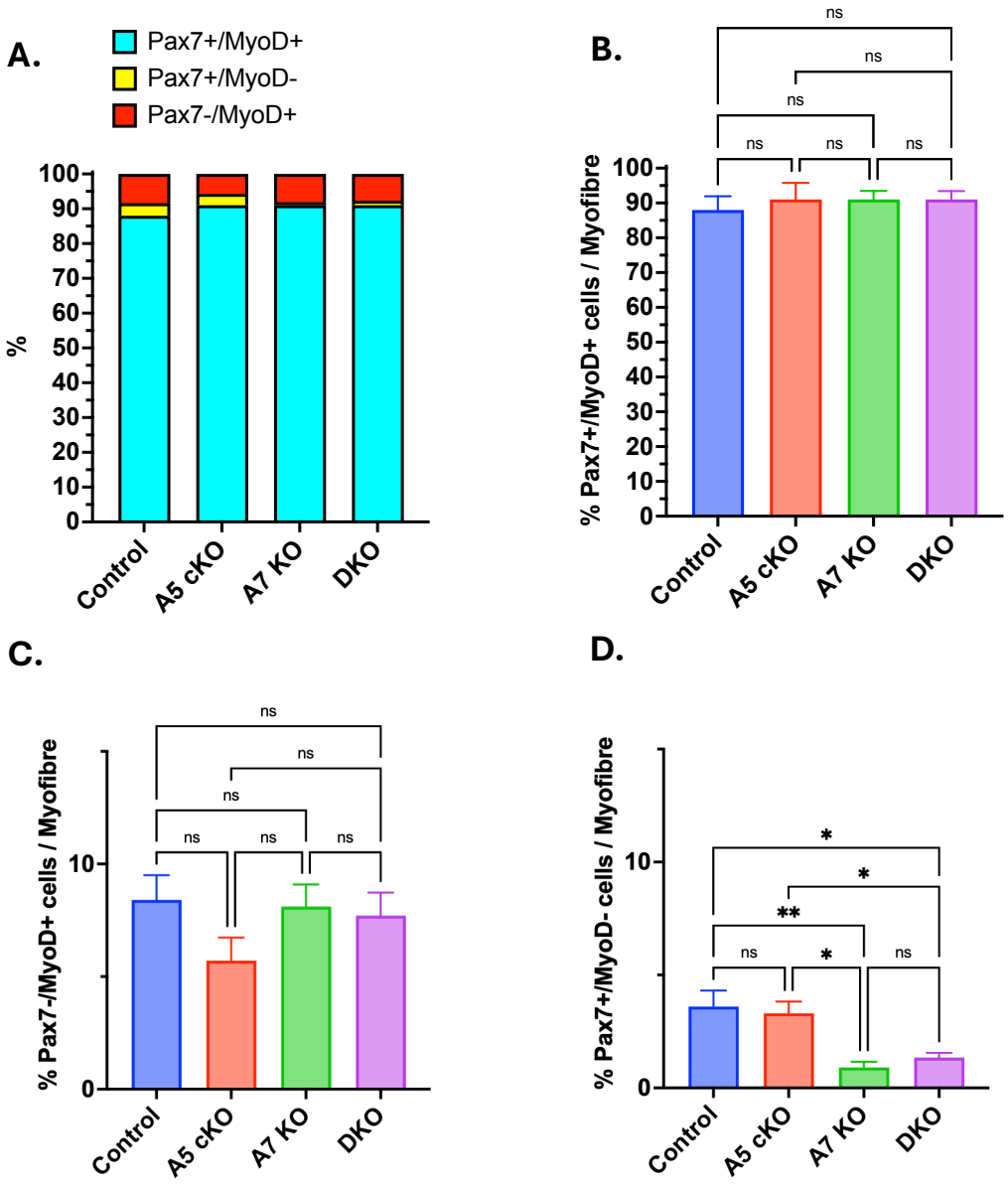


Figure 5.8. Loss if integrin α7 results in fewer Pax7 +ve / MyoD -ve myoblasts at T48. (A) Stacked bar chart shows proportional expression of Pax7 and MyoD at T48. **(B)** Mean (+SEM) percentage of Pax7 +ve / MyoD +ve cells per myofibre at T48**. (C)** Mean (+SEM) percentage of Pax7 -ve / MyoD +ve cells per myofibre at T48. **(D)** Mean (+SEM) percentage of Pax7 +ve / MyoD -ve cells per fibre at T48, n = 5 mice**.**

At T48, as shown in Fig 5.7, the majority of cells were MyoD+ / MyoG- (Fig. 5.9A & B). Immunostaining revealed approximately 5% of control and integrin α7 KO cells were MyoD+ / MyoG+ (Fig. 5.9C), indicating committed myogenic progression. However, MyoG expression was significantly reduced in α5 cKO cells compared to controls (n = 5, p = 0.0006) and notably completely absent in DKO cells (Fig 5.9C). There was also a significant difference in the proportion of MyoD- / MyoG- cells in both the α7 KO and DKO (n = 5, f = 7.357, p = 0.0026)

(Fig. 5.9D), these double negative cells would presumably be Pax7+ and destined for self-renewal.

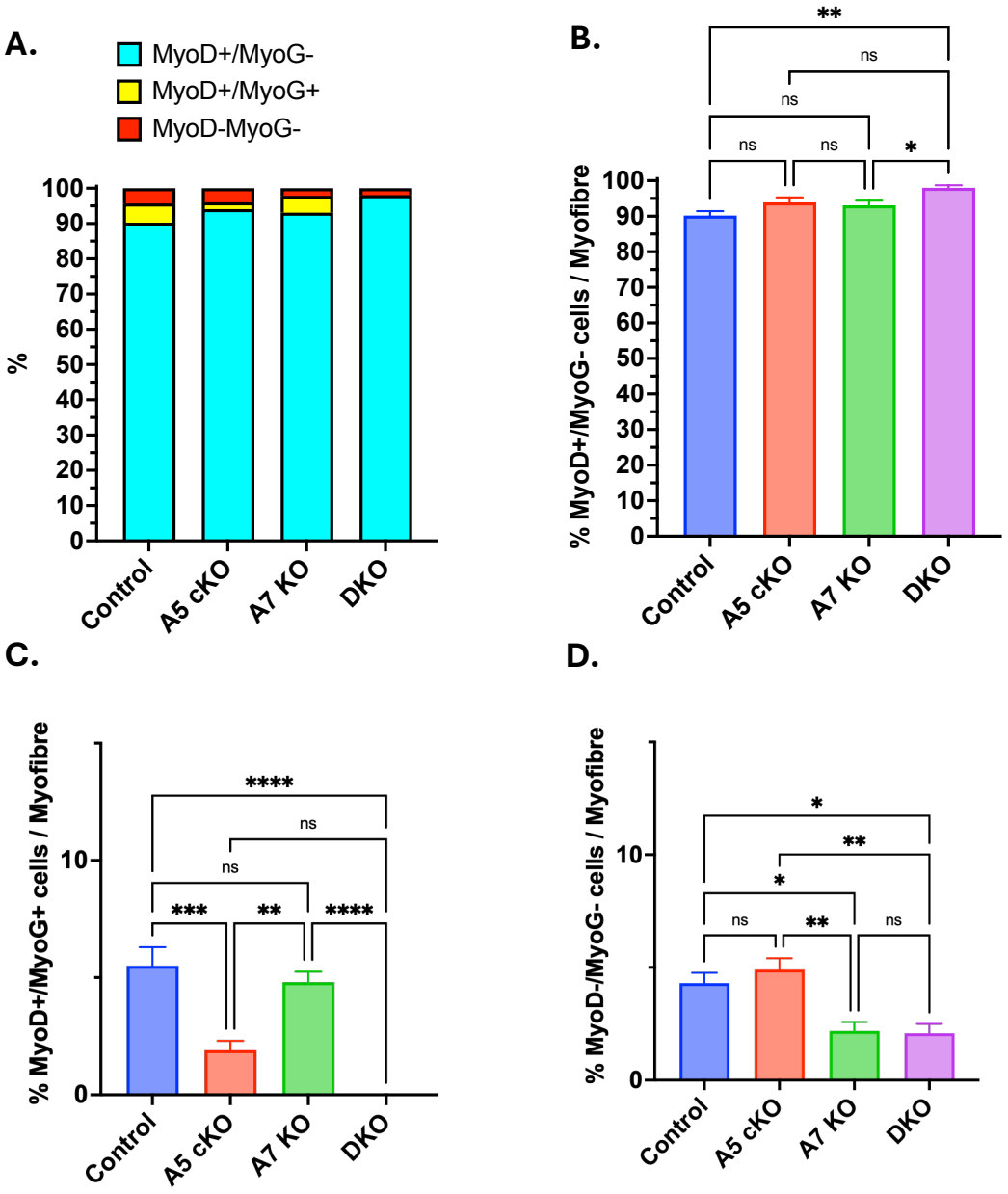


Figure 5.9. Loss of integrin α5 results in fewer MyoG +ve myoblasts at T48. **(A)** Stacked bar chart shows proportional expression of MyoD and MyoG at T48. **(B)** Mean (+SEM) percentage of MyoD +ve / MyoG -ve cells per fibre at T48. **(C)** Mean (+SEM) percentage of MyoD +ve / MyoG +ve cells per fibre at T48. **(D)** Mean (+SEM) percentage of MyoD -ve / MyoG -ve cells per fibre at T48, n = 5 mice.

5.6. Expression of Pax7, MyoD and MyoG in myogenic progenitors at 72 hrs after isolation.

Differentiating myoblast express MyoD and MyoG, whilst Pax7 becomes downregulated as cells progress towards terminal differentiation. Significant

differences in total cell number became more exaggerated at T72 (Fig 5.3.) and coimmunostaining of isolated fibres and associated cells with Pax7 and MyoD or MyoD and MyoG was again used to highlight differences in proportional MRF expression as myoblasts proliferate and differentiate (Fig. 5.10.).

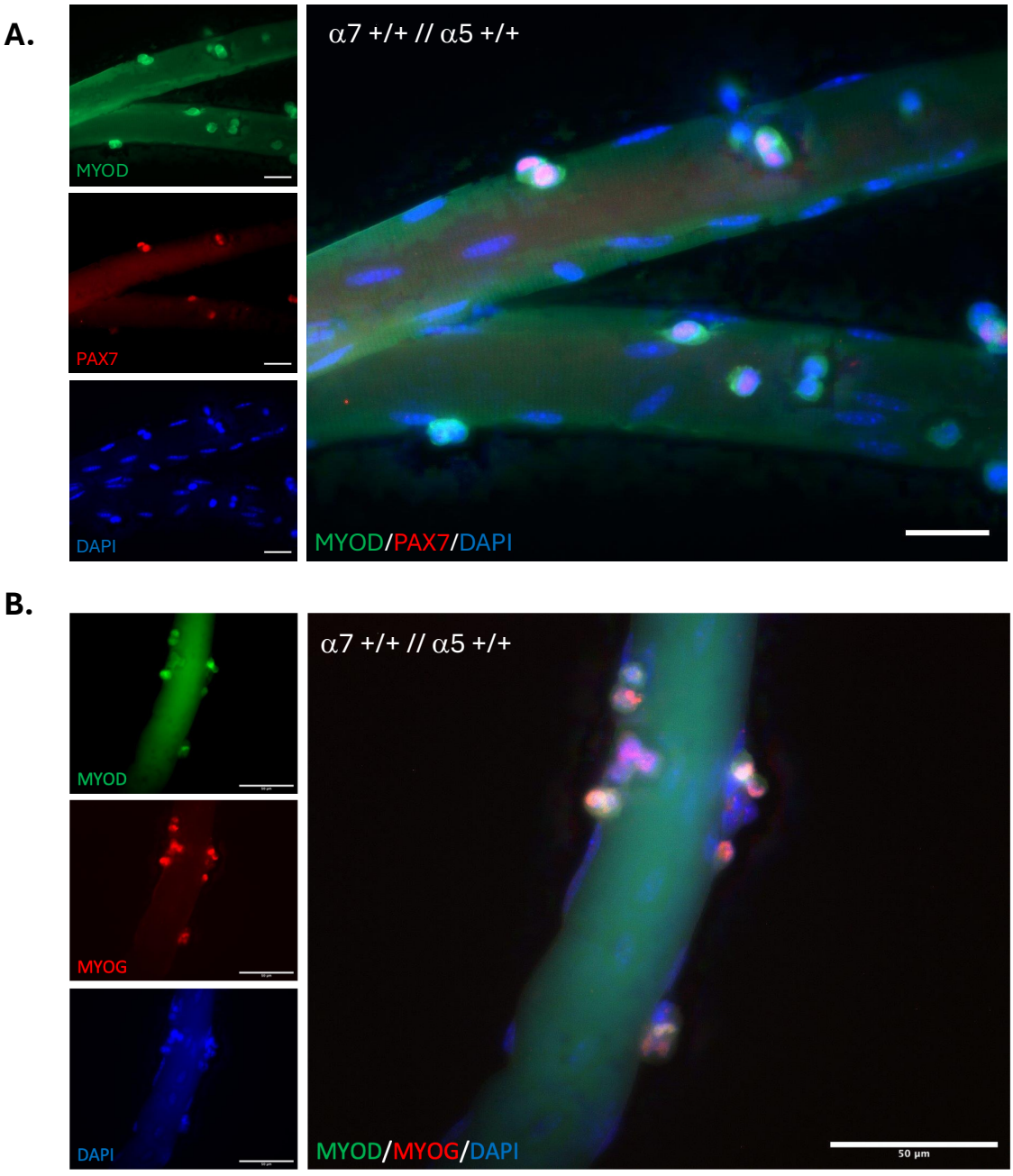


Figure 5.10. Representative images of isolated EDL myofibres and proliferating myoblasts immunostained against Pax7, MyoD and MyoG at T72. (A) MyoD (Green), Pax7 (Red) and DAPI (Blue). **(B)** MyoG (Green), MyoD (Red) and DAPI (Blue). Scale bars = 50 µm.

At T72, although control and α5 cKO mice exhibit significantly more myoblasts per myofibre (Fig. 5.3), the number of Pax7- cells had increased proportionally in all four groups compared to previous time points (Fig. 5.11A), indicating myogenic progression and commitment. Across the four groups, the majority of all cells were still MyoD+, a one-way ANOVA showed a significant difference in the proportion of MyoD+ cells between the DKO and control (n = 5, f = 3.958, p = 0.0275), (Fig. 5.11B). However, significant differences also persisted in the proportion of Pax7- / MyoD- cells (n = 5, f = 20.05, p = <0.0001), (Fig. 5.11C) and Pax7+ /MyoD- cells which would be destined for self-renewal (n = 5, f = 25.85, p = <0.0001), (Fig.5.11D).

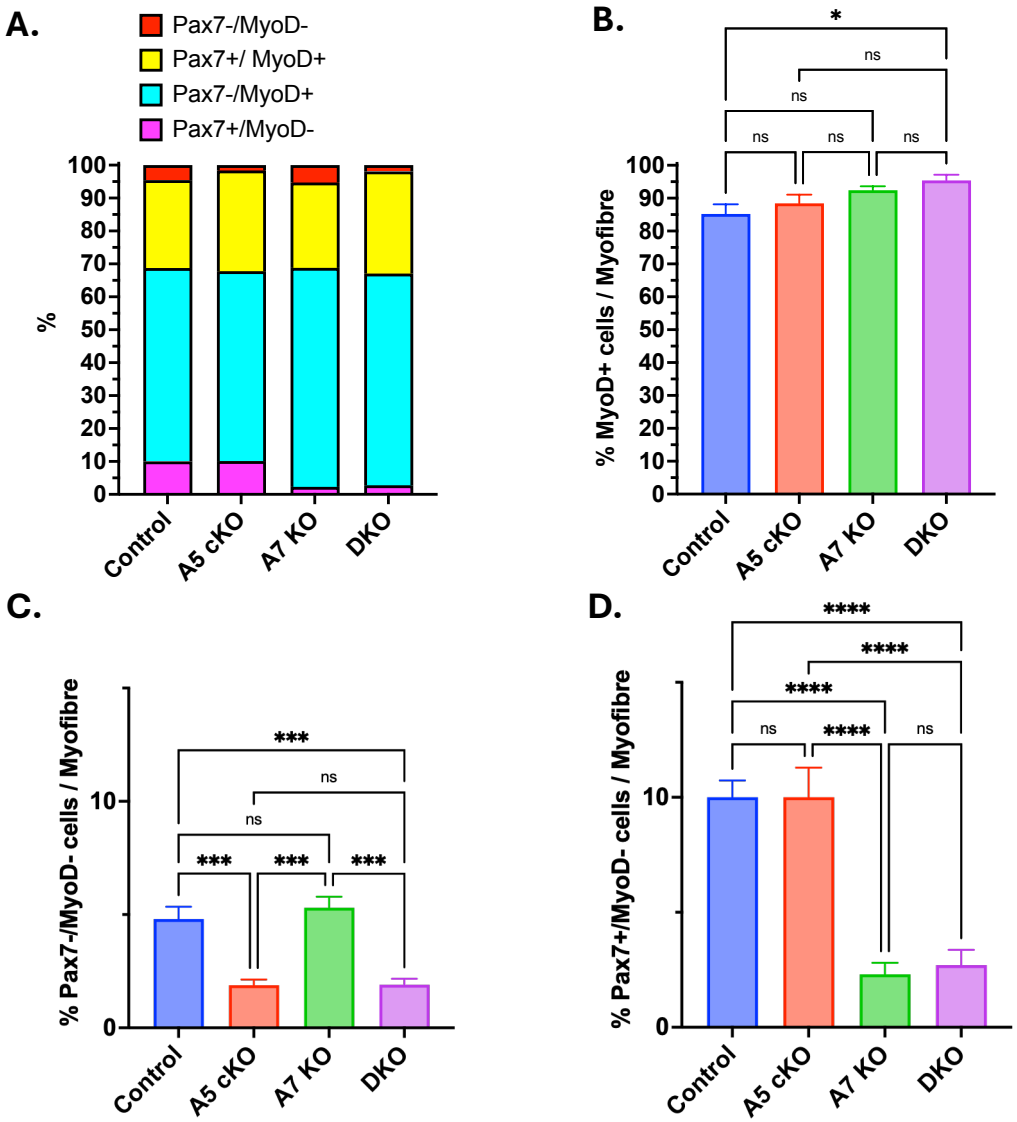


Figure 5.11. Loss of integrins results in fewer MyoD -ve myoblasts at T72. **(A)** Stacked bar chart shows proportional expression of Pax7 and MyoD at T72. **(B)** Mean (+SEM) percentage of MyoD +ve cells per fibre at T72. **(C)** Mean (+SEM) percentage of Pax7 -ve / MyoD -ve cells per fibre at T72. **(D)** Mean (+SEM) percentage of Pax7 +ve / MyoD -ve cells per fibre at T72, n = 5 mice.

Coimmunostaining against MyoD and MyoG (Fig. 5.10B) confirmed that the majority of cells are still MyoD+ at this time point (Fig. 5.12A). However, the proportion MyoG+ cells was significantly reduced when integrin α5 was absent (n = 5, f = 15.9, p = <0.0001), (Fig 5.12B). The proportion of MyoD- / MyoG- cells also closely matched the proportion of Pax7+ / MyoD- cells (Fig 5.11A & 5.12A), again demonstrating a reduced potential for self-renewal when integrin α7 is absent.

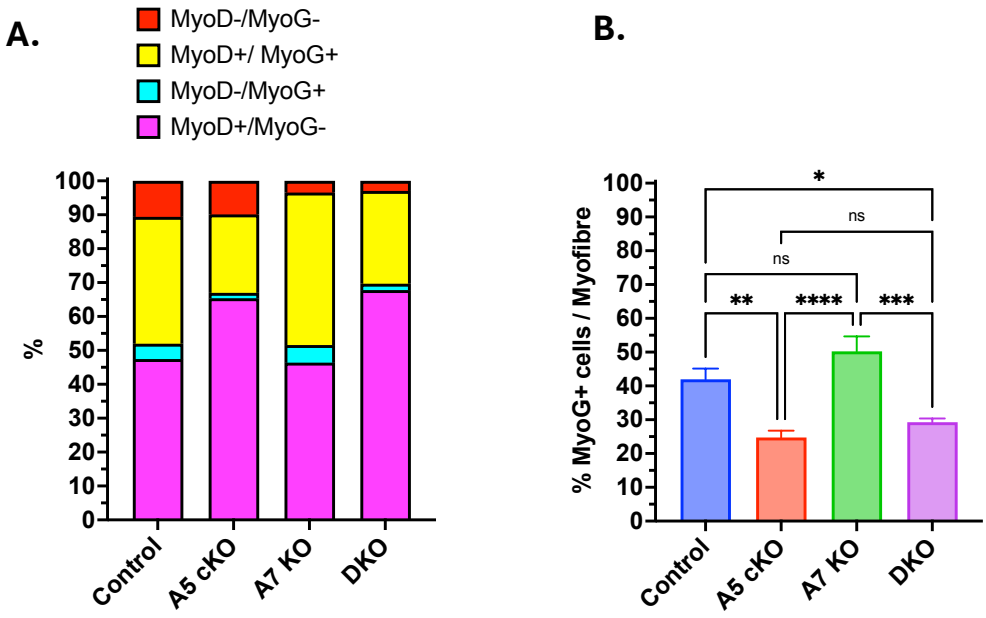


Figure 5.12. Loss of integrin α5 results in fewer MyoG +ve myoblast at T72. **(A)** Stacked bar chart shows proportional expression of MyoD and MyoG at T72. **(B)** Mean (+SEM) percentage of MyoG +ve cells per fibre at T72, n = 5 mice.

5.7. Expression of Pax7, MyoD and MyoG in myogenic progenitors at 96 hrs after isolation.

Coimmunostaining against Pax7 and MyoD (Fig. 5.13A) or MyoD and MyoG (Fig. 5.13B) allowed insight into the total number of cells and progression towards either terminal differentiation or self-renewal. At T96 there was huge disparity in total number of cells per myofibre, with significantly fewer integrin α7 KO or DKO cells visible (Fig. 5.3).

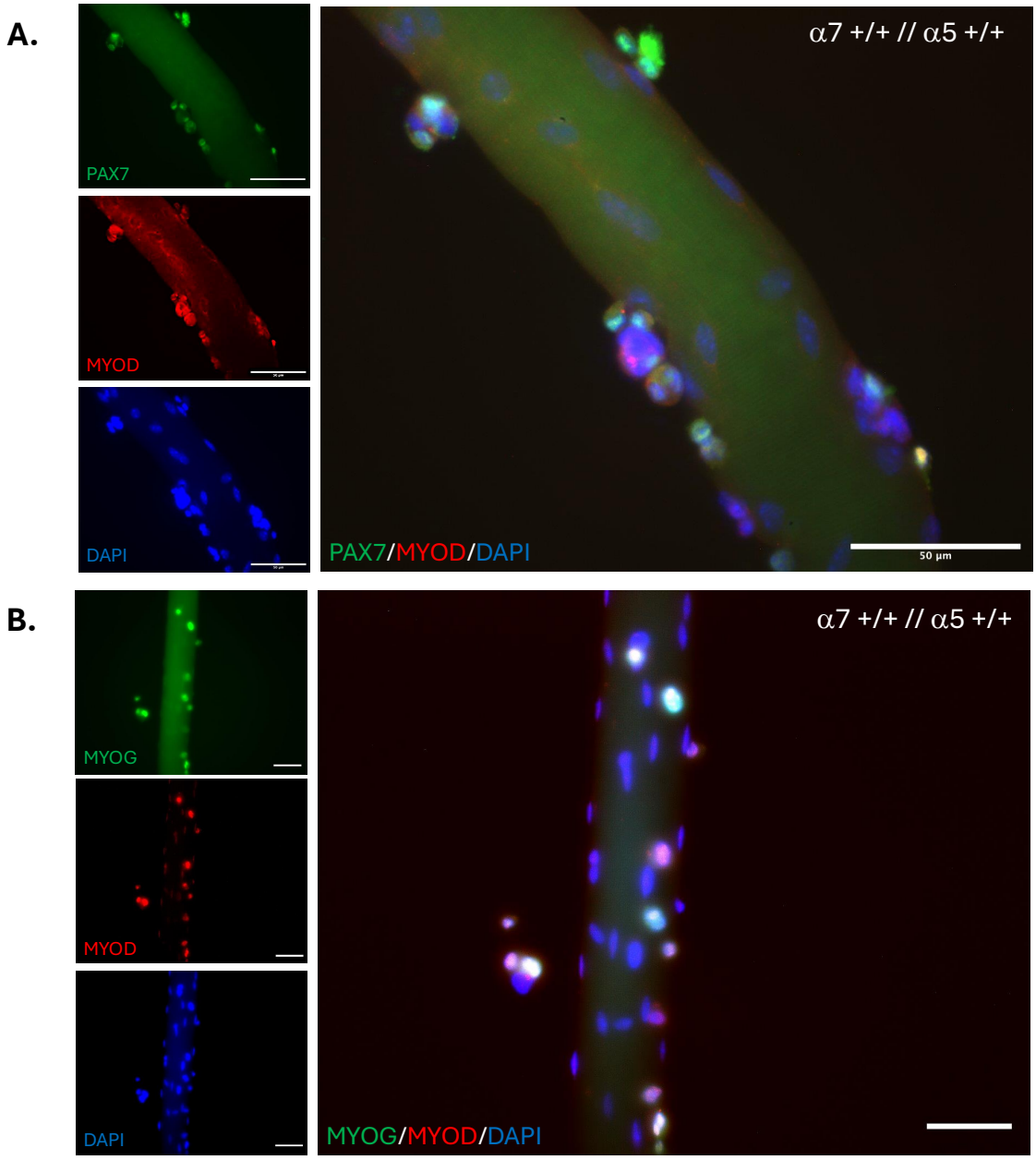


Figure 5.13. Representative images of isolated EDL myofibres and proliferating myoblasts immunostained against Pax7, MyoD and MyoG at T96. (A) Pax7 (Green), MyoD (Red) and DAPI (Blue). **(B)** MyoG (Green), MyoD (Red) and DAPI (Blue). Scale bars = 50 µm.

At T96 the majority of cells continued to express MyoD (Fig. 5.14A &B) and a one-way ANOVA and ad-hoc Tukey's test again highlighted a significant difference between the control and DKO in the proportion of MyoD+ cells ($n = 5$, $p = 0.0043$). However, the proportion of cells which maintained Pax7, to stay Pax7+ / MyoD+ was significantly greater in the integrin α5 cKO and DKO ($n = 5$, $f = 58.95$, $p = <0.0001$) (Fig. 5.14C), possibly indicating delayed myogenic progression. Although the number of Pax7+ / MyoD- cells had increased across

the four groups compared to other time points (Fig. 5.3), there was proportionally still significantly less cells displaying this 'stem cell' phenotype when integrin $\alpha 7$ was absent (n = 5, f = 31.01, p = <0.0001) (Fig. 5.14D).

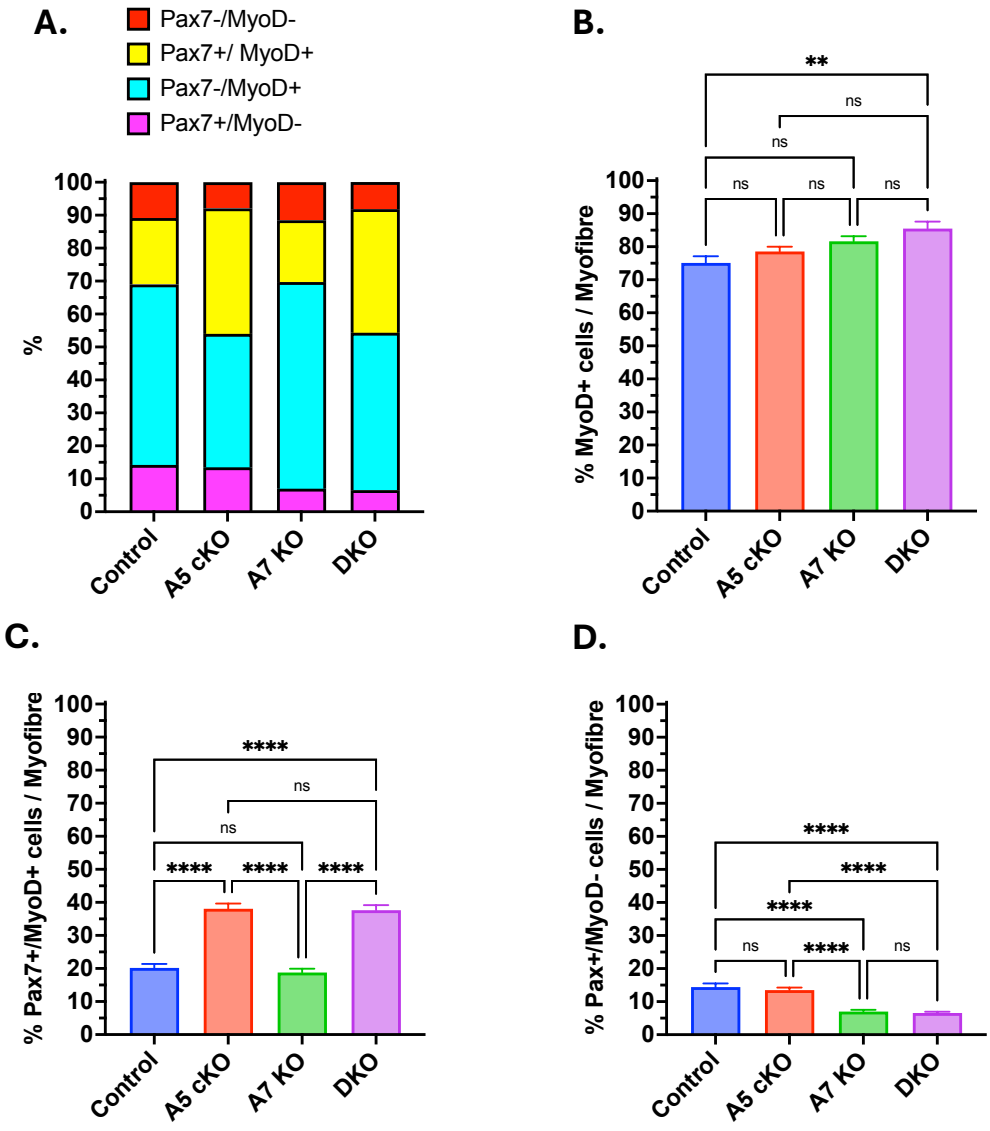


Figure 5.14. Loss of integrins slows myoblast differentiation and impairs self-renewal at T96. (A) Stacked bar chart shows proportional expression of Pax7 and MyoD at T96. **(B)** Mean (+SEM) percentage of MyoD +ve cells per fibre at T96. **(C)** Mean (+SEM) percentage of Pax7 +ve / MyoD +ve cells per fibre at T96. **(D)** Mean (+SEM) percentage of Pax7 +ve / MyoD -ve cells per fibre at T96, n = 5 mice.

Coimmunostaining against Myod and MyoG at T96 (Fig 5.13B) showed a greater proportion of cells had started to express MyoG across all four groups (Fig 5.15A). However, as at T72, the α5 cKO and DKO still had significantly less MyoG+ cells than either the control or α7 KO (Fig.5.15B).

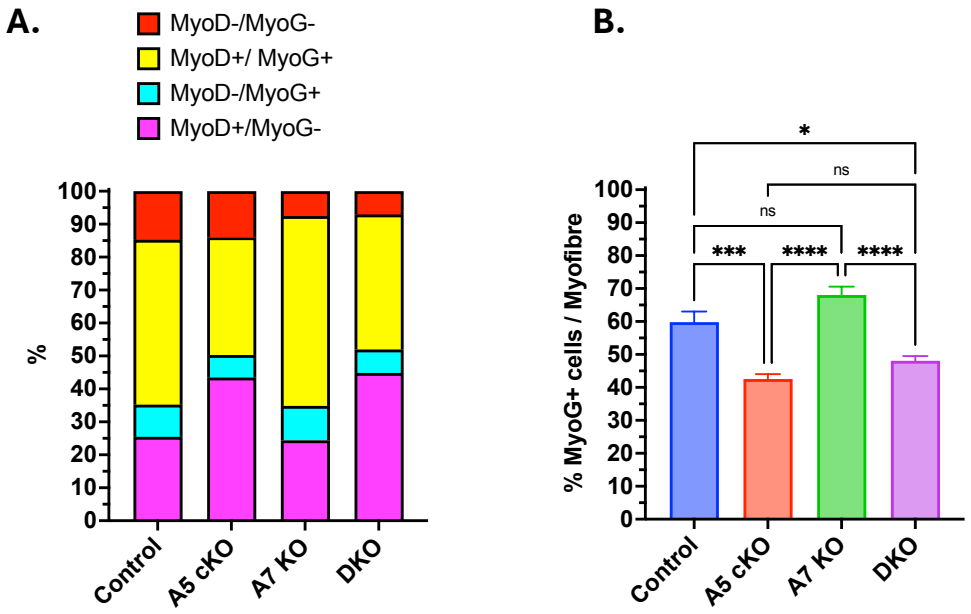


Figure 5.15. Loss of integrin α5 results in fewer MyoG +ve myoblast at T96. **(A)** Stacked bar chart shows proportional expression of MyoD and MyoG at T96. **(B)** Mean (+SEM) percentage of MyoG +ve cells per fibre at T96, n = 5 mice.

5.8. Summary.

The aim of this chapter was to investigate whether integrin deficiency in SCs affected the timing of key MRF expression, thereby altering the established progression of SCs and muscle progenitors as they proliferate and differentiate in response to activation. Differences in the rate of myogenic progression could contribute to the delayed or impaired regeneration observed in Chapter 3. We used single myofibre isolation, cell culture, coimmunostaining and fluorescence microscopy to label, visualise and count ex-vivo SCs and their progeny at set time points after activation.

It was immediately apparent that numbers of quiescent SCs were reduced when integrin α7 is absent, both the α7 KO and DKO mice displayed significantly fewer SCs per myofibre at T0, confirming the in-vivo data from Chapter 3. SCs lacking integrin α7 also proliferated at a reduced rate, which culminated as a huge

disparity in the total number of myogenic progenitors per myofibre at T96. This significant reduction in committed myogenic progenitors must be a contributing factor to the regenerative defect observed in the α7 KO and DKO mice. Although initially (T0) there was no significant difference between numbers of α5 cKO SCs and control SCs, the α5 cKOs did proliferate more slowly than controls, resulting in a significant difference by T48, which became exaggerated by T96.

At T0, integrin deficiency resulted in a greater proportion of Myf5+ SCs. The heterogeneity of Myf5 expression in quiescent SCs, is thought by some, to influence early fate decisions (Kuang et al., 2007). It is possible that Myf5+ cells are 'primed' ready to enter myogenesis, whereas Myf5- cells are more stable stem cells. By T24, no significant difference was apparent in terms of Pax7 or Myf5 expression. However, a greater proportion control SCs were MyoD+ than any of the integrin KOs. At T48 some key differences started to become apparent, the α7 KO and DKO displayed significantly reduced proportions of Pax7+ / Myod- cells, indicating a reduced potential for self-renewal, whilst the α5 cKO and DKO showed fewer MyoG+ cells, possibly indicating slightly delayed myogenic progression. These differences widened at later time points. By T72 and T96, it was clear that the loss of integrin α7 results in a significant reduction in the proportion of Pax7+ / MyoD- cells destined for self-renewal. Whilst the loss of integrin α5 results in delayed MyoG expression. A significantly higher proportion of cells lacking integrin α5 maintain a Pax7+ / MyoD+ phenotype for longer, limiting the induction of MyoG, which is a key requirement for myogenic progression and terminal differentiation.

Taking into account the reduced rates of proliferation, in conjunction with the differences in MRF expression, it is clear that integrin deficiency severely impacts SCs and impairs their normal function.

Chapter 6 .
Discussion & Conclusions.

6.1. Discussion.

Integrins α5β1 and α7β1 have been shown to play important roles in both muscle development and postnatal muscle homeostasis. The loss of integrin α5 is embryonically lethal (Yang et al,. 1993), whereas mice with chimeric expression of integrin α5 are viable but display signs of muscular dystrophy (Taverna et al., 1998). Integrin α7 KO mice have reduced numbers of live young and present with a dystrophic myopathy from around 3 weeks of age (Mayer et al., 1997). The integrin α7 KO mice also helped to illustrate a potential relationship between integrin α5β1 and α7β1 in skeletal muscle. In WT muscle integrin α5β1 is postnatally displaced by integrin α7β1 at the MTJ, however this integrin switch does not occur in the integrin α7 KO mice. Integrin α5 expression is instead maintained and induces an accumulation of fibronectin around the MTJ. The integrin α5β1 / fibronectin link represents an inferior gain of function compared to the integrin α7β1 / laminin link resulting in the phenotype observed by Mayer and colleagues (Nawrotzki et al., 2003) As yet, no study has sought to establish if the same mechanism exists in SCs, how SC function would be affected by the loss of one or both of these integrins, and in turn how this would impact adult muscle regeneration after an acute injury.

6.1.1. Impaired muscle regeneration after an acute injury in vivo.

Our in vivo injury model utilised α-SMA expression and quantification of regenerating myofibre size to demonstrate that although regeneration is delayed in the absence of either integrin α5β1 or integrin α7β1, there is a much more severe, prolonged regenerative defect when both integrins are absent. However, although scarce, the presence of newly formed centrally nucleated myofibres in DKO mice at 10 DPI suggests that myogenesis is not completely impaired. By 30 DPI the number of regenerating myofibres had increased, undergone a degree of hypertrophy and downregulated α-SMA but remained significantly smaller than controls. This could potentially be a result of reduced numbers of muscle progenitors, an inability for muscle progenitors to fuse with existing myofibres, or both. SC numbers were reduced in mice lacking integrin α7, both pre and post injury. Control and α5 cKO mice displayed a strong proliferative response to injury, whereas α7 KO and DKO did not. By 30 DPI SC numbers in vivo had returned to their pre-injury levels across all four groups Unfortunately we did not calculate

the fusion index as part of this study, so cannot say for certain if reduced myoblast fusion contributed to any regenerative defect.

At 10 DPI the α5 cKO mice displayed a relatively mild regenerative defect compared to either the α7 KO or DKO mice. The conditional nature of the α5 KO and acute nature of tamoxifen treatment raises questions in terms of protein turnover. Whilst the constitutive nature of the α7 KO raises further questions regarding the role of integrin α7β1 in the wider musculature, beyond SCs, and how this might also impact regeneration. Chapter 4 demonstrated that integrin α5 is only expressed after SC activation, for this reason we can be confident that the majority of SCs used in this study lack any integrin α5 protein because they only become activated upon isolation, by which point they have had an entire course of tamoxifen. However, a small population of cells may have been activated in vivo, prior to isolation, whereby small amounts of functional protein could potentially still be present in isolated SCs, which in theory could ameliorate the pathological severity. Integrin α7β1 is highly concentrated at the MTJ, whilst also expressed along the sarcolemma and at NMJs. It is known to be an indispensable link between the cytoskeleton and BM at the MTJ and along the sarcolemma, acting independently of the DGC (Mayer et al. 1997). However, its role at NMJs is less clear. Evidence suggests that integrin α7β1 interacts with acetylcholine receptors (AChRs) to induce clustering at the post synaptic membrane in an agrin dependant fashion, prior to NMJ formation (Burkin et al,. 2000). Whilst integrin α7 deficiency has also been shown to result in reduced axonal regeneration in axotomized facial motoneurons, potentially leading to a delay in target reinnervation (Werner et al., 2000). Innervation has been shown to be non-essential for myogenesis to proceed, but that it is a requirement for myofibre hypertrophy and maturation (Tintignac et al., 2015). Reduced levels of innervation after injury leads to abortive myogenesis, resulting in numerous immature myofibres (Borisov et al., 2005), similar to the phenotype observed in mice lacking integrin α7 at 10 DPI and the DKO at 30 DPI. Taken together, this evidence indicates that the loss of integrin α7β1 could potentially influence the rate of motoneuron extension and reinnervation of regenerating myofibres after an acute injury. This would have a negative effect on regeneration and exacerbate any phenotype caused solely by defects in SC function.

At first glance, the data from chapter 3 supports a hypothesis that there is some functional compensation occurring between integrins α5β1 and α7β1. Direct

mechanical compensation is unlikely, as the two integrins do not share the same extracellular ligand, and as we demonstrated in chapter 4, integrin α5 is not expressed in quiescent satellite cells (SCs). Instead, any functional overlap is more likely to arise from shared downstream signalling effects, resulting in similar gene expression responses following injury. These effects are primarily mediated by the common β1 subunit but may also involve shared intracellular effectors activated downstream of either the α5 or α7 integrin subunits.

The β1 integrin subunit is the most promiscuous integrin chain, contributing to 12 distinct heterodimers (Figure 1.11) and functioning to integrate ECM cues with intracellular responses. In humans, five cytoplasmic splice variants of β1 have been described, in contrast, mice express only β1A and β1D (Armulik et al., 2002). The β1A variant, which is ubiquitously expressed, supports dynamic adhesion and signalling, whereas β1D is restricted to cardiac and skeletal muscle and confers reduced signalling potential but enhanced mechanical stability (Soto-Ribeiro et al., 2019). Functional compensation between these splice variants is non-reciprocal: β1A can substitute for β1D, but loss of β1A leads to early embryonic lethality, underscoring its essential role in integrin-mediated signalling during development (Nawrotzki et al., 2003). Beyond structural adhesion, β1 integrins are key regulators of satellite cell quiescence (Rozo et al., 2016). Whereas integrin α7β1 and β1-containing integrins more broadly have also been shown to regulate myoblast fusion (McClure et al., 2019; Schwander et al., 2003), indicating that integrin dependent signalling contributes directly to late myogenic differentiation as well as SC maintenance. These observations demonstrate the importance of β1 integrins in coordinating multiple stages of the myogenic programme.

Many signalling pathways have been implicated in regulating processes such as muscle hyperplasia, hypertrophy, atrophy, and regeneration. Many of these pathways are subject to integrin-dependent modulation, reflecting extensive crosstalk between integrin-associated signalling complexes (e.g. FAK, ILK, Src family kinases) and growth factor or morphogen pathways. Therefore, the loss of integrin α5β1, α7β1, or both would be expected to cause disruption to many of the signalling components that facilitate regeneration. HGF and FGF signalling, for example, are both instrumental in SC activation and proliferation (Liu. & Schneider., 2014; Miller et al., 2000) acting through ERK MAPK, p38α/β MAPKs, PI3K, PLCγ, and JAK/STAT signalling cascades (Pawlikowski et al., 2017), whilst

integrin crosstalk with their respective receptors, c-MET and FGFRs, is well characterised (Eliceiri., 2001; Jahangiri et al., 2017; Stanislovas. & Kermorgant., 2022). β1 integrins are required for appropriate integration of these signals, likely by facilitating receptor localisation, clustering, or downstream kinase activation. Consequently, disruption of β1-dependent integrin signalling in the DKO mice would be expected to profoundly impair HGF / FGF mediated control of SC activation and proliferation.

6.1.2. Integrin deficient satellite cell migration.

SC migration is not strictly required to initiate muscle regeneration but is essential for efficient coordinated repair. After an acute injury SCs become activated, proliferate and migrate to the site of injury. Previous live imaging and ex vivo myofibre studies have demonstrated that SCs undergo integrin dependant migration along the basal lamina, or its remnants as 'ghost fibres', prior to differentiation and fusion (Siegel et al., 2009; Webster et al., 2016). Integrins are constantly being recycled from the plasma membrane via endocytosis, a process which regulates adhesive capacity and drives migration (Caswell & Norman 2006). Integrins are detached from the trailing edge, are internalised to endosomes, then recycled to the plasma membrane at the leading edge of the cell. This recycling facilitates integrin clustering, focal adhesion formation and continued signalling (White et al., 2007), constantly informing the cell as to the make-up of their extracellular environment, thereby allowing the cells to behave in an appropriate manner. Disruption of key signalling components required for migration, such as integrin β1, results in activated SCs that facilitate disorganised regeneration, impaired fibre growth and increased fibrosis (Rozo et al., 2016).

In this study we utilised 3D cell culture techniques coupled with time-lapse microscopy to directly compare how the loss of integrins α5 and / or α7 affected SC migration. Extensive SC tracking across each of the four groups confirmed our hypothesis, that myofibre associated SC motility is primarily dependent upon adhesion to laminin via integrin α7β1. Our data clearly showed that integrin α7 KO and DKO SCs have significantly reduced motility and myofibre associated migration speed compared to both control and α5 cKO SCs. This data represents a potential contributing factor to the overall regenerative defect observed in α7 KO mice, shown in chapter 3. However, it does not offer clear insight into the severity of the DKO phenotype. Because the isolated myofibres were suspended in a

collagen rich gel, and SCs migrated along the laminin rich BM of each myofibre, it is a very one-sided story. Integrin α5β1 is a fibronectin receptor, so its loss is unlikely to affect SC migration along the BM, in an environment which is initially devoid of fibronectin, and which crucially, does not represent the environment which SCs would experience in vivo. SCs start to express and secrete fibronectin after activation and along with numerous other cell types, including fibroblasts and fibro-adipogenic progenitors, contribute towards ECM remodelling (Bentzinger et al. 2013). However, the contribution from SCs alone is minimal and would not be sufficient to produce the same fibronectin rich environment which is established in vivo approximately 3 - 5 days after an acute injury (Schuler et al., 2022) Coincidently, fibronectin upregulation occurs around the same time we observed significant upregulation of integrin α5 in isolated SCs ex vivo. Upregulation of integrin α5 at this time point would be essential to enable activated SCs and myoblasts to efficiently migrate through this developing fibronectin rich matrix. Therefore, we can postulate that the loss of integrin α5 in vivo, in a fibronectin rich environment, would potentially cause a similar defect in SC migration to the one observed in the α7 KO and DKO SCs in chapter 4, thereby contributing to the additional severity of the DKO phenotype observed in vivo.

Although the data collected from these experiments is unambiguous, it must be presented with the caveat that there were numerous technical difficulties, leading to some inconsistencies in parameters which should not be considered variables. Along with numerous software crashes midway through video acquisition, the CO_2 regulator frequently failed to maintain a constant 6% CO_2 saturation and fluctuated between 3% - 8%. DMEM is designed to be used at between 5% - 10% CO_2 saturation, anything beyond those parameters will result in the media assuming a non-physiological pH and could therefore have a significant effect of cell behaviour. A large proportion of myofibres also perished early during video acquisition, indicating that their environment was less than optimal. Ideally, this experiment should be repeated with an increased sample size and a more stable environment.

6.1.3. Integrin deficient satellite cell proliferation and cell cycle progression.

Following activation, SCs are able to divide symmetrically, to produce enough myoblasts to facilitate regeneration, and asymmetrically to produce both myoblasts and Pax7+ stem cells (Fig. 1.9) which return to quiescence and

repopulate the stem cell niche ready for future rounds regeneration. Cell fate decisions are not governed by a single factor, but by a combination of niche derived spatial and mechanical cues from various adhesion receptors, including integrins and cadherins, in conjunction with signalling pathways such as notch, Wnt and various growth factors (Kuang et al., 2007; Le Grand et al., 2009). Asymmetric expression of specific adhesion and signalling receptors drives niche orientated SC polarisation. Basal integrin α7β1 expression maintains cell / ECM adhesion with the BM, whilst apical expression of M-cadherin and notch 1 & 2 allow for cell / cell interaction between the SC and associated myofibre (Brun et al., 2017). These interactions not only play a crucial role in the maintenance of quiescence, but also help dictate activation and cell fate. Efficient activation, proliferation and self-renewal are all fundamental to maintaining skeletal muscle homeostasis and enabling multiple rounds of regeneration as and when required.

Here we analysed in vivo SC numbers, pre and post injury, and ex-vivo SC numbers and proliferation rates. We showed that in uninjured muscle, α7 KO and DKO mice harboured fewer SCs, potentially as a result of reduced proliferation in conjunction with either dysfunctional self-renewal or premature cell death. The loss of integrin α7 could disrupt SC polarity, thereby biasing proportions of symmetric vs asymmetric cell divisions, resulting in more committed myoblasts and reduced self-renewal. The loss of integrin α5β1 and / or α7β1 from SCs could also contribute to the inhibition of numerous integrin dependant pro-survival pathways, including FAK, ILK, PI3K/AKT, MEK/ERK and NFκB, potentially triggering apoptosis or anoikis, a particular form of apoptosis induced through the loss of cell adhesion (Blandin et al. 2015). However, caspase 3 staining of cryosections from the TA of mice from each of the four groups showed no increase in SC apoptosis / anoikis in response to integrin deficiency, implying SCs were either becoming senescent or simply failing to self-renew to maintain a stable population. After an acute injury, SCs from control and integrin α5 cKO mice proliferated extensively in vivo, whereas numbers of integrin α7 KO SCs remained relatively unchanged, and numbers of DKO SCs actually diminished at 10DPI before recovering to pre-injury levels by 30DPI. This response was largely reproduced in the ex-vivo regeneration model, which showed rapid expansion of both control and α5 cKO SCs, but a significantly reduced proliferative response when cells lacked integrin α7. Although the loss of integrin α7 limits ex vivo proliferative capacity, it does not affect proliferation rate or timing. There was no

significant difference in the time taken for SCs in each of the four groups to undergo their first, or subsequent divisions. Although some α7 KO SCs were capable of multiple rounds of mitosis, the majority only managed a single round or didn't divide at all. In contrast, a greater proportion of control and α5 cKO SCs managed to divide multiple times in the same time frame.

Cell cycle progression, through both the G1/S and G2/M checkpoints, is obviously fundamental to proliferation. Failure to proceed past either of these checkpoints, for whatever reason, results in cell cycle arrest and either apoptosis or senescence. The primary driver of proliferation and G1/S checkpoint progression is the ERK/MAPK pathway (Meloche. & Pouyssegur., 2007), whereas survival, growth and continued proliferation are dependent upon the P13/AKT/MTOR pathway (Manning. & Toker., 2017). Both pathways are known to be activated by a range of growth factors and modulated by integrins via FAK and ILK (Moreno-Layseca & Streuli. 2014; Pawlikowski et al., 2017; Rozo et al., 2016). Integrin mediated signalling has previously been linked with G1/S checkpoint progression (Moreno-Layseca & Streuli. 2014). Our data, gained via EdU staining of cultured SCs did show reduced proportions of a7 KO and DKO SCs entering S-phase at D5+1, possibly indicating G1/S checkpoint failure, however no differences were apparent at the later time points. We did see significant differences in rates of cell cycle completion though. Fewer cells lacking integrin α7 were able to transition from 4n, after DNA replication during S-phase, back to 2n after completing cytokinesis. This confirms that at some point after DNA replication, cells lacking integrin a7 must undergo some form of catastrophic event, thereby inducing cell cycle arrest. Previous studies have shown that β1 integrins play a role in mitotic spindle alignment by initiating changes in cell shape and polarity (LaFlamme et al., 2008; Streuli., 2009), if this process is perturbed, cell cycle arrest or mitotic catastrophe is a likely outcome. Impaired notch signalling has been shown to induce mitotic catastrophe in SCs leading to a reduction in SC number (Liu et al. 2018). Numerous studies have also shown that SC quiescence and self-renewal is maintained by notch signalling (Bjornson et al. 2012; Mourikis et al. 2012), which represses MyoD and MyoG via the HES and HEY family of transcriptional repressors, whilst also actively promoting Pax7 expression (Koch et al. 2013; Wen et al. 2011). Timely proliferation and differentiation is governed by a switch from notch to Wnt signalling. Multiple Wnt ligands, including Wnt4 Wnt5a/b and Wnt7a/b are expressed at specific time

points during regeneration in order to dictate appropriate SC behaviour (Polesskaya et al., 2003). For example, Wnt7a initiates rapid myoblast proliferation by activating the planar cell polarity pathway, inducing integrin α7 polarisation and an increase in planar, rather than apical basal, cell division (Le Grand et al. 2009; Von Maltzahn et al., 2012). Although not exclusively in SCs, there is increasing understanding of integrin / notch interaction and crosstalk, both directly (Campos et al., 2006; Deford et al., 2016; Sachan et al,. 2023) and indirectly via downstream signalling intermediates (Langa et al., 2023), offering further evidence that integrin deficiency results in reduced proliferation through a variety of mechanisms.

6.1.4. Integrin deficient satellite cell differentiation and self-renewal.

SC activation, followed by myoblast proliferation and differentiation is orchestrated by the well characterised sequential expression of MRFs, outlined in figure 5.2. Pax7 and Myf5 expression mark quiescent and activated SCs, followed by MyoD which marks myogenic commitment and proliferation. Self-renewal is governed by maintained Pax7 expression and downregulation of MyoD. Whereas downregulation of Pax7 and Myf5, followed by MyoG induction initiates terminal differentiation, culminating with the elongation of myocytes into myotubes prior to fusion and maturation into multinucleated myofibres. The whole process if tightly temporally controlled, any deviation from the standard programme is likely to have negative downstream ramifications for the regenerative process.

To assess whether loss of integrin α5β1 and / or α7β1 affects MRF expression, isolated myofibres and associated SCs from integrin deficient mice were cultured in differentiation media and immunostained against specific MRFs at various timepoints. Our data clearly demonstrates that integrin α5β1 is required for timely terminal differentiation, whereas integrin α7β1 is needed to maintain the stem cell pool via self-renewal. At T0 a significantly higher proportion of α5 cKO, α7 KO and DKO SCs expressed Myf5 compared to controls. Although not the sole determining factor of cell fate, early Myf5 expression is thought to ‘prime’ quiescent SCs, readying them for myogenic commitment, whilst Myf5- cells are more biased towards self-renewal (Kuang et al., 2007). At T24 there was no difference in either Pax7 or Myf5 expression. However, a reduced proportion of α5 cKO, α7 KO and DKO SCs had started to express MyoD, indicating delayed myogenic commitment. As previously discussed, notch signalling plays a

fundamental role in the maintenance of quiescent by promoting Pax7 expression whilst concomitantly repressing MyoD. Notch signalling is regulated by NUMB, an endocytic adaptor protein and notch antagonist which has been shown to directly interact with β1 integrins during endocytic trafficking (Nishimura. & Kaibuchi. 2007). Although not demonstrated in SCs, a reciprocal regulatory relationship has been proposed between β1 integrins and NUMB in cardiac progenitor cells (Gibbs et al., 2018), therefore reduced levels of β1 integrins could potentially result in reduced levels of NUMB, resulting in maintained notch signalling and inhibited MyoD expression in integrin deficient SCs. NUMB also plays a key role in SC self-renewal as it can be asymmetrically segregated upon cell division, thereby differentially inhibiting notch signalling to drive one daughter cell towards differentiation and the other towards self-renewal (Conboy. & Rando. 2002; Shinin et al., 2006) By T48 differences between the α5 cKO and α7 KO had become apparent. Fewer α5 cKO and DKO myoblasts had started to express MyoG, whilst α7 KO and DKO myoblast showed reduced Pax7 expression. These observations became more exaggerated at the later time points demonstrating that timely MyoG expression, and therefore terminal differentiation is modulated to some extent by integrin α5β1, whereas maintenance of Pax7 expression and self-renewal is, at least in part, regulated by integrin α7β1. DKO SCs displayed delayed myogenic commitment and differentiation coupled with fewer Pax7+ SCs at each time point. Taken together, these observations offer some evidence as to why we see a more pronounced phenotype in the DKO mice.

6.2. Conclusions.

In this thesis, we have demonstrated a critical requirement for integrins α5β1 and α7β1 in SCs. The phenotypical changes observed in skeletal muscle after an acute injury are as a direct result of changes to SC activation, proliferation, differentiation and capacity for self-renewal in the absence of one or both integrins. Due to the shared β1 subunit, partial compensation is likely. However, the data suggests that each is having an effect on a different aspect of SC function. Whereas integrin α7β1 primarily impacts SC proliferation and self-renewal, integrin α5β1 is required for efficient SC terminal differentiation. Synergistically their loss results in severely impaired SC function, resulting in significant fibrosis and delays to adult muscle regeneration. Collectively, these observations support a model in which integrin β1 dependent signalling acts as a

central mediator of mechanical and biochemical cues, coordinating multiple regenerative pathways. The loss of integrin α5β1 and / or α7β1 from SCs is therefore likely to produce broad changes in gene expression leading to systemic defects in behaviour, not through a single pathway, but via convergent disruption of interconnected signalling networks.

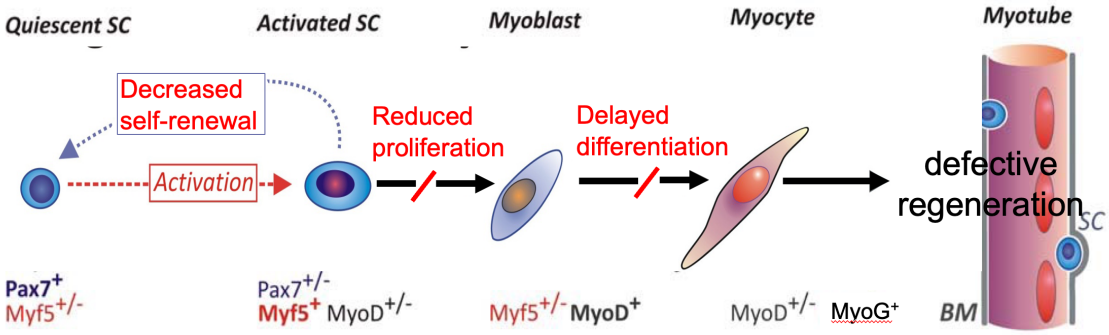


Figure 6.1. Graphical summary. Integrin α7 deficiency leads to a loss of SCs due to impaired self-renewal. Whereas integrin α5 ablation in SCs delays terminal differentiation. The severe regenerative phenotype observed in DKO mice is a compound effect demonstrating the crucial role for integrins α5β1 and α7β1 in SC function and adult skeletal muscle regeneration.

6.3. Future work.

Extensive work is still required to fully understand the roles of integrins α5β1 and α7β1 in SCs. The in-vivo comparison between conditional and constitutive KOs leaves some significant questions in terms of wider integrin α7 expression and how this impacts regeneration. Generation of an α7 cKO for comparison against the α5 cKO would answer these questions unequivocally, whilst also potentially opening new avenues for future research if differences between the constitutive and conditional α7 KOs were observed.

As previously mentioned, the generation of time-lapse videos was hampered by technical issues and should be repeated. It may also be beneficial to try and emulate a more physiologically relevant, fibronectin rich substrate for fibres to be mounted in. SC migration, within this fibronectin rich substrate, could then be analysed in conjunction with fibre associated migration to give a clearer picture of how SCs may function in vivo.

This thesis has demonstrated the phenotypical changes seen during muscle regeneration and in SC function in response to integrin deficiency but has not elucidated any mechanisms behind those changes. Extensive analysis of

numerous intracellular signalling networks is required, changes in the phosphorylation status or expression of key signalling components or intermediaries should be tested in primary cells where possible. However, due to the proliferation defect observed in α7 KO and DKO SCs, culturing them in sufficient numbers for most downstream applications, such as western blots, proteomics or sequencing, has proved technically very challenging. Establishing integrin deficient C2C12 myoblast lines using CRISPR would enable cells to be cultured in larger quantities, opening the possibility for more in depth analysis of signalling pathways and the individual components which may be impacted when specific integrins are absent. The C2C12 myoblast line, although able to answer some questions, is not a perfect model, therefore wherever possible, primary cells should still be used. New techniques, optimised for use on low abundance cells are becoming more common place. Utilising single cell transcriptomics (Cho. & Doles., 2018), single cell proteomics (Dowling et al., 2024) and phoshoproteomics (Gaizly. & Surinova., 2025) would shed light on many of the unanswered questions raised during this thesis, whilst costs for these techniques are constantly being driven down as the technology progresses, making them more accessible.

The use of advance staining and imaging techniques would also be highly beneficial. Multiplexed immunolabelling, such as the IBEX protocol (Radtke et al., 2022), enables the visualisation of up to 50 protein targets on a single tissue section, allowing us to investigate multiple overlapping markers at once, possibly helping to classify rare cell types or sub-populations, or highlighting colocalisation of numerous protein targets at the same time. High resolution imaging techniques such as immune-gold EM, could also be used to show the subcellular location of integrins or other proteins of interest. Whilst serial blockface SEM could generate 3D reconstructions of muscle tissue at a subcellular level, enabling insight into the 3D microenvironment of muscle fibres and possibly the SC niche.

References.

1. Ahmad, K., Shaikh, S., Chun, H. J., Ali, S., Lim, J. H., Ahmad, S. S., Lee, E. J. & Choi, I. (2023). Extracellular matrix: the critical contributor to skeletal muscle regeneration-a comprehensive review. Inflammation and Regeneration. (1):58.

2. Ahmad, K., Shaikh, S. M., Ahmed, S. S., Lee, E. J. & Choi, I. (2020). Crosstalk between extracellular matrix and skeletal muscle: implications for myopathies. Frontiers in Pharmacology. 11. 142.

3. Alanko, J., Mai, A., Jacquemet, G., Schauer, K., Kaukonen, R., Saari, M., Goud, B. & Ivaska, J. (2015). Integrin endosomal signalling suppresses anoikis. Nature Cell Biology. 17(11): 1412-1421.

4. Armand, O., Boutineau, A. M., Mauger, A., Pautou, M. P. & Kieny, M. (1983). Origin of satellite cells in avian skeletal muscles. Archives D'anatomie Microscopique et de Morphologie Experimental. 72(2). 163-181.

5. Armulik, A. (2002). Splice variants of human beta 1 integrins: origin, biosynthesis and functions. Frontiers in Biosciences. 7:d219-d227.

6. Asfour, H. A., Allouh, M. Z. & Said, R. S. (2018). Myogenic regulatory factors: The orchestrators of myogenesis after 30 years of discovery. Experimantal Biology and Medicine. 243. 118-128.

7. Aumailley, M. (2013). The laminin family. Cell adhesion & Migration. 7(1). 48-55.

8. Barczyk, M., Carracedo, S. & Gullberg, D. (2010). Integrins. Cell Tissue Research. 339, 269-280.

9. Behan, W. M. H., Cossar, D. W., Madden, H. A. & McKay, I. C. (2002). Validation of a simple, rapid, and economical technique for distinguishing type I and II fibres in fixed and frozen skeletal muscle. Journal of Clinical Pathology. 55(5). 375-380.

10. Bentzinger, C. F., Wang, Y. X. & Rudnicki, M. A. (2012). Building muscle: molecular regulation of myogenesis. Cold Spring Harbor Perspectives in Biology. 4(2). a008342.

11. Bentzinger, C. F., Wang, Y. X., Maltzahn, J. V., Soleimani, V. D., Yin, H. & Rudnicki, M. A. (2013). Fibronectin regulates Wnt7a signalling and satellite cell expansion. Cel Stem Cell. 12(1). 75-87.

12. Bintliff, S. W. & Walker, B. E. (1960). Radioautographic study of skeletal muscle regeneration. American Journal of Anatomy. 106. 233-246.

13. Biral, D., Betto, R., Danieli-Betto, D. & Salviati, G. (1988). Myosin heavy chain composition of single fibres from normal human muscle. The Biochemical Journal. 250. 307-308.

14. Bischoff, R. (1994). The satellite cell and muscle regeneration. Myology. McGraw-Hill. New York. 97-118.

15. Bjornson, C. R. R., Cheung, T. H., Liu, L., Tripathi, P. V., Steeper, K. M. & Rando, T. A. (2012). Notch signalling is necessary to maintain quiescence in adult muscle stem cells. Stem Cells. 30(2). 232-242.

16. Borisov, A. B., Dedkov, E. I. & Carlson, B. M. (2005). Abortive myogenesis in denervated skeletal muscle: differentiative properties of satellite cells, their migration, and block of terminal differentiation. Anatomy and Embryology. 209(4). 269–279.

17. Brun, C. E., Chevalier, F. P., Dumont, N. A. & Rudnicki, M. A. (2017). The satellite cell niche in skeletal muscle. Biology and Engineering of Stem Cell Niches. 10. 145-166.

18. Burkin, D. J., Kim, J. E., Gu, M. & Kaufman, S. J. (2000). Laminin and $\alpha 7\beta 1$ integrin regulate agrin-induced clustering of acetylcholine receptors. Journal of Cell Science. 113(16). 2877-2886.

19. Burkin, D. J., Wallace, G. Q., Nicol, K. J., Kaufman, D. J. & Kaufman, S. J. (2001) Enhanced expression of the a7b1 integrin reduces muscular dystrophy and restores viability in dystrophic mice. Journal of Cell Biology. 152(6). 1207-1218.

20. Campos, L. S., Decker, L., Taylor, V.& Skarnes, W. (2006). Notch, epidermal growth factor receptor and beta1-integrin pathways are coordinated in neural stem cells. The Journal of Biological Chemistry. 281(8). 5300-5309.

21. Caswell, P. T. & Norman, J. C. (2006). Integrin trafficking and the control of cell migration. Traffic. 7(1). 14-21.

22. Chal, J. & Pourquie, O. (2017). Making muscle: Skeletal myogenesis in vivo and in vitro. Development. 144(12). 2104-2122.

23. Charge, S. B. P. & Rudnicki, M. A. (2004). Cellular and molecular regulation of muscle regeneration. Physiological reviews. 84(1):209-38.

24. Cheah, M. & Andrews, M. R. (2018). Integrin activation: implications for axon regeneration. Cells. 7(3). 20.

25. Chen, X. & Liu, Y. (2009). Role of matrix metalloproteinases in skeletal muscle. Cell adhesion and migration. 3(4):337-341.

26. Cheng, Y. S. Champliaud, M. F., Burgeson, R. E., Marinkovich, M. P. & Yurchenco, P. D. (1997). Self-assembly of laminin isoforms. Journal of Biological Chemistry. 272(50. 31525-31532.

27. Cho, D. S. & Doles, J. D. (2017). Single cell transcriptome analysis of muscle satellite cells reveals widespread transcriptional heterogeneity. Gene. 15(636). 54-63.

28. Conboy, I. M. & Rando, T. A. (2002). The regulation of notch signalling controls satellite cell activation and cell fate determination in postnatal myogenesis. Developmental Cell. 3(3). 397-409.

29. Crisafulli, S., Sultana, J., Fontana, A., Salvo, F., Messina, S. & Trifiro, G. (2020). Global epidemiology of Duchenne muscular dystrophy: an updated systemic review and meta-analysis. Orphanet Journal of Rare Diseases. 15(141).

30. Cruz-Migoni, S.B., Imran, K.M., Wahid, A., Rahman, O., Briscoe, J., & Borycki, A.G. (2019). A switch in cilia-mediated Hedgehog signalling controls muscle stem cell quiescence and cell cycle progression. bioRxiv.

31. Csapo, R., Gumpenberger, M. & Wessner, B. (2020). Skeletal muscle extracellular matrix – what do we know about its composition, regulation, and physiological roles? A narrative review. Frontiers in Physiology. 11. 253.

32. Davies, J. A. (2001). Encyclopaedia of Life Sciences – Extracellular Matrix. DOI:10.1038/npg/els.001274.

33. Deford, P., Brown, K., Richards, R. L., King, A., Newburn, K., Westover, K. & Albig, A. R. (2016). MAP2 controls notch via interactions with RGD binding integrins: identification of a novel ECM – integrin – notch signalling axis. Experimental Cell Research. 341(1). 84-91.

34. De Franceschi, N., Hamidi, H., Alanko, J., Sahgal, P. & Ivaska, J. (2015). Integrin traffic – the update. Journal of Cell Science. 128(5): 839-852.

35. Divekar, D. & Mayer, U. (2014). Integrins in muscle disease and repair. UEA PhD thesis – unpublished.

36. Domogatskaya, A., Rodin, S. & Tryggvason, K. (2012). Functional diversity of laminins. Annual Review of Cell and Developmental Biology. 28. 523-553.

37. Dowling, P., Trollet, C., Muraine, L., Negroni, E., Swandulla, D. & Ohlendieck, K. (2024). The potential of proteomics for in-depth bioanalytical investigations of satellite cell function in applied myology. Expert Review of Proteomics. 21(5-6) : 229-235.

38. Eliceiri, B. (2001). Integrin and growth factor receptor crosstalk. Circulation Research. 89(12). 10.1161.

39. Enomoto, M, I., Boettiger, D. & Menko, A. S. (1993). Alpha 5 integrin is a critical component of adhesion plaques in myogenesis. Developmental Biology. 155(1). 180-197.

40. Flintoff-Dye, N. L., Wesler, J., Rooney, J., Scowen, P., Tamowski, S., Hatton, W. & Burkin, D. J. (2005). Role for the a7b1 integrin in vascular development and integrity. Developmental Dynamics. 234. 11-21.

41. Giancotti, F. (2000). Complexity and specificity of integrin signalling. Nature Cell Biology 2, E13–E14.

42. Gibbs, B., Shenje, L., Anderson, P., Miyamoto, M. & Kwon, C. (2018). β1-integrin is a cell-autonomous factor mediating the numb pathway for cardiac progenitor maintenance. Biochemical and Biophysical Research Communications. 500(2). 256-260.

43. Graham, Z. A., Gallagher, P. M. & Cardozo, C. P. (2015). Focal adhesion kinase and its role in skeletal muscle. Journal of Muscle Research and Cell Motility. 36(0). 305-315.

44. Gros, J., Manceau, M., Thome, V. & Marcelle, C. (2005). A common somitic origin for embryonic muscle progenitors and satellite cells. Nature. 435(7044). 954-958.

45. Guardiola, O., Andolfi, G., Tirone, M., Lavarone, F., Brunelli, S. & Minchiotti, G. (2017). Induction of acute skeletal muscle regeneration by cardiotoxin injection. Journal of Visualized Experiments. 119:54515.

46. Guo, C., Willem, M., Werner, A., Raivich, G., Emerson, M., Neyses, L. & Mayer, U. Absence of α7 integrin in dystrophin-deficient mice causes a myopathy similar to Duchenne muscular dystrophy. Human Molecular Genetics. 15(6). 989-998.

47. Hawke, T. J. & Garry, D. J. (2001). Myogenic satellite cells: Physiology to molecular biology. Journal of Applied Physiology. 91. 534-551.

48. Hayashi, Y. K., Chou, F. L., Engvall, E., Ogawa, M., Matsuda, C., Hiraayashi, S., YoKochi, K., Ziober, B. L., Kramer, R. H., Kaufman, S. J., Ozawa, E., Goto, Y., Nonake, I., Tsukahara, T., Wang, J. Z., Hoffman, E. P. & Arahata, K. (1998).

Mutations in the integrin alpha7 gene cause congenital myopathy. Nature Genetics. 19(1). 94-97.

49. Heller, K. N., Montgomery, C, L., Janssen, P. M., Reed Clark, K., Mendell, J. R. & Rodino-Klapac, L. R. (2013). AAV-mediated overexpression of human a7 integrin leads to histological and functional improvement in dystrophic mice. Molecular Therapy. 21(3). 520-525.

50. Hernandez-Torres, F., Rodriguez-Outeirino, L., Franco, D. & Aranega, A. E. (2017). Pitx2 in embryonic and adult myogenesis. Frontiers in Cell and Developmental Biology. 5. 46.

51. Heydemann, A. (2018). Skeletal muscle metabolism in Duchenne and Becker muscular dystrophy-implications for therapies. Nutrients. 10(6), 796.

52. Hinz, B. & Lagares, D. (2020). Evasion of apoptosis by myofibroblasts: a hallmark of fibrotic diseases. National Reviews Rheumatology. 16 : 11 – 31.

53. Hirunsai, M., Srikuea, R. & Yimlamai, T. (2015). Heat stress promotes extracellular matrix remodelling via TGF-beta1 and MMP-2/TIMP-2 modulation in tenotomised soleus and plantaris muscles. International Journal of Hyperthermia. 31(4). 336-348.

54. Hynes, R. O. (1976). Cell surface proteins and malignant transformation. Biochimica at Biophysica Acta – Reviews on Cancer. 458(1). 73-107.

55. Hynes, R. O. (1987). Integrins: a family of cell surface receptors. Cell. 4. 549-554.

56. Hynes, R. O. (1992). Integrins: Versatility, modulation, and signalling in cell adhesion. Cell. 69. 11-25.

57. Ilic, D., Furuta, Y., Kanazawa, S., Takeda, N., Sobue, K., Nakatsuji, N., Nomura, S., Fujimoto, J., Okada, M., Yamamoto, T. & Aizawa, S. (1995). Reduced cell motility and enhanced focal adhesion contact formation in cells from FAK-deficient mice. Nature. 377. 539-544.

58. Ishihara, J., Ishihara, A., Fukunaga, K., Sasaki, K., White, M. J. V., Briquez, P. S. & Hubbell, J. A. (2018). Laminin heparin-binding peptides bind to several growth factors and enhance diabetic wound healing. Nature Communications. 9. 2163.

59. Jahangiri, A., Nguyen, A., Chandra, A., Sidorov, M. K., Yagnik, G., Rick, J., Han, S. W., Chen, W., Flanigan, P. M., Schneidman-Duhovny, D., Mascharak, S., De Lay, M., Imber, B., Park, C. C., Matsumoto, K., Lu, K., Bergers, G., Sali, A., Weiss, W. A. & Aghi, M. K. (2017). Cross-activating c-met / β1 integrin complex drives metastasis and invasive resistance in cancer. Medical Sciences. 114(41). 8685-8694.

60. Janssen, I., Heymsfield, S. B., Wang, Z. M. & Ross, R. (2000). Skeletal muscle mass and distribution in 468 men and women aged 18-88 yr. Journal of Applied Physiology. 89, 81-88.

61. Jayadev, R. & Sherwood, D. R. (2017). Basement membranes. Current Biology. 27. 207-211.

62. Jensen, J., Rustad, P. I., Kolnes, A. J. & Lai, Y. (2011). The role of skeletal muscle glycogen breakdown for regulation of insulin sensitivity by exercise. Frontiers in Physiology. 2:112.

63. Jo, D., Yoon, G., Kim, O. Y. & Song, J. (2022). A new paradigm in sarcopenia: Cognitive impairment caused by imbalance myokine secretion and vascular dysfunction. Biomedicine & Pharmacotherapy. 147. 112636.

64. Johnson, S. E. & Allen, R. E. (1995). Activation of skeletal muscle satellite cells and the role of fibroblast growth factor receptors. Experimental Cell Research. 219(2). 449-453.

65. Kassar-Duchossoy, L., Giacone, E., Gayraud-Morel, B., Jory, A., Gomes, D. & Tajbakhsh, S. (2005). Pax3/Pax7 mark a novel population of primitive myogenic cells during development. Gens & Development. 19(12). 1426-1431.

66. Kim, H., Kim, M. C. & Asada, H. H. (2019). Extracellular matrix remodelling induced by alternating electrical and mechanical stimulations increases the contraction of engineered skeletal muscle tissues. Scientific Reports. 9(1). 2732.

67. Koch, U., Lehal, R. & Radtke, F. (2013). Stem cells living with notch. Development. 140(4). 689-704.

68. Koopman, R., Hai Ly, C. & Ryall, J. G. (2014). A metabolic link to skeletal muscle wasting and regeneration. Frontiers in Physiology. 5, 1-11.

69. Kuang, S., Gillespie, M. A. & M. A. Rudnicki. (2008). Niche regulation of muscle satellite cell self-renewal and differentiation. Cell Stem Cell. 2(1). 22-31.

70. Kuang, S., Kuroda, K., Le Grand, F. & Rudnicki, M. A. (2007). Asymmetric self-renewal and commitment of satellite stem cells in muscle. Cell. 129(5). 999-1010.

71. Kuhl, U., Ocalan, M., Timpl, R. & von der Mark, K. (1986). Role of laminin and fibronectin in selecting myogenic versus fibrogenic cells from skeletal muscles cells in vitro. Developmental Biology. 117(2). 628-635.

72. LaFlamme, S. E., Nieves, B., Colello, D. & Reverte, C. G. (2008). Integrins as regulators of mitotic machinery. Current Opinion in Cell Biology. 20(5). 576-582.

73. Larsson, L., Sjodin, B. & Karlsson, J. (1978). Histochemical and biochemical changes in 2 human skeletal muscle with age in sedentary males, age 22 – 65 years. Acta Physiogica. 103. 31-39.

74. Lee, J.O., Rieu, P., Arnaout, M.A., and Liddington, R. (1995). Crystal structure of the A domain from the alpha subunit of integrin CR3 (CD11b/CD18. Cell. 80. 631-638.

75. Le Grand, F., Jones, A. E., Seale, V., Scime, A. & Rudnicki, M. A. (2009). Wnt7a activates the planar cell polarity pathway to drive symmetric expansion of satellite stem cells. Cell Stem Cell. 4(6). 535-547.

76. Lepper, C., Partridge, T. A. & Fan, C-H. (2011). An absolute requirement for Pax7-positive satellite cells in acute injury-induced skeletal muscle regeneration. Development. 138(17). 3639 – 3646.

77. Liu, J., Burkin, D. J. & Kaufman, S. J. (2009). Increasing $\alpha 7\beta 1$ integrin promotes muscle cell proliferation, adhesion, and resistance to apoptosis without changing gene expression. American Journal of Physiology, Cell Physiology. 294(2). 627-640.

78. Liu, L., Charville, G. W., Cheung, T. H., Yoo, B., Santos, P. J., Schroeder, M. & Rando, T, A. (2018). Impaired notch signalling leads to decrease in p53 activity and mitotic catastrophe in aged muscle stem cells. Cell Stem Cell. 23(4). 544-556.

79. Liu, Y. & Schneider, M. F. (2014). FGF2 activates TRPC and Ca^{2+} signalling leading to satellite cell activation. Frontiers in Physiology. 5. 10.3389.

80. Lonsdale, P. D., & Mayer, U. (2022). Investigating the role of $\alpha 5$ and $\alpha 7$ integrins in satellite cell function and adult skeletal muscle regeneration. UEA MScR thesis - unpublished

81. Loomis, T. & Smith, L. R. (2023). Thrown for a loop: fibro-adipogenic progenitors in skeletal muscle fibrosis. American Journal of Physiology, Cell Physiology. 325(4) : 895 – 906.

82. Loreti, M., & Sacco. A. (2022). The jam session between muscle stem cells and the extracellular matrix in the tissue microenvironment. Npj Regenerative Medicine. 7. 16

83. Lu, F., Zhu, L., Bromberger, T., Yang, J., Yang, Q., Liu, J., Plow, E. F., Moser, M. & Qin, J. (2022). Mechanism of integrin activation by talin and its cooperation with kindlin. Nature Communications. 13. 2362.

84. MacCalman, C. D., Bardeesy, N., Holland, P. C., and Blaschuk, O. (1992). Noncoordinate developmental regulation of N-cadherin, N-CAM, integrin, and fibronectin mRNA levels during myoblast terminal differentiation. Developmental Dynamics. 195. 127-132.

85. Makarenkova, H. P., Gonzalez, K. N., Kiosses, W. B. & Meech, R. (2009). Barx2 controls myoblast fusion and promotes MyoD-mediated activation of the smooth muscle α-actin gene. The Journal of Biological Chemistry. 284(22), 14866-14874.

86. Manning, B. D. & Toker, A. (2017). AKT/PKB Signalling: Navigating the Network. Cell. 169(3). 381–405.

87. Mauro, A. (1961). Satellite cell of skeletal muscle fibres. The Journal of Biophysical and Biochemical Cytology. 9. 493-495.

88. Mayer, U. (2003). Integrins: redundant or important players in skeletal muscle. The Journal of Biological chemistry. 278(17), 14587-14590.

89. Mayer, U., Saher, G., Fassler, R., Bornemann, A., Echtermeyer, F., von der Mark, H., Miosge, N., Poschl, E. & von der Mark, K. (1997). Absence of integrin α7 causes a novel form of muscular dystrophy. Nature Genetics. Vol. 17: 318-323.

90. McClure, M. J., Ramey, A. N., Rashid, M., Boyan, B. D. & Schwartz, Z. (2019). Integrin α7 regulates connexin 43, M-cadherin, and myoblast fusion. American Journal of Physiology, Cell Physiology. 316, C876-C887.

91. Meloche, S. & Pouyssegur, J. (2007). The ERK1/2 mitogen-activated protein kinase pathway as a master regulator of the G1- to S-phase transition. Oncogene. 26(22). 3227–3239.

92. Miller, K. J., Thaloor, D., Matteson, S. & Pavlath, G. K. (2000). Hepatocyte growth factor affects satellite cell activation and differentiation in regenerating skeletal muscle. American Journal of Physiology, Cell Physiology. 278(1). C174-181.

93. Montarras, D., Morgan, J., Collins, C., Relaix, F., Zaffran, S., Cumano, A., Partridge, T. & Buckingham, M. (2005). Direct isolation of satellite cells for skeletal muscle regeneration. Science. 309(5742). 2064-2067.

94. Moreno-Layseca, P., Icha, J., Hamidi, H. & Ivaska, J. (2019). Integrin trafficking in cells and tissues. Nature Cell Biology. 21(2): 122 – 132.

95. Mourikis, P., Sambasivan, R., Castel, D., Rocheteau, P., Bizzarro, V. & Tajbakhsh, S. (2012). A critical requirement for notch signalling in maintenance of the quiescent skeletal muscle stem cell state. Stem Cells. 30. 243-252.

96. Mouw, J. K. & Weaver, O. G. (2014). Extracellular matrix assembly: a multiscale deconstruction. Nature Reviews. 15(12). 771-785.

97. Nawrotzki, R., Willem, M., Miosge, N., Brinkmeier, H. & Mayer, U. (2003). Defective integrin switch and matrix composition at alpha 7-deficient myotendinous junctions precede the onset of muscular dystrophy in mice. Human Molecular Genetics. 12(5), 483-495.

98. Nishimura, T. & Kaibuchi, K. (2007). Numb controls integrin endocytosis for directional cell migration with aPKC and PAR-3. Developmental Cell. 13(1). 15-28.

99. Ocalan, M., Goodman, S. L., Kuhl, U., Hauschka, S. D. & von der Mark, K. (1988). Laminin alters cell shape and stimulates motility and proliferation of murine skeletal myoblasts. Developmental Biology. 125. 158-167.

100. Ono, Y., Urata, Y., Goto, Shinji., Nakagawa, S., Humbert, P. O., Li, T-S. & Zammit, P. S. (2015). Muscle stem cell fate is controlled by the cell polarity protein Scrib. Cell Reports. 10(7). 1135-1148.

101. Ortenblad, N., Nielsen, J., Boushel, R., Soderlund, K., Saltin, B. & Holmberg, HC. (2018). The muscle fibre profiles, mitochondrial content, and enzyme activities of the exceptionally well-trained arm and leg muscles of elite cross-country skiers. Frontiers in Physiology. 9. 1031.

102. Ott, M. O., Bober, E., Lyons, G., Arnold, H. & Buckingham, M. (1999). Early expression of the myogenic regulatory gene myf-5, in precursor cells of skeletal muscle in the mouse embryo. Development. 111(4). 1097-1107.

103. Otto, A., Schmidt, C., Luke, G., Allen, S., Valasek, P., Muntoni, F., Lawrence-Watt, D. & Patel, K. (2008). Canonical Wnt signalling induces satellite-cell proliferation during adult skeletal muscle regeneration. Journal of Cell Science. 121(17). 2939-2950.

104. Pasut, A., Jones, A. E. & Rudnicki, M. (2013). Isolation and culture of individual myofibres and their satellite cells from adult skeletal muscle. Journal of Visualized Experiments. 73:50074.

105. Pawlikowski, B., Vogler, T. O., Gadek, K. & Olwin, B. B. (2017). Regulation of skeletal muscle stem cells by fibroblast growth factors. Developmental Dynamics. 246(5). 359-367.

106. Pedersen, B. K. (2013). Muscle as a secretory organ. Comprehensive Physiology. 3(3). 1337-1362.

107. Periasamy, M., Herrera, J. L. & Reis, F. C. G. (2017). Skeletal muscle thermogenesis and its role in whole body energy metabolism. Diabetes and Metabolism Journal. 41(5). 327-336.

108. Pette, D. & Staron, R. S. (2000). Myosin isoforms, muscle fibre types, and transitions. Microscopy Research and Techniques. 50. 500-509.

109. Pezzo, B. (2013). Muscle cells: development, disorders and regeneration. Hauppauge. N.Y. Nova Science.

110. Piccioni, A., Gaetani, E., Palladino, M., Gatto, I., Smith, R. C., Neri, V., Marcantoni, M., Giarretta, I., Silver, M., Straino, S., Capogrossi, M., Landolfi, R. & Ploa, R. (2014). Sonic hedgehog gene therapy increases the ability of the dystrophic skeletal muscle to regenerate after injury. Gene Therapy. 21. 413-421.

111. Pisconti, A., Banks, G. B., Babaeijandaghi, F., Dalla Betta, N., Rossi, F. M. V., Chamberlain, J. S. & Olwin, B. B. (2016). Loss of niche-satellite cell interactions in syndecan-3 null mice alters muscle progenitor cell homeostasis improving muscle regeneration. Skeletal Muscle. 6. 34.

112. Polesskaya, A., Seale, P. & Rudnicki, M. A. (2003). Wnt signalling induces the myogenic specification of CD45+ adult stem cells during muscle regeneration. Cell. 113(7). 841-852.

113. Radtke, A. J., Chu, C. J., Yaniv, Z., Yao, L., Marr, J., Beuschel, R. T., Ichise, H., Gola, A., Kabat, J., Lowekamp, B., Speranza, E., Croteau, J., Thakur, N., Jonigk, D., Davis, J. L., Hernandez, J. M. & Germain, R. N. (2022). IBEX: an iterative immunolabeling and chemical bleaching method for high-content imaging of diverse tissues. Nature Protocols. (2):378-401.

114. Rahimov, F. & Kunkel, L. M. (2013). Cellular and molecular mechanisms underlying muscular dystrophy. Journal of Cell Biology. Vol. 201. 4. 499-510.

115. Relaix, F., Montarras, D., Zaffran, S., Gayraud-Morel, B., Rocancourt, D., Tajbakhsh, S., Mansouri, A., Cumano, A. & Buckingham, M. (2006). Pax3 and Pax7 have distinct and overlapping functions in adult muscle progenitor cells. Journal of Cell Biology. 172(1). 91-102.

116. Robson, L.G. (2017). Vertebrate embryo: myogenesis and muscle development. In eLS, John Wiley & Sons, Ltd (Ed.). doi:10.1002/9780470015902.a0026598.

117. Rocheteau, P., Gayraud-Morel, B., Siegl-Cachedenier, I., Blasco, M. A. & Tajbakhsh, S. (2012). A subpopulation of adult muscle stem cells retains all template DNA strands after cell division. Cell. 148(1-2). 112-125.

118. Rogers, L. K. & Mayer, U. (2006). Insights into integrin function in skeletal muscle. *Integrins and Development.* Landes Bioscience, pp. 138-151.

119. Rozo, M., Li, L. & Fan, C. (2016). Targeting β1-integrin signalling enhances regeneration in ages and dystrophic muscle in mice. Nature Medicine. Vol. 22. 8: 889-896.

120. Ryall, J. G., Schertzer, J. D. & Lynch, G. S. (2008). Cellular and molecular mechanisms underlying age-related skeletal muscle wasting and weakness. Biogerontology. 9. 213-228.

121. Sachan, N., Sharma, V., Mutsuddi, M. & Mukherjee, A. (2023). Notch signalling: multifaceted role in development and disease. The FEBS Journal. 291(14). 3030-3059.

122. Sado, Y., Kagawa, M., Naito, I., Ueki, Y., Seki, T., Momota, R., Oohashi, T. & Ninomiya, Y. (1998). Organisation and expression of basement membrane collagen IV genes and their roles in human disorders. The Journal of Biochemistry. 123. 767-776.

123. Sakai, T., Li, S., Docheva, D., Grashoff, C., Sakai, K., Kostka, G., Braun, A., Pfeifer, A., Yurchenco, P. D. & Fassler, R. (2003). Integrin-linked kinase (ILK) is required for polarizing the epiblast, cell adhesion, and controlling actin accumulation. Genes & Development. 17(7). 926-940.

124. Sampath, S. C., Sampath, S. C., Ho, A. T. V., Corbel, S. Y., Millstone, J. D., Lamb, J., Walker, J., Kinzel, B., Schmidt, C. & Blau, H. M. (2018). Induction of muscle stem cell quiescence by the secreted niche factor Oncostatin M. Nature Communications. 9. 1531.

125. Schiaffino, S. (2010). Fibre types in skeletal muscle: a personal account. Acta Physiologica. 199. 451-463.

126. Schmidt, M., Schuler, S. C., Huttner, S. S., Von Eyss, B. & Von Maltzahn, J. (2019). Adult stem cells at work: regenerating skeletal muscle. Cellular and Molecular Life Sciences. 76. 2559-2570.

127. Schneider, S. M., Sridhar, V., Bettis, A. K., Heath-Barnett, H., Balog-Alvarez, C., Guo, L., Johnson, R., Jaques, S., Vitha, S., Glowcwski, A. C., Kornegay, J. N. & Ngheim, P. P. (2018). Glucose metabolism as a pre-clinical

biomarker for the golden retriever model of Duchenne muscular dystrophy. Molecular Imaging and Biology. 20(5). 780-788.

128. Schuler, S. C., Liu, Y., Dumontier, S., Grandbois, M., Le Moal, E., Cornelison, D. D. & Bentzinger, C. F. (2022). Extracellular matrix: Brick and mortar in the skeletal muscle stem cell niche. Frontiers in Cell and Developmental Biology. 10. 1056523.

129. Schwander, M., Leu, M., Stumm, M., Dorchies, O. M., Ruegg, U. T., Schnitty, J. & Muller, U. (2003). Beta1 integrins regulate myoblast fusion and sarcomere assembly. Developmental Cell. 4(5). 673-685.

130. Scott, W., Stevens, J. & Binder-Macleod, S. A. (2001). Human skeletal muscle fibre type classifications. Physical Therapy. 81(11) 1810-1816.

131. Seale, P., Saborin, L. A., Girgis-Gabardo, A. Mansouri, A., Gruss, P. & Rudnicki, A. (2000). Pax7 Is Required for the Specification of Myogenic Satellite Cells. Cell, Vol. 102: 777-786.

132. Severinsen, M. C. K. & Pedersen, B. K. (2020). Muscle-organ crosstalk: The emerging role of myokines. Endocrine Reviews. 41(4). 594-609.

133. Shinin, V., Gayraud-Morel, B., Gomes, D., Tajbakhsh, S. (2006). Asymmetric division and cosegregation of template DNA strands in adult muscle satellite cells. Nature Cell Biology. 8. 677-682.

134. Siegel, A. L., Atchison, K., Fisher, K. E., Davis, G.E. & Cornelison, D. D. (2009) 3D timelapse analysis of muscle satellite cell motility. Stem Cells. 27(10). 2527–2538.

135. Smerdu, V., Karsch-Mizrachi, I., Campione, M., Leinwand, L. & Schiaffino, S. (1994). Type IIX myosin heavy chain transcripts are expressed in type IIB fibres of human skeletal muscle. American Journal of Physiology. 267. C1723-1728.

136. Soto-Ribeiro, M., Kastberger, B., Bachmann, M., Azizi, L., Fouad, K., Jacquier, M-C., Boettiger, D., Bouvard, D., Bastmayer, M., Hytonen, V-P. & Wehrle-Haller, B. (2019). b1D integrin splice variant stabilizes integrin dynamics and reduces integrin signalling by limiting paxillin recruitment. Journal of Cell Science. 132(8), p.jcs224493.

137. Stanislovas, J. & Kermorgant, S. (2022). C-met-integrin cooperation: Mechanisms, tumorigenic effects, and therapeutic relevance. Frontiers in Cell and Developmental Biology. 10:994528.

138. Steffensen, B., Magnuson, V. L., Potempa, C. L., Chen, D. & Klebe, R. J. (1992). Alpha 5 integrin subunit expression changes during myogenesis. Biochimica et Biophysica Acta. 1137(1). 95-100.

139. Strace, G., Aprahamian, T., Flex, A., Gaetani, E., Biscetti, F., Smith, R. C., Percorini, G., Pola, E., Angelini, F., Stigliano, E., Castellot Jr, J. J., Losordo, D. W. & Pola, R. (2009). Sonic hedgehog regulates angiogenesis and myogenesis during post-natal skeletal muscle regeneration. Journal of cell and Molecular Medicine. 13(8b). 2424-2435.

140. Streuli, C. H. (2009). Integrins and cell-fate determination. Journal of Cell Science. 122(2). 171-177.

141. Sun, Z., Costell, M. & Fassler, R. (2019). Integrin activation by talin, kindlin and mechanical forces. Nature Cell Biology. 21. 25-31.

142. Tajbakhsh, S., Rocancourt, D., Cossu, G. & Buckingham, M. (1997). Redefining the genetic hierarchies controlling skeletal myogenesis: Pax3 and Myf-5 act upstream of MyoD. Cell. 89(1). 127-138.

143. Talbot, J. C. & Maves, L. (2016). Skeletal muscle fibre type: using insights from muscle developmental biology to dissect targets for susceptibility and resistance to muscle disease. Wiley Interdisciplinary Reviews: Developmental Biology. 5(4). 518-534.

144. Tamkun, J. W., DeSimone, D. W., Fonda, D., Patel, R. S., Buck, C., Horwitz, A. F & Hynes, R. O. (1986). Structure of integrin, a glycoprotein involved in the transmembrane linkage between fibronectin and actin. Cell. 42. 271-282.

145. Taverna, D., Disatnik, M-H., Rayburn, H., Bronson, R. T., Yang, J., Rando, T. A. & Hynes, R. O. (1998). Dystrophic muscle in mice chimeric for expression of a5 integrin. The Journal of Cell Biology. Vol. 143(3). 849 – 859.

146. Tidball, J. G. & Vilalta, S. A. (2010). Regulatory interactions between muscle and immune system during muscle regeneration. American Journal of Physiology – Regulatory, Integrative and Competitive Physiology. 298(5):R1173-87.

147. Tintignac, L. A., Brenner, H-R. & Ruegg, M. A. (2015). Mechanisms regulating neuromuscular junction development and function and causes of muscle wasting. Physiological Reviews. 95(3). 809-852.

148. Tomatis, D., Echtermayer, F., Schober, S., Balzac, F., Francesco Retta, S., Silengo, L. & Tarone, G. (1999). The muscle-specific laminin receptor a7b1 integrin negatively regulates a5b1 fibronectin receptor function. Experimental Cell Research. 246. 421-432.

149. Timpl, R. & Brown, J. C. (1996). Supramolecular assembly of basement membranes. Bioessays.18. 123-132.

150. Vignier, N., Moghadaszzdeh, B., Gary, F., Beckmann, J., Mayer, U. & Guicheney, P. (1999). Structure, genetic localization, and identification of the cardiac and skeletal muscle transcripts of the human integrin a7 gene (ITGA7). Biochemical and Biophysical Research Communications. 260. 357-364.

151. Von der Mark, H., Williams, I., Wendler, O., Sorokin, L., Von der Mark, K. & Poschl, E. (2001). Alternative splice variants of a7b1 integrin selectively recognize different laminin isoforms. The Journal of Biological Chemistry. 277(8), 6012-6016.

152. Von Maltzahn, J., Chang, N.C., Bentzinger, C. F. & Rudnicki, M. A. (2012). Wnt signalling in myogenesis. Trends in Cell Biology. 22(11). 602-609.

153. Wachtler, F. & Christ, B. (1992). The basic embryology of skeletal muscle formation in vertebrates: the avian model. Seminars in Developmental Biology. 3. 217-227.

154. Wang, H-V., Chang, L-W., Brixius, K., Wickstrom, S. A., Montanez, E., Thievessen, I., Schwander, M., Muller, U., Mayer, U. & Fassler, R. (2008). Integrin-linked kinase stabilizes myotendinous junctions and protects muscle from stress-induced damage. Journal of Cell Biology. 180(5). 1037-1049.

155. Webster, M.T., Manor, U., Lippincott-Schwartz. J. & Fan, C. M. (2016). Intravital imaging reveals ghost fibres as architectural units guiding myogenic progenitors during regeneration. Cell Stem Cell. 18(2). 243–252.

156. Wen, Y., Bi, P., Liu, W., Asakura, A., Keller, C. & Kuang, S. (2011). Constitutive notch activation upregulates Pax7 and promotes the self-renewal of skeletal muscle satellite cells. Molecular and Cellular Biology. 32(21). 2300-2311.

157. Werner, A., Willem, M., Jones, L. L., Kreutzberg, G. W., Mayer, U. & Raivich, G. (2000). Impaired axonal regeneration in α7 integrin-deficient mice. Journal of Neuroscience. 20(5). 1822-1830.

158. White, D. P., Caswell, P. T. & Norman, J. C. (2007). αvβ3 and α5β1 integrin recycling pathways dictate downstream Rho kinase signalling to regulate persistent cell migration. Journal of Cell Biology. 177(3):515–525.

159. White, J. P. (2021). Amino acid trafficking and skeletal muscle protein synthesis: a case of supply and demand. Frontiers in Cell and Developmental Biology. 9:656604.

160. Yamada. K. M. & Sekiguchi, R. (2018). Basement membranes in development and disease. Current Topics in Developmental Biology. 130. 143-191.

161. Yang, J. T., Rayburn, H. & Hynes, R. O. (1993). Embryonic mesodermal defects in α5 integrin-deficient mice. Development. Vol. 119: 1093-1105.

162. Yurchenco, P. D. & Orear, J. J. (1994). Basal lamina assembly. Current Opinion in Cell Biology. 6(5). 674-681.

163. Zamir, E. & Geiger, B. (2001). Components of cell-matrix interactions. Journal of Cell Science. Vol. 114(20). 3577-3579.

164. Zamir, E. & Geiger, B. (2001). Molecular complexity and dynamics of cell-matrix interactions. Journal of Cell Science. Vol. 114(20). 3583-3590.

165. Zammit, P. S., Golding, J. P., Nagata, Y., Hudon, V., Partridge, T. A. & Beauchamp, J. R. (2004). Muscle satellite cells adopt divergent fates: a mechanism for self-renewal? Journal of Cell Biology. 166(3). 347-357.

166. Zammit, P. S. (2017). Function of the myogenic regulatory factors Myf5, MyoD, Myogenin and MRF4 in skeletal muscle, satellite cells and regenerative myogenesis. Seminars in Cell & Developmental Biology. 72. 19-32.

167. Ziober, B. L., Vu, M. P., Waleh, N., Crawford, J., Lin, C. S. & Kramer, R. H. (1993). Alternative extracellular and cytoplasmic domains of the integrin a7 subunit are differentially expressed during development. Journal of Biological Chemistry. 268, 26773-26783.

168. Zofkie, W., Southard, S. M., Braun, T. & Lepper, C. (2021). Fibroblast growth factor 6 regulates sizing of the muscle stem cell pool. Stem Cell Reports. 16(12). 2913-2927.

Appendix.

Appendix 1.1. Number of myofibres analysed in uninjured muscle to calculate Fmin in acute injury model.

Genotype	Mouse ID	Number of myofibres	Number of images	Number of sections
Control	296	1383	24	6
	361	990	17	5
	367	2095	24	6
	531	702	12	3
	519	1266	24	6
	9993	1901	24	6
	2010	1504	24	6
a5 cKO	294	1315	23	6
	6385	1530	20	5
	6387	1558	23	6
	6391	1552	24	6
	6509	1301	23	6
	6569	1315	23	6
	6599	1311	23	6
a7 KO	439	1504	24	6
	530	1272	23	6
	532	1420	23	6
	9994	1462	20	5
	2009	1424	24	6
	2101	1503	24	6
	2103	1424	24	6
DKO	295	1422	24	6
	360	1797	24	6
	529	1205	23	6
	6514	1425	24	6
	6566	1797	24	6
	6601	1205	23	6
	6609	1259	23	6

Appendix 1.2. Number of myofibres analysed at 10DPI to calculate Fmin in acute injury model.

Genotype	Mouse ID	Number of myofibres	Number of images	Number of sections
Control	296	2013	18	5
	361	2852	24	6
	367	2770	24	6
	531	1631	12	3
	519	2604	24	6
	9993	3274	22	6
	2010	3182	24	6
a5 cKO	294	1842	16	4
	6385	2646	16	4
	6387	2671	16	4
	6391	1902	20	5
	6509	1842	16	4
	6569	2761	24	6
	6599	1839	17	5
a7 KO	439	2771	23	6
	530	3116	24	6
	532	2919	24	6
	9994	2275	15	4
	2009	2051	23	6
	2101	2673	23	6
	2103	2898	22	6
DKO	295	3320	23	6
	360	1139	24	6
	529	2591	24	6
	6514	3320	23	6
	6566	1139	24	6
	6601	2591	24	6
	6609	2588	24	6

Appendix 1.3. Number of myofibres analysed at 30DPI to calculate Fmin in acute injury model.

Genotype	Mouse ID	Number of myofibres	Number of images	Number of sections
Control	614	2842	23	6
	9969	2218	23	6
	9975	1931	22	6
	2196	2218	23	6
	2136	2381	23	6
	2152	2013	22	6
a5 cKO	606	1598	23	6
	6297	2708	24	6
	6345	2953	22	6
	6341	3077	23	6
	6589	2897	24	6
	6542	2953	22	6
a7 KO	9990	2505	23	6
	6349	3097	21	6
	6350	2329	22	6
	2199	2509	23	6
	2139	2979	22	6
	2154	2501	23	6
DKO	612	1581	16	4
	622	1966	20	5
	6339	2957	24	6
	6587	2229	22	6
	6541	2392	22	6
	6556	2167	21	6

Appendix 1.4. Number of myofibres and SCs analysed to determine the timing of integrin a5 expression (n = 3 mice).

Time point	Number of myofibres		Number of SCs	
	Control	a7 KO	Control	a7 KO
T0	30	27	53	39
T24	34	24	74	45
T48	29	27	127	55
T72	26	29	219	72

Appendix 1.5. Number of myofibres and SCs analysed to determine myofibre associated migration speed (n = 4 mice).

Genotype	Mouse ID	Number of myofibres	Number of SCs
Control	2432	12	49
	2475	12	47
	2531	11	46
	2452	12	47
a5 cKO	6661	11	47
	6745	9	39
	6749	10	42
	6799	10	42
a7 KO	2431	9	51
	2450	5	27
	2490	8	39
	2530	8	37
DKO	6746	8	39
	6766	8	36
	6801	11	39
	6818	9	40

Appendix 1.6. Statistical analysis of SC mitotic potential (Fig. 4.4).

0 Divisions		
ANOVA summary		
F	62.68	
P value	<0.0001	
P value summary	****	
Tukey's test	**Summary**	**Adjusted P Value**
Control vs. A5 cKO	ns	0.9571
Control vs. A7 KO	****	<0.0001
Control vs. DKO	****	<0.0001
A5 cKO vs. A7 KO	****	<0.0001
A5 cKO vs. DKO	****	<0.0001
A7 KO vs. DKO	ns	0.6172

1 Division		
ANOVA summary		
F	9.108	
P value	0.0009	
P value summary	***	
Tukey's test	**Summary**	**Adjusted P Value**
Control vs. A5 cKO	**	0.0065
Control vs. A7 KO	***	0.0009
Control vs. DKO	**	0.0087
A5 cKO vs. A7 KO	ns	0.7771
A5 cKO vs. DKO	ns	0.9988
A7 KO vs. DKO	ns	0.6947

2 Divisions		
ANOVA summary		
F	9.156	
P value	0.0009	
P value summary	***	
Tukey's test	**Summary**	**Adjusted P Value**
Control vs. A5 cKO	ns	0.6848
Control vs. A7 KO	*	0.0227
Control vs. DKO	ns	0.0526
A5 cKO vs. A7 KO	**	0.0024
A5 cKO vs. DKO	**	0.0057
A7 KO vs. DKO	ns	0.9725

3 Divisions		
ANOVA summary		
F	37.15	
P value	<0.0001	
P value summary	****	
Tukey's test	**Summary**	**Adjusted P Value**
Control vs. A5 cKO	ns	0.0803
Control vs. A7 KO	****	<0.0001
Control vs. DKO	****	<0.0001
A5 cKO vs. A7 KO	****	<0.0001
A5 cKO vs. DKO	***	0.0001
A7 KO vs. DKO	ns	0.9982

4+ Divisions		
ANOVA summary		
F	6.144	
P value	0.0056	
P value summary	**	
Tukey's test	**Summary**	**Adjusted P Value**
Control vs. A5 cKO	ns	0.1952
Control vs. A7 KO	*	0.0353
Control vs. DKO	**	0.004
A5 cKO vs. A7 KO	ns	0.7835
A5 cKO vs. DKO	ns	0.2192
A7 KO vs. DKO	ns	0.7027

Appendix 1.7. Number of myofibres and SCs analysed to determine timing of MRF expression (n = 4 mice).

Time point	MRF target	Number of myofibres				Number of SCs			
		Control	a5c KO	a7 KO	DKO	Control	a5c KO	a7 KO	DKO
T0	Pax7/Myf5	52	40	40	37	212	196	76	68
T24	Pax7/Myf5	44	36	31	40	240	208	68	64
	Pax7/MyoD	29	48	40	50	218	248	87	104
T48	Pax7/MyoD	34	30	42	38	628	536	132	156
	MyoD/MyoG	36	36	44	41	648	524	160	179
T72	Pax7/MyoD	45	40	30	38	2392	1588	284	316
	MyoD/MyoG	52	36	29	30	2512	1648	262	280
T96	Pax7/MyoD	34	42	32	40	3404	2748	532	556
	MyoD/MyoG	40	40	22	28	3572	2884	404	448